



UNIVERSITEIT VAN PRETORIA  
UNIVERSITY OF PRETORIA  
YUNIBESITHI YA PRETORIA

# **Inhibition of lysine-specific demethylase 1 as an antimalarial target by polyamine analogues**

---

by

B Barnard

28171404

Submitted in partial fulfilment of the degree:

*Magister Scientiae* Biotechnology (Specialisation Biochemistry)

Department of Biochemistry

Faculty of Natural and Agricultural Sciences

University of Pretoria

Pretoria

## **Submission declaration**

### **This page states:**

I, Bernice Barnard, declare that the thesis/dissertation, which I hereby submit for the degree (*Magister Scientiae*) in the Department of Biochemistry, at the University of Pretoria, is my own work and has not previously been submitted by me for a degree at this or any other tertiary institution.

Signature:

Date:

**Plagiarism declaration:**

**University of Pretoria  
Faculty of Natural and Agricultural Sciences  
Department of Biochemistry**

Full name: **Bernice Barnard**

Student number: **28171404**

Title of work: **Inhibition of lysine-specific demethylase 1 as an antimalarial target by polyamine analogues**

**Declaration:**

1. I understand what plagiarism entails and am aware of the University's policy in this regard.
2. I declare that this dissertation is my own, original work. Where someone else's work was used (whether from a printed source, the internet or any other source due acknowledgement was given and reference was made according to departmental requirements.
3. I did not make use of another student's previous work and submit it as my own.
4. I did not allow and will not allow anyone to copy my work with the intention of presenting it as his or her own work.

Signature: \_\_\_\_\_ Date: \_\_\_\_\_

## **Acknowledgements**

I would like to thank my supervisor, Prof. Lyn-Marie Birkholtz for her advice, patience and faith in my capabilities. For all the opportunities she created in benefit of my future.

A special thank you to Prof. Abraham Louw for his wonderful advice, love and support.

I would like to thank Dr. Pieter Burger for bioavailability predictions and Kathryn Wicht for assisting with the  $\beta$ -haematin inhibition assays at the University of Cape Town. Thanks to the students of the Malaria group and the staff at the Department of Biochemistry (University of Pretoria).

The South African National Research Foundation, the University of Pretoria and the South African Malaria Initiative (SAMI) for funding this project.

I want to thank my mom, Hannelie Barnard, for being an incredible role model and for always believing in me. The special people in my life, Barnie and Annelise Barnard, Dave and Alison Redgate, Marna de Beer, Nabila Ismail, Natasha Gouws and last but not least, Gavin Evans. Thank you for your unconditional faith, love and support in my capabilities.

Thank you to God for giving me strength, confidence and hope. “Vertrou op God en nie op jou eie insig nie, en Hy sal jou nooit in die steek laat nie.” Karla Dornacher

## Summary

According to the World Health Organization, malaria has been classified as one of the three most important infectious diseases in Africa. The number of malaria cases is still on the increase in various countries, such as Rwanda and Zambia, which highlights the fragility of malaria control and the need to maintain and improve control programs. An innovative strategy for developing new antimalarial agents is through targeting epigenetic regulatory mechanisms in the malarial parasite, *Plasmodium falciparum*. Histone post-translational modifications (PTMs) are factors contributing to epigenetic regulation in *P. falciparum* parasites. The epigenetic regulatory enzyme, Lysine-specific demethylase 1 (LSD1), has the ability to remove methyl groups from mono- and dimethylated lysine residues and is a regulator of gene expression through the modulation of chromatin structure. Polyamine analogues have been described as epi-drugs that target cell cycle development by blocking epigenetic control mechanisms in mammalian cells. A library of polyamine analogues were tested in cancer cells and found to specifically inhibit LSD1. In addition, these analogues were shown to have antiplasmodial activity against a drug-sensitive parasite strain, with IC<sub>50</sub> values ranging from 88-100 nM but were metabolically unstable *in vivo*. In an attempt to overcome this *in vivo* hurdle, the leading compound was fluorinated at four different positions and tested for improved antiplasmodial activity and selectivity towards the parasites. Furthermore, the effect of the compounds on epigenetic regulatory mechanisms, through inhibition of LSD1 activity, was investigated. The analogues showed inhibition of parasite proliferation at low nanomolar concentrations and were very selective towards the parasites with low resistance indices. The leading compound showed reversible cytotoxicity towards parasite proliferation in addition to inhibitory activity against LSD1 and therefore, epigenetic regulatory changes. The approach taken in this dissertation is novel as none of the currently available antimalarials target LSD1 and as such, adds valuable information to future perspectives for drug design.

## **TABLE OF CONTENTS**

<b>Summary</b> .....	<b>V</b>
<b>List of figures</b> .....	<b>IX</b>
<b>List of tables</b> .....	<b>X</b>
<b>Abbreviations</b> .....	<b>XI</b>
<b>Chapter 1: General introduction</b> .....	<b>1</b>
<b>1.1. Malaria as a parasitic disease</b> .....	<b>2</b>
<b>1.2. Intraerythrocytic developmental cycle of <i>Plasmodium</i></b> .....	<b>2</b>
<b>1.3. Multifaceted malaria control</b> .....	<b>5</b>
<b>1.4. Antimalarial drug discovery and development</b> .....	<b>5</b>
<b>1.4. Epigenetics in <i>P. falciparum</i> parasites</b> .....	<b>8</b>
<b>1.4.1. Higher organisation-level epigenetic regulation</b> .....	<b>11</b>
<b>1.4.2. Chromatin-level epigenetic regulation</b> .....	<b>12</b>
1.4.2.1. ATP-dependent chromatin remodelers .....	13
1.4.2.2. Transcription factors.....	13
1.4.2.3. Non-coding RNA .....	13
<b>1.4.3. Nucleosome-level epigenetic regulation</b> .....	<b>14</b>
1.4.3.1. Variant histones and nucleosome stability .....	14
1.4.3.2. Histone post-translational modifications.....	15
<b>1.5. Histone methylation</b> .....	<b>21</b>
<b>1.6. Histone demethylation</b> .....	<b>22</b>
1.6.1. Jumonji C-Domain-Containing histone demethylases .....	23
1.6.2. Lysine-Specific Demethylase 1 .....	25
<b>1.7. Polyamines and polyamine analogues</b> .....	<b>29</b>
<b>1.8. Null hypothesis of research objective</b> .....	<b>32</b>
<b>1.9. Aims</b> .....	<b>33</b>
<b>Chapter 2: Materials and Methods</b> .....	<b>34</b>
<b>2.1. <i>In silico</i> compound pharmacokinetics</b> .....	<b>35</b>
<b>2.2. <i>In vitro</i> cultivation of <i>P. falciparum</i></b> .....	<b>35</b>
<b>2.3. <i>In vitro</i> assessment of antiplasmodial activity</b> .....	<b>36</b>
<b>2.4. <i>In vitro</i> culturing of human hepatocellular liver carcinoma cells</b> .....	<b>37</b>
<b>2.5. Lactate dehydrogenase cytotoxicity determinations in mammalian cells</b> .....	<b>38</b>

<b>2.6. Recovery of parasite proliferation</b> .....	<b>39</b>
<b>2.7. Detergent Initiated <math>\beta</math>-Haematin Crystallisation assay</b> .....	<b>39</b>
<b>2.8. Lysine-Specific Demethylase 1 Chemiluminescence assay optimisation</b> .....	<b>40</b>
2.8.1. Kinetic study of luminol activity .....	40
2.8.2. Reagent effects on chemiluminescence .....	41
2.8.3. LSD1 enzymatic activity .....	41
2.8.4. LSD1 activity on isolated parasites .....	42
<b>2.9. Comparison of histone isolation protocols</b> .....	<b>42</b>
2.9.1. <i>Issar et al., 2008</i> Protocol .....	43
2.9.2. Merrick and Duraisingh, 2010 Protocol .....	44
2.9.3. <i>Trelle et al., 2009</i> Protocol .....	45
<b>2.10. Protein quantitation analysis</b> .....	<b>46</b>
<b>2.11. SDS-Polyacrylamide Gel Electrophoresis</b> .....	<b>46</b>
<b>2.12. Mass spectrometry analysis</b> .....	<b>47</b>
<b>2.13. Statistical Analyses</b> .....	<b>49</b>
<b>Chapter 3: Results</b> .....	<b>50</b>
<b>3.1. ADME profile of fluorinated polyamine analogues</b> .....	<b>51</b>
<b>3.2. Antiplasmodial activity of polyamine analogues in <i>P. falciparum</i></b> <b>parasites</b> .....	<b>56</b>
<b>3.3. Selectivity indices of the fluorinated polyamine analogues</b> .....	<b>59</b>
<b>3.4. Recovery of parasites after short-term exposure with compounds 1 and</b> <b>3</b> .....	<b>60</b>
<b>3.5. <math>\beta</math>-Haematin Crystallisation Studies</b> .....	<b>62</b>
<b>3.6. LSD1 Chemiluminescence Assay Optimisation</b> .....	<b>64</b>
3.6.1. Kinetic study of chemiluminescence .....	64
3.6.2. Reagent effect on chemiluminescence .....	65
3.6.3. Inhibition of human recombinant LSD1 enzyme activity .....	66
3.6.4. Antiplasmodial activity of tranlylcypropromine .....	67
3.6.5. <i>P. falciparum</i> LSD1 activity .....	69
<b>3.7. Isolation of <i>P. falciparum</i> histones</b> .....	<b>70</b>
3.7.1. Protein concentration standard curve .....	70
3.7.2. Concentrations of <i>P. falciparum</i> acid extracted histone proteins .....	71
3.7.3. SDS-PAGE separation of <i>P. falciparum</i> acid extracted histone preparations. ....	72
<b>3.8. Mass spectrometry analysis of isolated histone samples</b> .....	<b>75</b>

<b>Chapter 4: Discussion .....</b>	<b>76</b>
<b>Chapter 5: Concluding discussion.....</b>	<b>94</b>
<b>References.....</b>	<b>97</b>
<b>Appendix 1.....</b>	<b>105</b>
<b>Solubility .....</b>	<b>105</b>
<b>Permeability.....</b>	<b>105</b>
<b>Metabolic stability studies .....</b>	<b>106</b>
<b><i>In vivo</i> pharmacokinetic evaluation .....</b>	<b>107</b>



## **List of figures**

**Figure 1.1:** The intraerythrocytic life cycle of *P. falciparum*.

**Figure 1.2:** Four primary mechanisms of epigenetic regulation.

**Figure 1.3:** Heterochromatin and euchromatin.

**Figure 1.4:** Four canonical *P. falciparum* histone proteins.

**Figure 1.5:** Mode of catalysis of Jumonji-C demethylases.

**Figure 1.6:** LSD1 in complex with CoREST and a peptide substrate.

**Figure 1.7:** LSD1 enzyme complex.

**Figure 1.8:** The mode of catalysis of LSD1.

**Figure 1.9:** Monoamine oxidase inhibitors exhibiting LSD1 inhibition.

**Figure 1.10:** Three natural polyamines.

**Figure 1.11:** Structure of verlindamycin.

**Figure 1.12:** Structure of compound 30.

**Figure 3.1:** Antimalarial activity of polyamine analogues in *P. falciparum* parasites.

**Figure 3.2:** Recovery data of the two leading polyamine analogues.

**Figure 3.3:**  $\beta$ -haematin sigmoidal IC<sub>50</sub> graphs.

**Figure 3.4:** Kinetic study of luminols' activity.

**Figure 3.5:** Effect of various reagents on chemiluminescent activity.

**Figure 3.6:** Recombinant human LSD1 activity.

**Figure 3.7:** Tranylcypromine dose response curve in *P. falciparum* parasites.

**Figure 3.8:** Effect of compounds on parasite LSD1 activity.

**Figure 3.9:** Line graph of BSA standard absorbance readings.

**Figure 3.10:** AnyKD SDS-PAGE gel showing separated histone bands.

## **List of tables**

**Table 1.1:** Three classes of HDAC enzymes.

**Table 1.2:** Histone post-translational modifications.

**Table 3.1:** Solubility and permeability determinations

**Table 3.2:** Alkylated 3-6-3 carbon backbone fluorinated polyamine analogues.

**Table 3.3:** ADME Data of the fluorinated polyamine analogue series.

**Table 3.4:** Quantitative estimate of "drug likeness".

**Table 3.5:** *In vitro* antiplasmodial activity of fluorinated polyamine analogues.

**Table 3.6:** Cytotoxicity and selectivity determination of fluorinated polyamine analogues.

**Table 3.7:** Concentrations of acid extracted *P. falciparum* histones (Fresh vs frozen samples)

**Table 3.8:** Concentrations of acid extracted *P. falciparum* histones loaded onto an AnyKD SDS-PAGE gel.

**Table 3.9:** Histones identification and coverage determined using mass spectrometry.

## **Abbreviations**

ADME	Absorption, distribution, metabolism and excretion
AOL	Amine oxidase-like domain
BBB	Blood brain barrier
CAPS	3-(cyclohexylamino)-1-propanesulfonic acid
CQ	Chloroquine
DBL	Duffy binding-like family of proteins
DUBs	Ubiquitin-deconjugating enzymes
<i>E. coli</i>	<i>Escherichia coli</i>
H <sub>2</sub> O <sub>2</sub>	Hydrogen peroxide
H3	Histone 3
H3K9me3	Trimethylated lysine 9 of histone 3
HATs	Histone acetyltransferases
HDACs	Histone deacetylases
HIA	Human intestinal absorption
HKMTs	Histone lysine methyltransferases
HRP	Horseradish peroxidase
IDC	Intraerythrocytic developmental cycle
JmjC	Jumonji C-domain containing histone demethylases
LSD	Lysine-specific demethylase
MAO	Monoamine oxidases
MMV	Medicines for Malaria Venture
MTA	5'-methyl-thioadenosine
ncRNA	Non-coding RNA
PAO	Polyamine oxidases
PBS	Phosphate buffer saline
PDCA	Pyridine-2,4-dicarboxylic acid
<i>P. falciparum</i>	<i>Plasmodium falciparum</i>
<i>PfH3</i>	<i>Plasmodium falciparum</i> histone 3
<i>PfRh</i>	Reticulocyte homology family of proteins
PI	Protease Inhibitor Cocktail
PTMs	Post-Translational Modifications
QED	Quantitative estimate of "drug likeness"

RI	Resistance index
<i>rif</i>	Rifins - Repetitive interspersed family of proteins
RT	Room temperature
SDS-PAGE	Sodium dodecyl sulfate – polyacrylamide gel electrophoresis
SI	Selectivity Index
<i>stevor</i>	Subtelomeric variable open reading frame proteins
SUMO	Small Ubiquitin-like MOdifier
TCA	Tricarboxylic acid
TEMED	Tetramethylethylenediamine
Ubls	Ubiquitin-like proteins
WHO	World Health Organisation

# Chapter 1

---

## General introduction

## 1.1. Malaria as a parasitic disease

The World Health Organisation (WHO) has ranked malaria as one of the most serious causes of death worldwide and the second most prevalent cause of death in Africa after HIV/AIDS. It affects people in 108 countries worldwide, causing  $\pm$  250 million clinical malaria cases annually (WHO, 2013).

The five Plasmodia species causing malaria in humans are *Plasmodium malariae*, *Plasmodium vivax*, *Plasmodium knowlesi*, *Plasmodium falciparum* and *Plasmodium ovale*. As the most virulent of the Plasmodia species affecting humans, *P. falciparum* parasites, which is the source of about 85% of the malaria cases in Africa, cause the most medically severe form of malaria and is socio-economically debilitating. *P. falciparum* parasite resistance is rendering most of the currently used antimalarials ineffective in most parts of the world (Birkholtz *et al.*, 2012).

The parasite has an intricate life cycle and inhabits the female *Anopheles* mosquito vector and the human host. Due to the immense increase in parasite numbers during the intraerythrocytic developmental cycle (IDC) and the ability to quickly adapt to various environmental conditions for survival in both hosts, *P. falciparum* parasites have many unique life cycle control mechanisms.

## 1.2. Intraerythrocytic developmental cycle of *Plasmodium*

During the blood meal taken by an uninfected mosquito, mature gametocytes are transferred from the malaria carrier to the mosquito. These gametocytes develop into male and female gametes that fuse to produce a zygote in the stomach of the mosquito. The zygote undergoes rapid meiosis and develops into an oocyst, which matures into a motile ookinete. After 10-22 days, motile sporozoites develop, known as the infective parasite stage. They migrate to the salivary glands of the mosquito from where they are injected into the human host's bloodstream. Within 30 min, the sporozoites infect the host's hepatocytes, where they differentiate and mature intra-cellularly to form merozoites (Figure 1.1)(Tilley *et al.*, 2011).

Hepatocyte lysis releases merozoites that infect healthy host erythrocytes and initiate the IDC (also known as erythrocytic schizogony/asexual life cycle), which is responsible for much of the disease pathology. The IDC, as depicted in Figure 1.1, spans about 48 hours. During this time, the parasite develops through ring, trophozoite and schizont stages, releasing an average of 20-32 merozoites (daughter cells). These daughter merozoites can subsequently infect uninfected erythrocytes, leading to marked parasite loads within a few replication cycles. Mature gametocytes develop after 1-3 weeks of asexual cycling and they are responsible for the continued spread of malaria (Tilley *et al.*, 2011).

Invading merozoites (lemon shaped, Figure 1.1) contain a basally located nucleus, minimal cytoskeleton, secretory vesicles, ribosomes, mitochondria and a plastid. Uniquely, the merozoite surface is covered in a bristly coat used to attach to erythrocyte surfaces but the coat is “shed” after the merozoite enters the erythrocyte. During invasion, the composition and shape of the erythrocyte surface is changed by the release of compounds from the parasite rhoptries, micronemes and dense granules. The intraerythrocytic parasite develops within a parasitophorous vacuole, which is formed primarily from the secretion of the lipid-rich rhoptries. To optimise survival within the parasitophorous vacuole, the parasite is believed to export about 400 proteins such as kinases, adhesins and proteases that have a profound effect on remodelling the infected erythrocyte (Goldberg and Cowman, 2010).

Within the trophozoites, the plastid and mitochondrion lengthens and the number of free ribosomes increases greatly. The endoplasmic reticulum enlarges and an unusual type of Golgi complex is present. Various membranous structures are referred to as Maurer’s clefts and their function is thought to be involved in trafficking of substances from the parasite to the erythrocyte and maybe *vice versa*. The schizont form of the parasite undergoes multiple rounds of nuclear division and ingests haemoglobin until late in the life cycle.

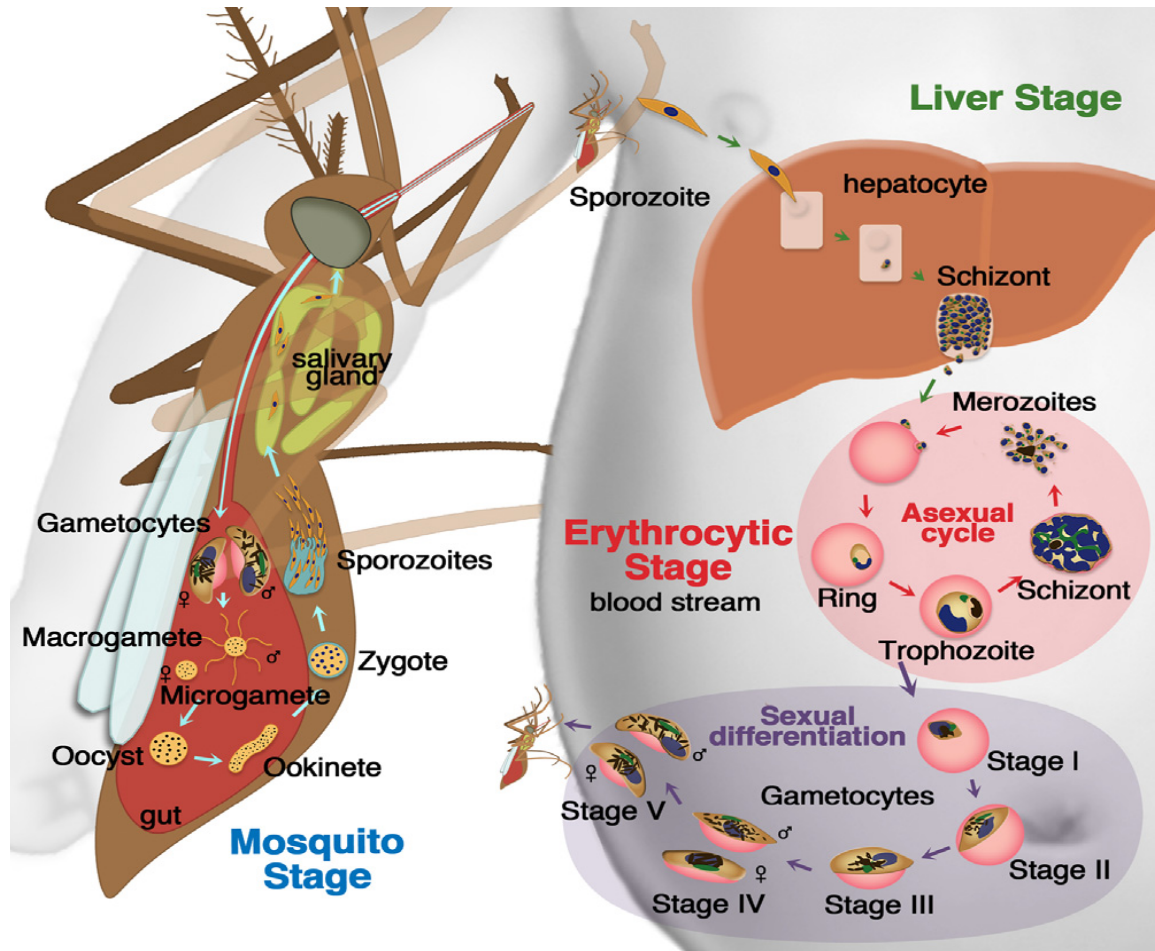


**Figure 1.1: The life cycle of *Plasmodium* parasites.** Released from the mosquito salivary glands, sporozoites move through the host bloodstream to the liver, where they develop into the schizont stage of the parasite life cycle. Hepatic schizonts release merozoites from ruptured hepatocytes, which infect healthy host erythrocytes. During the intraerythrocytic developmental cycle, the parasite matures through the ring, trophozoite and schizont stages to re-release merozoites with the ability to re-infect healthy erythrocytes. During the sexual differentiation of the parasites, male and female gametocytes mature through 5 stages of sexual development and are the mode of transmission to uninfected mosquitos (Griffith *et al.*, 2007; JAMA 2007). Within the mosquito midgut, the male and female gametocytes fuse, forming an oocyst, which develops into a motile ookinete. The zygote forms mature sporozoites by means of rapid meiosis, which are transferred to the mosquito salivary glands, from where the re-infection process starts anew (Tilley *et al.*, 2011).

Haem, a toxic by-product of haemoglobin digestion, is complexed by biomineralisation into a non-toxic crystalline form known as haemozoin and it is retained in the food vacuole of the parasite (Pagola *et al.*, 2000). Merozoites are formed within the schizont with the assembly of various organelles, starting at apical organelle formation and following a specific sequence of steps (Bannister *et al.*, 2000). Many of these above mentioned



unique parasite survival tactics have been exploited as antimalarial drug targets.

### **1.3. Multifaceted malaria control**

Due to the alarming rate of *P. falciparum* drug resistance development, including the recent detection of parasite resistance to artemisinin (mainline antimalarial chemotherapy) at the Thai-Cambodia border (Yeung *et al.*, 2009), drug development and novel drug target identification remains essential to sustained malaria control endeavours. Due to the complex nature of malaria as a disease, three main approaches to disease elimination and eradication are focussed on: 1) vector control, 2) vaccines and 3) chemotherapy.

Current vector control attempts are based on insecticide treated bed nets (ITNs) and indoor residual spraying (IRS), both mostly using a single class of insecticides known as pyrethroids. These are used because they are economical, have a long residual effect, show low toxicity towards humans and have a quick knockdown effect (Calderón *et al.*, 2013). Needless to say, novel insecticides are required for improved vector control. Furthermore, vaccines are mostly still in development stages. A leading vaccine candidate currently in the pipeline (phase III clinical trials) is a fusion protein of both *P. falciparum* and Hepatitis B surface antigens combined with a potent adjuvant (Calderón *et al.*, 2013). Other vaccine candidates are thought to be 5-10 years behind the above mentioned candidate (Calderón *et al.*, 2013).

### **1.4. Antimalarial drug discovery and development**

As vaccines and vector control compounds progress through clinical trials, the central strategy to malaria control remains treatment of disease symptoms, reducing morbidity and mortality. Novel antimalarial chemotherapy must preferably have a rapid onset of action in a single dose, address drug-resistance problems and be safe for use in children and pregnant women (Maser *et al.*, 2012). Owing to the complex parasite life cycle, various hosts and quick adaptation responses of malaria parasites, drug discovery targeting

all the life stages is a key aspect for malaria eradication. The four stages that need to be considered on for drug discovery are the liver stage, the blood stage, the transmission stages and the mosquito stages, as depicted in Figure 1.1 (Biamonte *et al.*, 2013).

The best current antimalarial chemotherapy approach to malaria treatment is the use of artemisinin combination therapies (ACTs). Artemisinin is used for its fast acting treatment of disease symptoms but it has a short half-life. Therefore, artemisinin is combined with slow clearing drugs (E.g. lumefantrine) to act on residual parasites. The mode of action of artemisinin is thought to involve the cleavage of a peroxide bond by  $Fe^{2+}$  in haem proteins, thereby generating oxygen radicals, which are toxic to the parasite. Artemisone, currently in phase II trials, provides a single dose cure in monkeys whereas the combination of artemisinin and naphthoquine are in phase III trials, showing promise as a single dose cure (Félix *et al.*, 2013).

ACT treatments replaced the combination therapy of sulfadoxine-pyrimethamine, which supplanted chloroquine. Chloroquine interferes with the development of haemozoin crystals in the digestive vacuole of the parasites, resulting in toxic haem created during haemoglobin digestion. Resistance to chloroquine is now found all over the world, due to various mutations in the chloroquine resistance transporter, which allows for an increased efflux of chloroquine to the cytosol from the acidic digestive vacuole of the parasites. A drug called ferroquine is currently undergoing phase II clinical trials as it shows promising results against chloroquine-resistant phenotypes, accumulating in their digestive vacuoles (Biamonte *et al.*, 2013).

In terms of folate pathway enzymes as validated drug targets, novel structure-based designs have developed compound P218, which overcomes all clinically relevant dihydrofolate reductase mutations, inhibiting nucleic acid synthesis (Biamonte *et al.*, 2013). Compounds DSM265 and DSM190 (Phase I clinical trials) are both bioavailable and have nanomolar *in vitro* activity. Their mode of action seems to be *de novo* pyrimidine synthesis inhibition, via inhibition of dihydroorotate dehydrogenase (Biamonte *et al.*, 2013).

Looking at the antimalarial pipeline, two compounds – spiroindolones and albitiazolium – are progressing through phase II trials with noteworthy results. As a replacement to preventative treatments, spiroindolones have been found to target the *Pf*ATPase4 cation channel, disturbing Na<sup>+</sup> homeostasis within the parasite. Albitiazolium mainly targets the transport of choline into the parasites. Choline is required for the synthesis of phosphatidylcholine, which is the main lipid in the cell membranes of parasites. This compound has been found to accumulate irreversibly in the parasite and a single-dose cure seems to be possible (Biamonte *et al.*, 2013).

On-going drug discovery ventures are looking for structurally distinct compounds and antimalarials with a distinct, novel mode of action (Calderón *et al.*, 2013). Founded in Switzerland, the Medicines for Malaria Venture (MMV) is a non-profit organisation driven to decrease the burden of malaria in disease-endemic countries by discovering new, effective and affordable antimalarials. An online global malaria medicine portfolio, designed by MMV, is updated every three months and accessible to all who are interested in antimalarial research. Furthermore, for successful future antimalarial ventures MMV has created guidelines. These include expectations that the possible novel antimalarial compounds must have 50% effective concentration (EC<sub>50</sub>) values smaller than or equal to 10 nM, a parasite reduction rate faster than artemisinin derivatives and a single-digit mg/kg activity of the 90% eradication dosage (ED<sub>90</sub>) in *P. falciparum* infected SCID mice (Burrows *et al.*, 2014). Additionally, an MMV box set containing 400 compounds with antimalarial activity against the asexual *P. falciparum* stage was constructed and made available free of charge (Wells *et al.*, 2009). The MMV box set aims at discovering the targets and modes of action of these known active compounds.

An important part of eventual malaria elimination and eradication is the design of compounds that are able to inhibit both the progression of parasites to sexual development as well as the transmission of the parasites from the mosquito to the host. Current transmission blocking agents are being narrowed down to compounds targeting the later stages (especially stage V)

of gametocyte maturation, as this is the stage taken up by the mosquito vector (Biamonte *et al.*, 2013). Currently, only primaquine is recommended for use targeting hypnozoites and mature gametocytes of all malaria species. The mechanism of action of primaquine is not yet understood, but active metabolites are thought to destroy the mitochondrial structures of the parasites. However, primaquine cannot be used by individuals with glucose-6-phosphate dehydrogenase deficiency as it will cause haemolytic anaemia, therefore, it is not widely used. Other than primaquine, methylene blue (monoamine oxidase inhibitor) has recently been discovered to inhibit gametocytes of all stages, abolishing almost all transmission to mosquitoes at concentrations acceptable to humans (Biamonte *et al.*, 2013). However, there are a number of other compounds (E.g. Ketotifen and epoxomicin) targeting gametocytes, which are currently being studied (Biamonte *et al.*, 2013; Wells *et al.*, 2009).

As not enough information is yet available on the epigenetic factors and enzymes as potential drug targets, research in this specific area is currently a hot topic for malaria drug design and development. Epigenetic factors are important for the cycling of parasites through their complex life cycle, providing novel targets such as histone acetyl transferases and histone deacetylases (Biamonte *et al.*, 2013). In the following section, epigenetics and epigenetic drug targets in *P. falciparum* parasites will be discussed in more detail.

#### **1.4. Epigenetics in *P. falciparum* parasites**

Various types of regulatory mechanisms are engaged by *P. falciparum* parasites to sustain the intricate and rapid transitions between morphological states and long-term antigenic variations, which allow for parasite survival and proliferation. These regulatory mechanisms include transcriptional and post-transcriptional regulation of gene expression, post-translational protein modification and translational repression among others (Merrick and Duraisingh, 2010).

Epigenetics defines the heritable changes of the phenotype or gene expression patterns in a cell, which occurs through mechanisms other than changes in the underlying DNA sequence and do not depend on different environmental conditions (Cui and Miao, 2010, Merrick and Duraisingh, 2010, Cortes *et al.*, 2012; Duffy *et al.*, 2014). Epigenetics is an important regulator of three components within the malaria parasite's biology: 1) the changes in gene expression, which occur during the IDC, 2) sexual and morphological changes and 3) the variant expression of gene families involved in virulence processes (Merrick and Duraisingh, 2010). The above components are synchronised by three primary mechanisms of epigenetic regulation in malaria parasites (Figure 1.2): 1) at a higher organisation level, which involves nuclear organisation, 2) at chromatin level and 3) at nucleosome level (Hoeijmakers *et al.*, 2012).

The chemical modifications of DNA bases (Figure 1.2 - a) occurs frequently in eukaryotes, but has not been discovered in *P. falciparum* parasites (Trelle *et al.*, 2009). Similarly, in eukaryotes, the core histones are separated by a linker histone (H1), which is not present in *P. falciparum* (Duffy *et al.*, 2012). The absence of H1 is correlated with the lack of higher-order organisation of *P. falciparum* nuclear DNA (Cui and Miao, 2010). Nucleosome-level regulation (Figure 1.2 - b) is influenced by: 1) post-translational modifications (PTMs), 2) variant histone proteins and 3) nucleosome stability. All three processes affect the nucleosome in terms of its composition, properties and/or placement (Hoeijmakers *et al.*, 2012). Chromatin-level epigenetic regulation (Figure 1.2 - c) denotes chromatin-associated proteins involved in the conversion of euchromatin to heterochromatin and *vice versa*, by means of the recruitment of chromatin remodelers and transcription factors, which affect changes in chromatin structure. It also associates non-coding RNA molecules with gene silencing and the higher-order packaging of chromatin. Higher organisation-level regulation (Figure 1.2 - d) signifies the organised storage of chromatin within the nucleus.

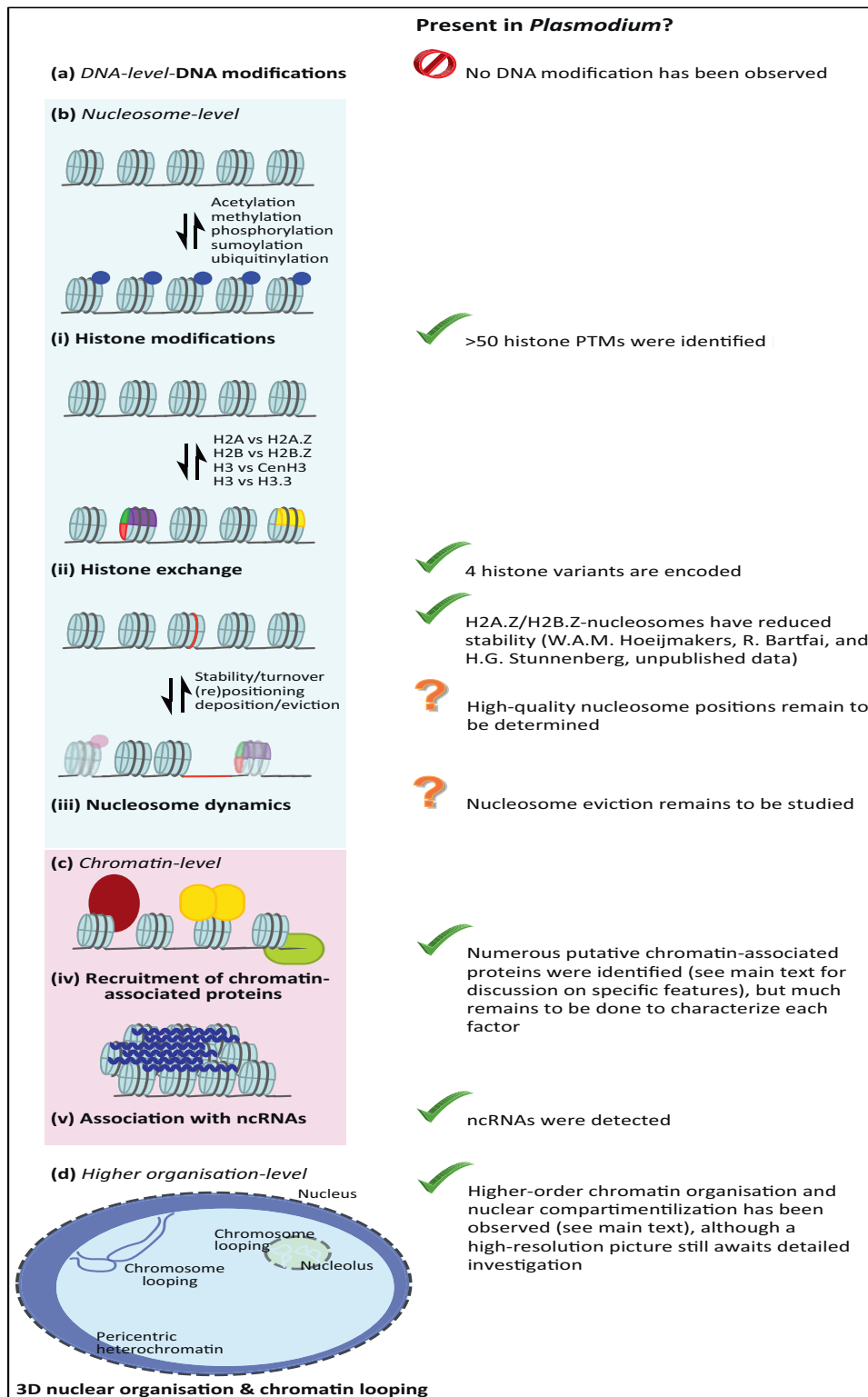


**Figure 1.2: Four primary levels of epigenetic regulation.** *Plasmodium* parasites apply three levels of epigenetic regulation, namely nucleosome level (b), chromatin level (c) and higher organisation-level (d). DNA-level epigenetic regulation (a) DNA modification has not been observed within *Plasmodium* parasites. Each level of regulation consists of different mechanisms, indicated in bold (i-v). Figure adapted from (Hoeijmakers *et al.*, 2012).

Regions of similar functions tend to cluster to nuclear sub-compartments via chromosome looping (Hoeijmakers *et al.*, 2012). Each level of *P. falciparum* parasite epigenetic regulation is discussed in more detail individually, in the sections to follow.

#### **1.4.1. Higher organisation-level epigenetic regulation**

About 10% of the *P. falciparum* parasite genome resides in a heterochromatic state and 90% resides in the transcription-permissive euchromatic state (Figure 1.3) (Hoeijmakers *et al.*, 2012). Each state is marked by classic “silent” or “active” post-translational marks, respectively (Section 1.4.3). Parasite chromatin undergoes stage-specific packaging changes during cycling through the IDC, and nuclear organisation affects gene expression as well as gene positioning, thereby affecting transcriptional regulation. This affects the movement of silenced genes from compact heterochromatin to less condensed euchromatin, permitting access to transcription machinery. Furthermore, the combination of heterochromatin/euchromatin spatial organisation within the nucleus could be changed and adapted according to processes activated (Weiner *et al.*, 2011, Sims *et al.*, 2009).

Studies show that during the parasite ring stage, there is no clear distinction between heterochromatin and euchromatin, which correlates to the low transcription levels observed during this stage. During the parasite trophozoite stage, heterochromatin is scattered throughout the nucleoplasm and is interspersed with euchromatin, but during the parasite schizont stage, there is a clear distinction between heterochromatin and euchromatin (Figure 1.3). The changes here correlate with transcriptome changes in processes involved in survival, metabolic functions and specialised re-infection functions such as egress and re-invasion (Weiner *et al.*, 2011, Sims *et al.*, 2009). The high level of transcription during both trophozoite and schizont stages correlates to the presence of euchromatin.

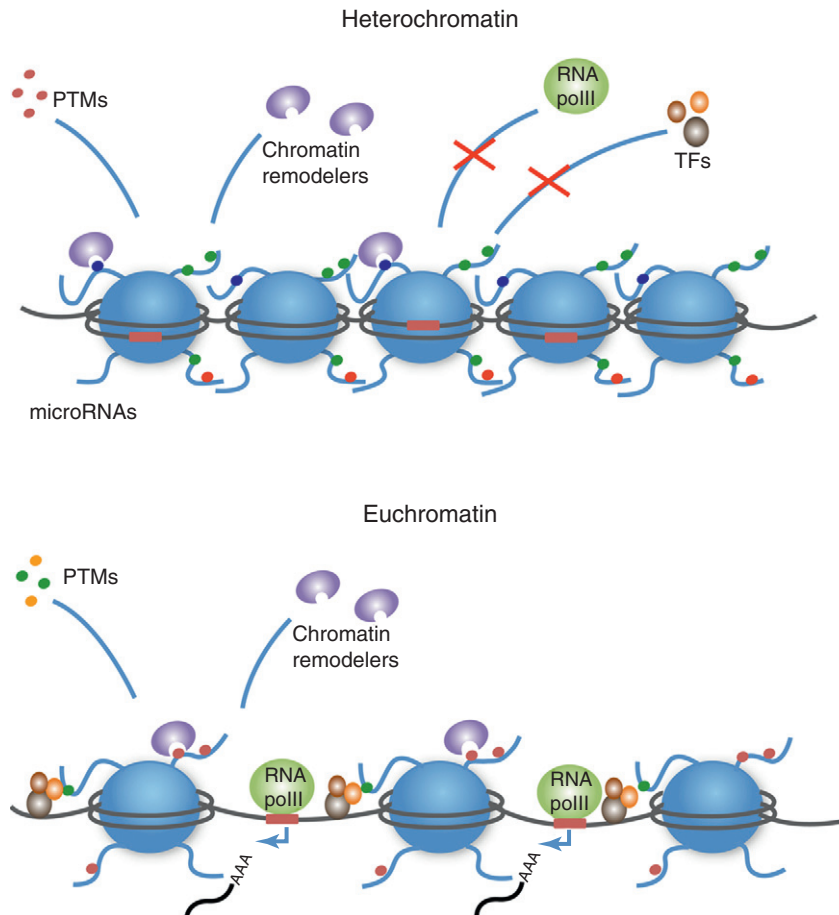


**Figure 1.3: *P. falciparum* parasite heterochromatin and euchromatin.** There are two functional chromatin forms. Heterochromatin is condensed, transcriptionally silent whereas euchromatin is relaxed, transcriptionally active. Heterochromatin prevents access to chromatin remodelers, whereas access is granted by euchromatin. Chromatin remodelers include ATP-dependent remodelers, histone modifying enzymes and specialised macromolecular compounds. These molecules are important for maintaining the respective heterochromatin and euchromatin states (Croken *et al.*, 2012).

### 1.4.2. Chromatin-level epigenetic regulation

The genome of *P. falciparum* is 23.26 Mbp in size, encodes more than 6000 genes and is organised into 14 chromosomes (Hernandez-Rivas *et al.*, 2010, Salcedo-Amaya *et al.*, 2009). Chromatin-level epigenetic regulation involves a conserved collection of chromatin-associated remodelers as well as an association with non-coding RNA. A low level of recognised transcription factors are affected, even though the parasite directs a tightly regulated transcriptional program (Cui *et al.*, 2008a).



#### **1.4.2.1. ATP-dependent chromatin remodelers**

Chromatin remodelers are protein complexes with the ability to alter nucleosome structure and composition, leading to changes in nucleosome composition and affecting the access of transcription factors and RNA polymerases to the nucleosomes (Croken *et al.*, 2012). The ATP-dependent chromatin remodelers also conduct the post-replicative replacement of canonical histones with histone variants. As an example, the SWI2/SNF2 family of protein complexes play a role in mobilising nucleosomes along DNA strands by receiving energy from ATP hydrolysis. Although the functions of this family are not well understood, *P. falciparum* parasites contain at least eleven SWI2/SNF2 ATPases (Lopez-Rubio *et al.*, 2007). The global positioning of nucleosomes during the IDC of *P. falciparum* seems to be quite stable. However, changes in chromatin structure and nucleosomal occupancy at promoters are associated with *var* gene activation. Therefore, SWI2/SNF2 ATPases might play a role in antigenic variation (Westenberger *et al.*, 2009).

#### **1.4.2.2. Transcription factors**

To date, few transcription factors have been identified and/or experimentally verified in parasitic protozoa. A plant-like transcription family known as AP2 has been identified in *P. falciparum* parasites and they are sequence-specific regulators of gene expression, acting directly or indirectly with chromatin remodelers (e.g. *PfGCN5*). Some *PfAP2* transcription factors are involved in epigenetic regulation via heterochromatin formation, genome integrity of sub-telomeric regions and targeting of silenced *var* genes to heterochromatin rich clusters (Croken *et al.*, 2012). Other transcription factors identified are *Pfmyb1* (involved in the IDC) and two non-sequence specific transcription factors containing the mobility group box (HMGB) motif (involved in the IDC and sexual stages) (Gomez *et al.*, 2010).

#### **1.4.2.3. Non-coding RNA**

Non-coding RNA (ncRNA) molecules do not encode proteins but associate with chromatin, often recruiting repressive histone modifying complexes (Hoeijmakers *et al.*, 2012). Although the topic of ncRNAs enforcing epigenetic

regulation is still controversial in *Plasmodium*, recent evidence shows that long ncRNAs are associated with *P. falciparum* centromeres. ncRNA could be involved in telomeric silencing in the absence of a functional RNA interference (RNAi) system. Proposed methods of silencing include stalling polymerases or the formation of RNA duplexes preventing translation (Merrick and Duraisingh, 2010). The dynamics of the chromatin state is affected by the synergistic and antagonistic relationships formed between the histone PTMs and the chromatin-associated proteins, who also have the ability to bind more than one histone PTM (Cui and Miao, 2010).

### **1.4.3. Nucleosome-level epigenetic regulation**

Epigenetic regulation at nucleosome level affects the composition, position and placement of these chromatin-packaging structures. The two factors influencing individual nucleosome epigenetic regulation are discussed in more detail below.

#### **1.4.3.1. Variant histones and nucleosome stability**

Variant histones have similar but not identical amino acid sequences to canonical histones, creating structurally and functionally specialised chromatin domains (Petter *et al.*, 2013). They are incorporated into the genome in a replication-independent manner (ATP-dependent chromatin remodelers), carry different modifications and have distinct functions (Hoeijmakers *et al.*, 2012). The presence of histone variants has been found to reduce nucleosome stability (Hoeijmakers *et al.*, 2012) but facilitates access of transcription factors, promoting transcription.

Research has shown that the variant H2A.Z is associated with a transcriptional permissive state due to predominantly being acetylated, possibly recruiting histone modifying complexes (Bartfai *et al.*, 2010). The double-variant nucleosomes (H2A.Z/H2B.Z) display reduced nucleosome stability in *P. falciparum* parasites and provide a transcriptionally permissive environment, which is concurrent with the pattern of acetylated PTMs found on these nucleosomes (Hoeijmakers *et al.*, 2012).

### 1.4.3.2. Histone post-translational modifications

Nucleosomes consist of DNA wrapped around an octamer of histones (Figure. 1.4). This octamer is composed of two copies of each of the core canonical histones (H2A, H2B, H3 and H4) (Munshi *et al.*, 2009) and four variant histones namely, H2A.Z, H2Bv, H3.3 and the centromere specific H3 (CenH3) variant (Miao *et al.*, 2006, Gill *et al.*, 2010).

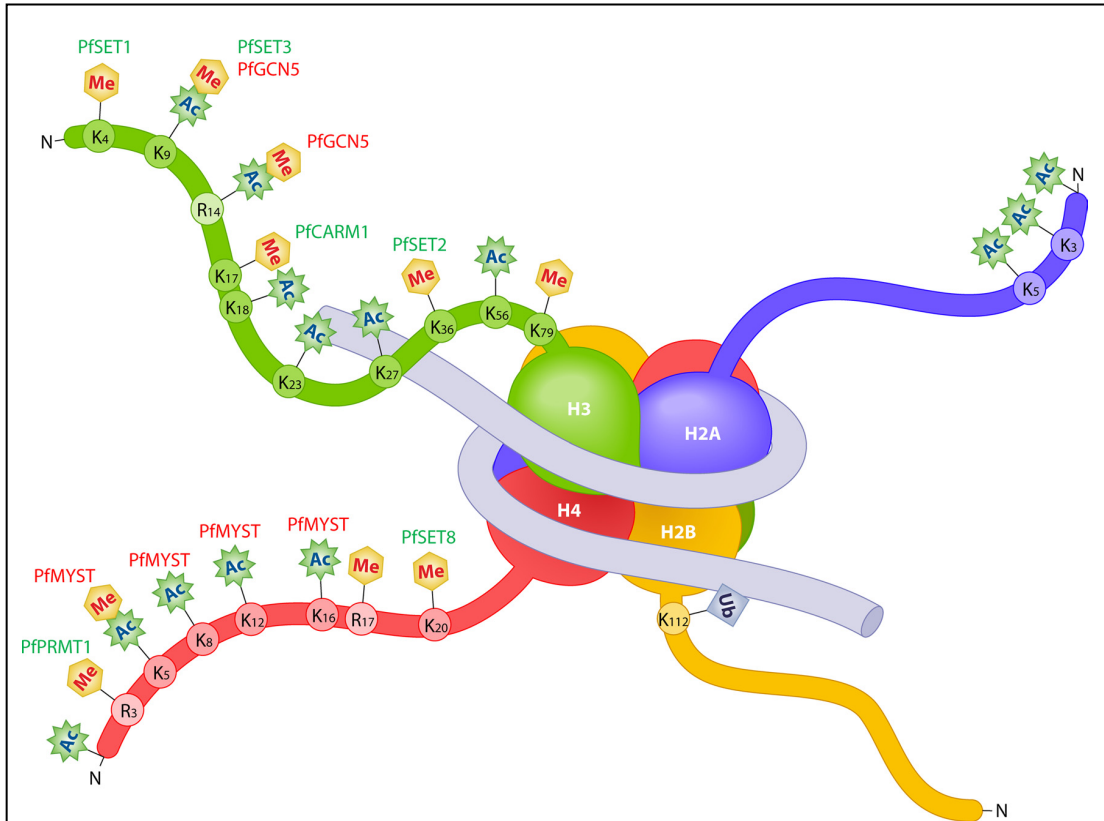


**Figure 1.4: Four canonical histones of *P. falciparum* parasites and their post-translational modifications (PTMs).** The four canonical histones form the nucleosome, which is the repeating unit structure of chromatin. The histones tails are subject to an array of PTMs such as methylation [Me], acetylation [Ac], and ubiquitination [Ub]. The PTMs are catalysed by various enzymes (*PfGCN5*, *PfSET1*, *PfSET2*, *PfCARM1*, *PfPRMT1*, *PfMYST*, and *PfSET8*) (Cui and Miao, 2010, Shechter *et al.*, 2007). The PTMs are a form of epigenetic regulation, which is an important factor in cycling the parasites through a complex life cycle.

Each histone octamer consists of a globular C-terminal domain (mediates histone-histone interactions) and dynamic N-terminal tails. These tails are rich in basic amino acids (lysine and arginine) and extend outwards from the nucleosome surface (Munshi *et al.*, 2009). It is primarily on these N-terminal tails that PTMs occur (Sullivan *et al.*, 2006). The PTMs affecting histones

result in the remodelling of chromatin into either euchromatin (accessible) or heterochromatin (inaccessible). Specialised adaptor proteins, known as “chromatin readers” bind the modifications, which are created by enzymes referred to as “chromatin writers”. Together, the actions of the chromatin readers and writers cause the above-mentioned chromatin remodelling via the recruitment of transcription factors and the RNA polymerase complex (Figure 1.4).

### **Chromatin “readers”**

Conserved protein domains have been discovered, which can be classified into several subgroups: 1) Bromodomains, 2) Royal Superfamily Proteins, 3) 14-3-3 proteins, 4) Plant Homeodomain (PHD) Fingers and 5) WD40 Repeat Containing Proteins and 6) Chromodomains. These domains specifically bind/recognise histone PTMs and are referred to as histone “readers”. The recognition of specific PTMs by these “readers” facilitates downstream events via the recruitment of chromatin-associated proteins. Bromodomains are acetyllysine-binding modules whereas PHD fingers, the Royal superfamily and chromodomain protein folds are methyllysine-binding modules. The WD40 repeats are associated with the Su(var), E(z), Trithorax domain (SET1). *P. falciparum* parasites contains at least ten PHD domain proteins and more than ninety WD40 repeats. *PfMYST* (a histone acetyltransferases family) and heterochromatin protein 1 (*PfHP1*) contain single chromodomains whereas the helicase-DNA-binding protein 1 homologue contains double chromodomains. *PfHP1* is associated with the sub-telomeric and intra-chromosomal silent *var* genes and is essential for the IDC. *PfGCN5* (histone acetyltransferase) and *PfSET1* (histone deacetylases) both contain a single bromodomain (Cui and Miao, 2010).

### **Chromatin “writers”**

A protein that places a histone PTM at a specific residue on the histone tail is referred to as a chromatin “writer”. The PTMs placed by the chromatin “writers” modulate chromatin dynamics, condensation and cohesion but also

transcription, DNA replication and repair, as well as recruiting chromatin “readers” to specific genomic loci in a combinatorial manner. There are a variety of PTMs: acetylation, phosphorylation, sumoylation, ubiquitination and methylation among others (Figure 1.4). These modifications change chromatin structure directly by modulating the interactions of the DNA with various proteins as well as creating an epigenetic marker to retrieve specific effector proteins (Cui and Miao, 2010).

The “histone code” hypothesis confers that all the varieties and numbers of histone modifications in totality dictate a certain biological outcome. The “histone code” is interpreted by other proteins allowing them to control the structure and eventually function of chromatin fibres, directing the biological outcomes that follow (Cui and Miao, 2010). Histone modifications are an important part of epigenetic studies because the various histone modifications determine, in part, if a certain promoter is open and active or closed and repressed.

Research on *P. falciparum* histones has identified more than 70 reversible PTMs (Miao *et al.*, 2006; Duffy *et al.*, 2014) signifying more activation marks than silencing marks, which correlates to the euchromatin status of *P. falciparum* parasites (Hoeijmakers *et al.*, 2012). The sheer number of PTMs on canonical and variant histones as well as the possible synergistic relationships demonstrates the complexity of the “histone code” within the malaria parasite (LaCount *et al.*, 2005). The most abundant PTMs are histone lysine acetylation and methylation. Many PTMs in *Plasmodium* histones confer synergistic relations to epigenetic regulatory circuits by lying densely clustered. Several of the transcriptionally active and repressive markers associated with H3 and H4 methylation and acetylation in *P. falciparum* parasites are indicated in Table 1.1 (Cui *et al.*, 2008a; Duffy *et al.*, 2014).

- **Histone ubiquitylation and sumoylation**

Ubiquitylation in *P. falciparum* has been linked to transcriptional activation and silencing as well as mRNA stability (Ponder and Bogyo, 2007) and is often found on canonical histones H2A and H2B (Cui and Miao, 2010).

**Table 1.1: Validated histone 3 and histone 4 post-translational modifications and histone-modifying enzymes.** Each PTM is labelled as an active or silent marker, showing its presence during a certain IDC stage consistent with a chromatin state. PTM enzymes responsible for each modification are also shown (Cui *et al.*, 2008a; Duffy *et al.*, 2014).

PTMs	Marker	IDC Stage	Chromatin state	Enzyme
H3K4me1	Active	Trophozoite and Schizont	Euchromatin	<i>Pf</i> SET1;4;6
H3K4me2	Active	Trophozoite and Schizont	Euchromatin	<i>Pf</i> SET1;4;6
H3K4me3	Active	Trophozoite and Schizont	Euchromatin	<i>Pf</i> SET1;4;6
H3K9me3	Silent	Ring	Heterochromatin	<i>Pf</i> SET3
H3K9ac	Active	Trophozoite and Schizont	Euchromatin	<i>Pf</i> GCN5
H3K14ac	Active	Trophozoite and Schizont	Euchromatin	<i>Pf</i> GCN5
H3K27me	Silent	Ring	Heterochromatin	HKMT
H3K36me	Silent	Ring	Heterochromatin	<i>Pf</i> SET2
H3K79me	Silent	Ring	Heterochromatin	HKMT
H4ac	Active	Trophozoite and Schizont	Euchromatin	<i>Pf</i> MYST
H4K20me	Silent	Schizont	Heterochromatin	<i>Pf</i> SET8
H3R17me	Active	Trophozoite and Schizont	Euchromatin	HKMT
H4R3me	Active	Trophozoite and Schizont	Euchromatin	<i>Pf</i> PRMT1

Through three enzyme activities: 1) an ATP-dependent activating enzyme, 2) a conjugating enzyme and 3) a protein isopeptide ligase, ubiquitin (a 76-amino acid containing protein) is conjugated onto the histones, which are then targeted to the proteasome for degradation. During ubiquitylation, the C-terminal diglycine of ubiquitin forms an isopeptide bond with the amino group of the histone lysine side chain. Within *P. falciparum* parasites, two ubiquitin-like proteins have been classified: SUMO and Nedd8.

Small Ubiquitin-like Modifier (SUMO) conjugation, also referred to as the process of sumoylation, is a PTM implicated in a variety of cellular processes. The SUMO protein is structurally related to ubiquitin, of similar size and is attached to lysine residues within its target proteins but does however, not mark the protein for degradation. It is believed to modify its substrate's interactions with their partner proteins. Sumoylated proteins are involved with the regulation of transcription factors and chromatin remodelling proteins (Issar *et al.*, 2008). In *Plasmodium*, histone H4 is often found sumoylated and is associated with decreased gene expression (Cui and Miao, 2010). Opposing ubiquitylation, *P. falciparum* parasites also have ubiquitin-deconjugating enzymes (DUBs), which show specificities to both Nedd8 and

ubiquitin. DUBs have the ability to remove a single ubiquitin from a polyubiquitin chain and can remove ubiquitin from conjugated substrates (Ponder and Bogyo, 2007).

- **Histone acetylation**

Histone lysine residues are acetylated by histone acetyltransferases (HATs) and deacetylated by the opposing actions of histone deacetylases (HDACs). HATs bind transcription factors and chromatin remodelers (bromodomains), thereby directly or indirectly regulating gene expression, therefore acetylation is largely linked to active genes (Cui and Miao, 2010). As one of the most studied PTMs, acetylation is believed to neutralise the cationic charge found on the N-terminal amino tails of the histones. This affects the interaction between the histones and the DNA, making the DNA more accessible to transcription (Andrews *et al.*, 2012).

Five families of HATs are recognised: general transcription HATs, GNATs (GCN5 N-acetyltransferase), nuclear hormone-related HATS, MYSTs (MOZ, Ybf1/Sas3, Sas2 and Tip 60) and p300/CBP (CREB-binding protein). Within the malaria parasite genome, at least four HATs are found: PF08\_0034 (*PfGCN5*, preferentially acetylates lysine nine of histone 3 (H3K9) and H3K14 *in vitro*), PF11\_0192 (*PfMYST*, acetylates K5, K8 and K12 of H4), PFL1345c and PFD0795w. An essential *P. falciparum* gene encodes *PfGCN5*, which has an unusually long N-terminal extension involved in mediating protein complex formation and it appears to harbour the nuclear localisation signal. The H3K9 mark is enriched in the promoters of active genes, which is consistent with its role in gene activation (Cui and Miao, 2010). *PfMYST* is an essential *P. falciparum* gene involved in the regulation of the parasite cell cycle. Its over expression results in a defect in the parasite cell cycle, causing accelerated schizogony and fewer merozoites per schizont (Croken *et al.*, 2012).

Inhibition of HATs is most common using compounds curcumin and anacardic acid, resulting in hypoacetylation of lysine residues. Curcumin inhibits several cell signalling pathways and cell enzymes, shows synergistic activity with artemisinin and its mode of action is presumably due to the formation of

reactive oxygen species (Cui and Miao, 2007). Anacardic acid treatment results in the down regulation of developmentally regulated genes but this could be due to off-site effects as it inhibits a wide variety of enzymes in other organisms (Cui *et al.*, 2008b).

- **Histone deacetylation**

HDACs are responsible for removing acetyl residues, opposing the dynamic process of acetylation. Table 1.2 shows the three classes of HDACs that have been identified in *P. falciparum* parasites. PfHDAC1 is localised mainly in the nucleus, are small molecules and are expressed during multiple life cycle stages whereas *P. falciparum* class II HDAC proteins are present in both the nucleus and cytoplasm and are generally a bit larger. Both class I and II HDAC enzymes are zinc-dependent hydrolases. Class III HDACs (sirtuins) are an NAD-dependent subfamily involved in regulating the mutually exclusive expression of *var* genes (Patel *et al.*, 2009).

**Table 1.2: Three classes of *P. falciparum* parasite histone deacetylase enzymes.** *P. falciparum* proteins classified into three HDAC classes, showing their localisation within the parasite as well as the type of enzyme class they belong to.

HDAC Class	Protein	Localisation	Type
I	<i>Pf11260c</i>	Nucleus	Zn-dependent
II	<i>Pf14_069</i>	Nucleus and cytoplasm	Zn-dependent
II	<i>Pf10_0078</i>	Nucleus and cytoplasm	Zn-dependent
III	<i>PfSir2A</i>	Undetermined	NAD-dependent
III	<i>PfSir2B</i>	Undetermined	NAD-dependent

Class III HDAC, *PfSir2A* is involved in silencing the sub-telomeric *var* genes and is transcribed towards the telomere and intra-chromosomal *var* genes, playing a key role in the maintenance of telomere length (Tonkin *et al.*, 2009). A unique facet of *PfSirA* is that it shows ADP-ribosyl-transferase activity on all histones (Cui and Miao, 2010, French *et al.*, 2008). *PfSir2B* silences a subset of *var* genes containing a different promoter to the *PfSir2A* silenced genes (Andrews *et al.*, 2012). Although neither HDAC class III sirtuins are necessary



for survival, their regulation of *var* gene expression is a target for drug development.

Inhibition of HDAC class I and class II enzymes, are based on binding the Zn-containing tubular enzyme pockets (mode of action of apicidin). Due to apicidin having low selectivity and poor bioavailability, it is considered clinically unsuitable. Short-chain fatty acids have low activity against mammalian HDACs and have other targets, therefore cannot be classified as HDAC specific inhibitors (Andrews *et al.*, 2012). Synthetic HDAC inhibitor suberoylanilide hydroxamic acid (SAHA) and natural HDAC inhibitor trichostatin A (TSA) are hydroxamate based HDAC inhibitors (Trenholme *et al.* 2014). TSA is not clinically suitable even though it has a low nanomolar  $IC_{50}$  for *P. falciparum* killing *in vitro* and recent results show that it has a low gametocytocidal activity between 70-90 nM (Trenholme *et al.* 2014). SAHA has a less potent *in vitro*  $IC_{50}$  than TSA, but is more selective towards the parasite. It inhibits *ex vivo* parasite growth and shows promising antiproliferative action against *P. vivax*. Ultimately, HDAC specific inhibitors should consist of a metal chelating group joined by a carbon chain linker to a hydrophobic capping element, which confers potency and selectivity (Patel *et al.*, 2009).

### **1.5. Histone methylation**

Histone methyltransferase enzymes (HKMTs) are responsible for the methylation of positively charged histone lysine and arginine residues, which is associated with maintenance of sub-telomeric heterochromatin and gene regulation (Cui and Miao, 2010). Unlike acetylation, methylation does not alter the charge of the histone tail but instead influences its hydrophobicity and basicity thereby affecting the affinity of DNA binding molecules (Spannhoff *et al.*, 2009). HKMTs use S-adenosylmethionine as a co-substrate to transfer methyl groups (Spannhoff *et al.*, 2009) and differentiation between gene activation and silencing depends on the residue methylated and the valency of the methylation (Lopez-Rubio *et al.*, 2009). As an example, the differential methylation of histones H3 and H4 lysine residues can either activate or

repress gene transcription depending on the location of the lysine or arginine residues and the degree of methylation (mono-, di- or trimethylation) (Hou and Yu, 2010).

*P. falciparum* parasites encode a large family of ten methyltransferase members, which consists of the Su(var), E(z) and Trithorax (SET) domain (Cui *et al.*, 2008a). The SET domains contain mostly  $\beta$ -sheets with N-terminal (SET-N) and C-terminal sequences (SET-C). The SET-C regions are well conserved in all PfSETs whereas the SET-N regions vary considerably (Chookajorn *et al.*, 2007). With respect to parasite core histones, lysine methylation occurs mainly on H3 at K4, K9, K27, K36, K79 and on H4 at K20. Microarray analysis performed by Cui *et al.* indicated that during the IDC, transcript abundance of PfSET4 and PfSET8 peaked during the schizont stages (Cui *et al.*, 2008a). However, PfSET1, PfSET5 and PfSET7 (unknown PTM specificity) all had a constitutive pattern of expression. PfSET6 transcript levels peaked during the ring and early trophozoite stages, however PfSET2 transcripts are present at very high levels during the ring and schizont stages but decrease in the late trophozoite stage (Cui *et al.*, 2008a). Each IDC stage of peak transcription correlates to the chromatin state and PTM present, predicting the modification as an active or silent gene marker (Table 1.1). The silencing, heterochromatin histone marker H3K9me3 is negatively correlated with global gene expression and is associated with silent *var* genes whereas the active gene marker, di- and trimethylated H3K4, is associated with the *var* promoter that is actively transcribed (Lopez-Rubio *et al.*, 2007). *P. falciparum* parasites have three arginine methyltransferases of which only PfPRMT1 has been characterised. It is localised in the nucleus and cytoplasm, which correlates with its ability to methylate non-histone substrates as well as H4R3 (Miao *et al.*, 2006). Unlike lysine methylation, evidence shows that arginine methylation is mostly associated with gene activation.

## 1.6. Histone demethylation

The discovery of demethylases changed the view of methylation from an irreversible process to a reversible, dynamic process under enzymatic control

(Hou and Yu, 2010). Demethylases play an important role in chromatin-based cellular processes via the regulation of the steady-state levels of histone methylations (Hou and Yu, 2010). This regulation is based on demethylase enzymes broadly repressing gene expression with the removal of mono-, di- and tri-methylation marks from H3K4, among others (Zhu *et al.*, 2012). To date, two families of histone lysine demethylases have been identified: 1) Jumonji C-domain-containing histone demethylases (JHDMS) and 2) lysine-specific demethylases 1 (LSD1) (Cui *et al.*, 2008a).

### 1.6.1. Jumonji C-Domain-Containing histone demethylases

Jumonji C-Domain-Containing histone demethylases (JHDMS) have narrow substrate specificities, prefer different methylation states and often target a single lysine residue within a substrate. They belong to the superfamily of iron-dependent di-oxygenases and is a predicted metalloenzyme catalytic motif (Tian and Fang, 2007). They adopt a jellyroll-like  $\beta$ -fold, within which the active site is concealed (Cui *et al.*, 2008a). The jellyroll is surrounded by structural elements that help maintain the structural integrity of the catalytic core and contributes to substrate recognition (Hou and Yu, 2010).

JHDMS use the cofactors,  $\alpha$ -ketoglutarate and iron ( $\text{Fe}^{2+}$ ), to demethylate proteins in the presence of oxygen (Figure 1.5). During the demethylation reaction the substrate and the two cofactors react with an iron-oxo intermediate while bound to the enzyme active site. A bond forms between  $\alpha$ -ketoglutarate and iron resulting in the decarboxylation of  $\alpha$ -ketoglutarate. This decarboxylation results in the formation of succinate, carbon dioxide and  $\text{Fe}^{4+}$ -oxo species. The iron-oxo intermediate is reduced, while hydrogen is removed from the methylated substrate. Carbinolamine is formed, which degrades into formaldehyde and a demethylated product, while  $\text{Fe}^{2+}$  is regenerated (Spannhoff *et al.*, 2009).

JHDMS are able to remove all three degrees of methylation, as no free electron pair on the nitrogen is needed. *P. falciparum* encodes two JHDMS, *PfJmjC1* and *PfJmjC2*. *PfJmjC1* proteins seem to be specific for H3K36 and

have higher specificity for H3K9 demethylase activity due to the Serine-Alanine residue substitution in the substrate-binding pocket (Cui *et al.*, 2008a).

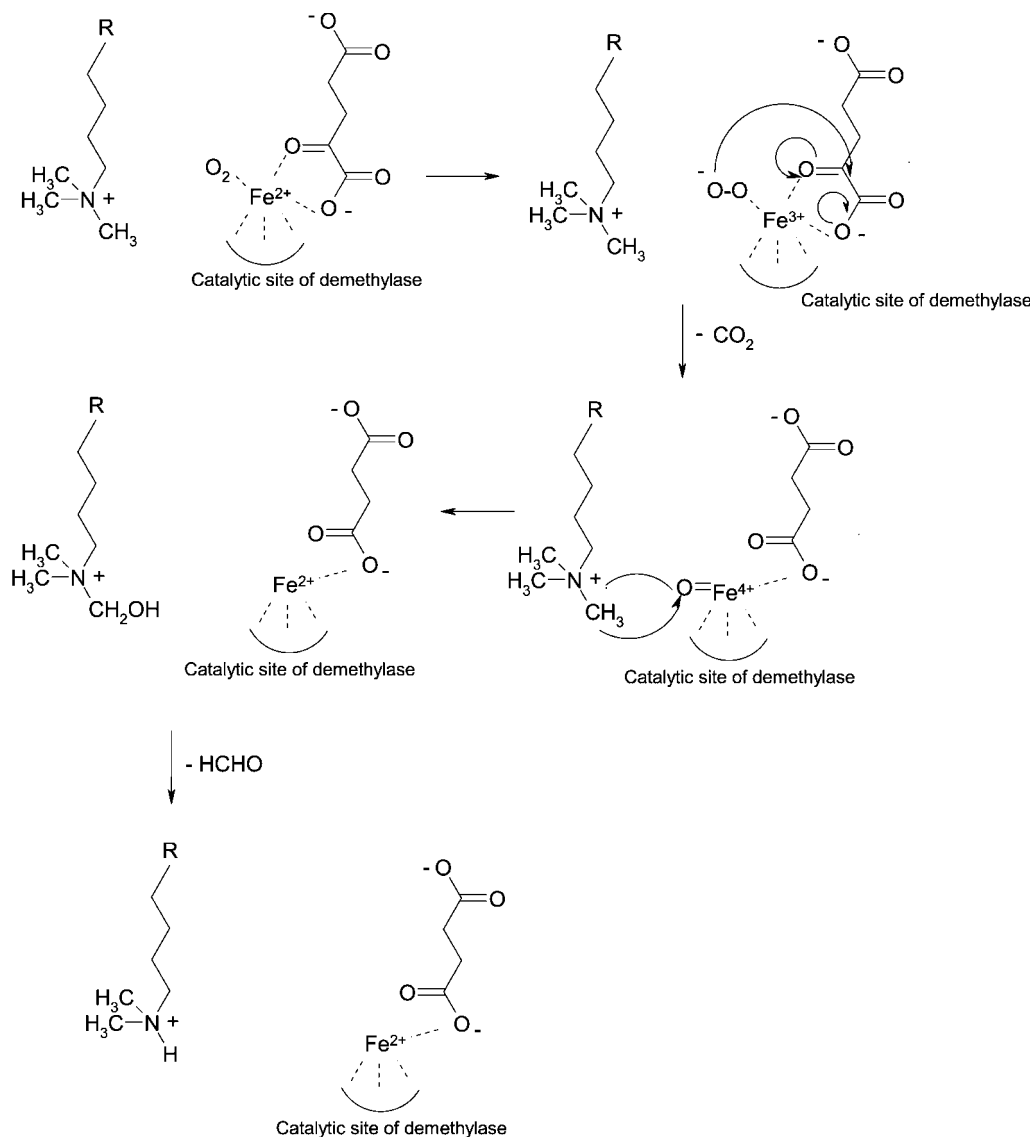


**Figure 1.5: Mode of catalysis of Jumonji C-Domain-containing histone demethylases.** During the demethylation reaction, the substrate and the two cofactors react with an iron-oxo intermediate, while bound to the enzyme active site. A bond forms between α-ketoglutarate and iron resulting in the decarboxylation of α-ketoglutarate, forming succinate, carbon dioxide and Fe<sup>4+</sup>-oxo species. The iron-oxo intermediate is reduced, while hydrogen is removed from the methylated substrate. Carbinolamine is formed, which degrades into formaldehyde and a demethylated product, while Fe<sup>2+</sup> is regenerated (Spannhoff *et al.*, 2009).

Compounds known as 8-hydroxyquinolines (8-HQs) could be used as templates for novel inhibitors of demethylases. These compounds inhibit human JmjD2 by binding with the iron residue in the enzyme active site. 5-

carboxy-8HQ interacts with the active site nickel via the 8-hydroxy and quinoline-nitrogen, displaying tight-binding inhibitory behaviour (King *et al.*, 2010).

Certain HDAC inhibitors such as pyridine-2,4-dicarboxylic acid (PDCA), have been found to inhibit the human JmjC2E at concentrations below 10  $\mu$ M. PDCA has to be modified to a pro-drug form to enable it to move through cell membranes (King *et al.*, 2010). Although there are currently no specific JHDM inhibitors, the known structures can be modified to synthesise more potent, selective inhibitors.

### 1.6.2. Lysine-Specific Demethylase 1

*P. falciparum* parasites encode at least one LSD1 (PFL0575w). LSD1 belongs to the superfamily of flavin adenine di-nucleotide (FAD)-dependent amine oxidases and consists of three structural domains: a C-terminal amine oxidase-like domain (AOL), an N-terminal SWIRM domain and a central protruding tower domain (Figure 1.6). The C-terminal AOL is made up of 2 subdomains: an FAD-binding domain and a substrate-binding domain. These subdomains build the catalytic centre of the enzyme at their interface (Spannhoff *et al.*, 2009), close to which a wide binding domain, acting as a second interaction site, can be found. The SWIRM domain is essential for enzyme stability and the tower domain regulates the enzyme's activity allosterically when interacting with other proteins (Spannhoff *et al.*, 2009).

LSD1 is not a free-functioning enzyme *in vivo*. It is a component of the transcriptional co-repressor complex containing the REST complex (CoREST) and HDAC1/2 (Figure. 1.6). The LSD1-CoREST complex demethylates mono- and dimethylated lysines in nucleosomes (Hou and Yu, 2010). Following a stepwise manner, HDAC1/2 deacetylates the histone to create a hypoacetylated histone tail for CoREST binding. BHC80 (PHD-domain-containing protein) binds to the demethylated histone lysine to prevent the restoration of methylation (Figure 1.7).

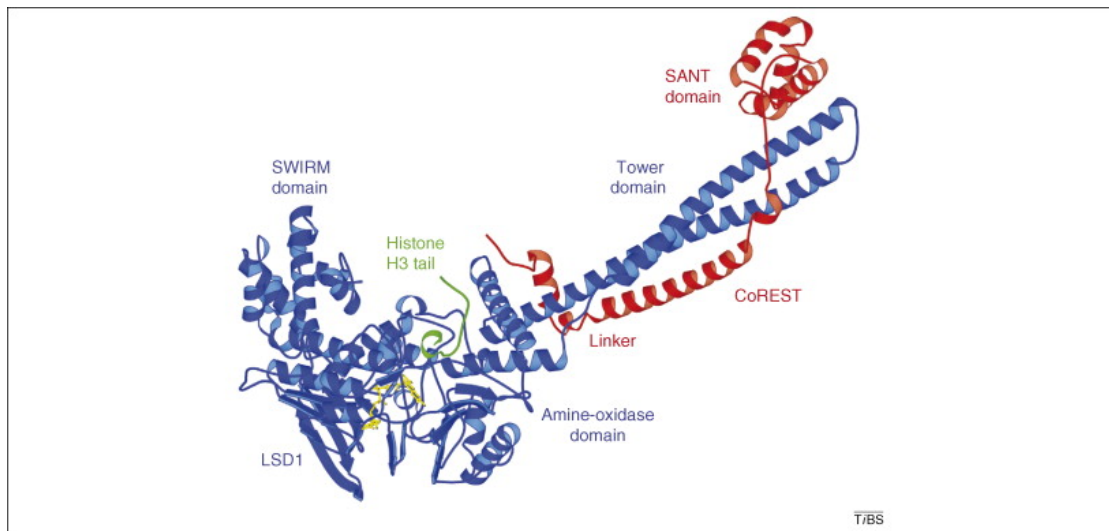


**Figure 1.6: Human LSD1 in complex with CoREST and a peptide substrate.** LSD (blue), consisting of a SWIRM domain, amine-oxidase domain and a tower domain. The tower domain allows for the association of LSD1 to the SANT domain of the CoREST complex (red). The histone tail, consisting of 16 residues (green), binds the amine oxidase domain (Forneris *et al.*, 2008).

The CoREST complex protects LSD1 from proteosomal degradation as well as aiding in targeting LSD1 to the histone (Spannhoff *et al.*, 2009).

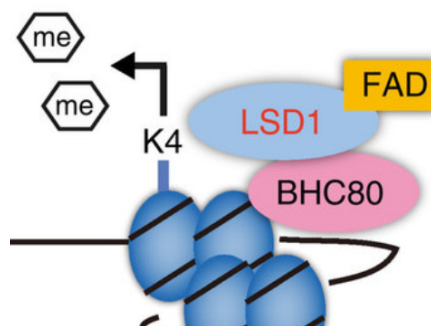


**Figure 1.7: LSD1 enzyme complex.** Following a stepwise manner, HDAC1/2 deacetylated the histone, creating a hypoacetylated tail for CoREST binding. FAD is reduced during the demethylation reaction, followed by BHC80 binding to the histone tail, preventing methylation restoration (Spannhoff *et al.*, 2009).

LSD1 demethylation reactions commence with the reduction of FAD to FADH<sub>2</sub>, which is then re-oxidized to hydrogen peroxide (H<sub>2</sub>O<sub>2</sub>) resulting in the formation of an imine intermediate. The intermediate is hydrolyzed in a non-enzymatic manner to carbinolamine, which spontaneously degrades resulting in a demethylated compound and formaldehyde (Figure. 1.8).

LSD1 removes methyl groups from mono- and dimethylated lysines in peptides or bulk histones but not in nucleosomes and it does not demethylate trimethylated lysines. A lone pair of electrons must be present on the unprotonated nitrogen of the methylated lysine to form the imine intermediate (Spannhoff *et al.*, 2009). Therefore, LSD1 is unable to demethylate trimethylated lysine residues but it is still able to recognise and bind to trimethylated lysines (Hou and Yu, 2010). The demethylation activity of LSD1 is hampered by the steric and electrostatic perturbations caused by the presence of epigenetic markers on H3. Therefore, HDAC enzymes must operate before LSD1 demethylation can commence (Forneris *et al.*, 2008).

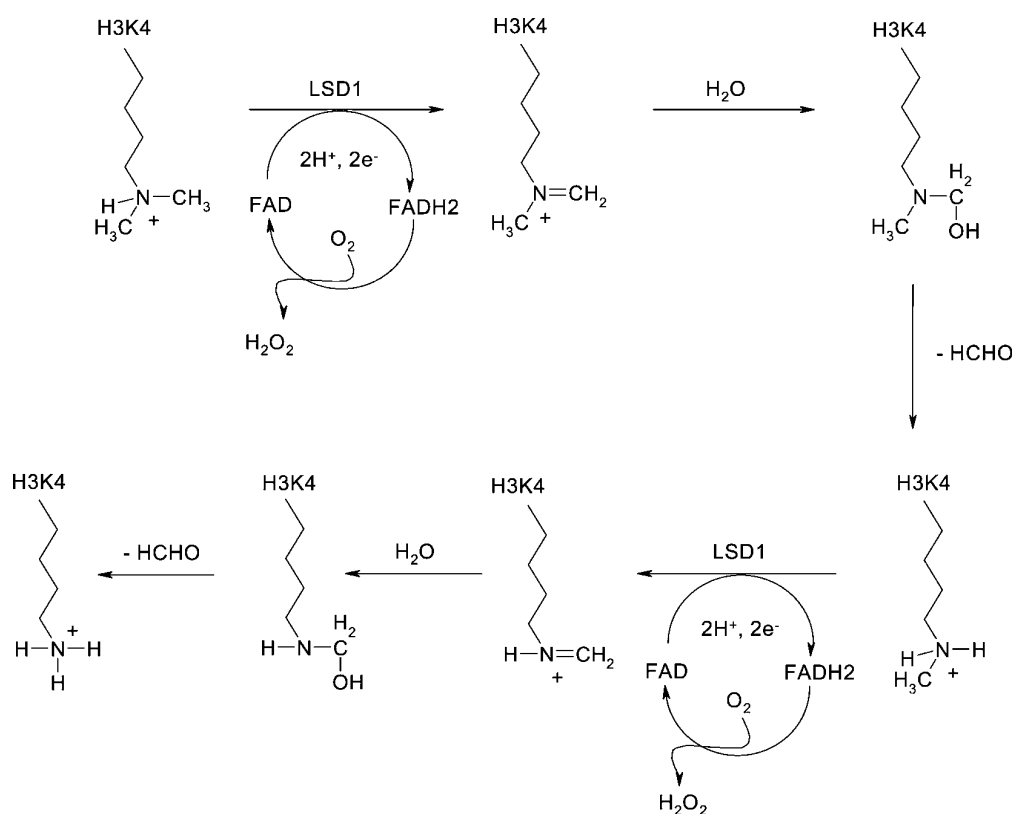


**Figure 1.8: The mode of catalysis of lysine-specific demethylase 1 (LSD1).** The reaction commences with the reduction of FAD to FADH<sub>2</sub> that is then re-oxidized to hydrogen peroxide (H<sub>2</sub>O<sub>2</sub>) resulting in the formation of an imine intermediate. The intermediate is hydrolysed in a non-enzymatic manner to carbinolamine, which spontaneously degrades resulting in a demethylated compound and formaldehyde (Spannhoff *et al.*, 2009).

There is a range of interesting interactions with other PTMs such as the acetylation of H3K9, which positively affects the catalytic activity of LSD1

whereas the phosphorylation of H3S10 negatively affects the catalytic activity of LSD1 (Spannhoff *et al.*, 2009).

The amino acid sequence of LSD1 has similarity to monoamine oxidases (MAOs) and polyamine oxidases (PAOs). MAOs bind to the mitochondrial membrane and play an important role in neurotransmitter metabolism. PAOs can be found in peroxisomes, where it degrades spermine, spermidine and other derivatives (Forneris *et al.*, 2008). Due to the structural and mechanistic similarities between LSD1 and amine oxidases, MAO inhibitors such as pargyline and tranylcypromine are able to inhibit LSD1 activity (Figure 1.9). They do however bind with low selectivity and potency (Woster and Casero, 2011).

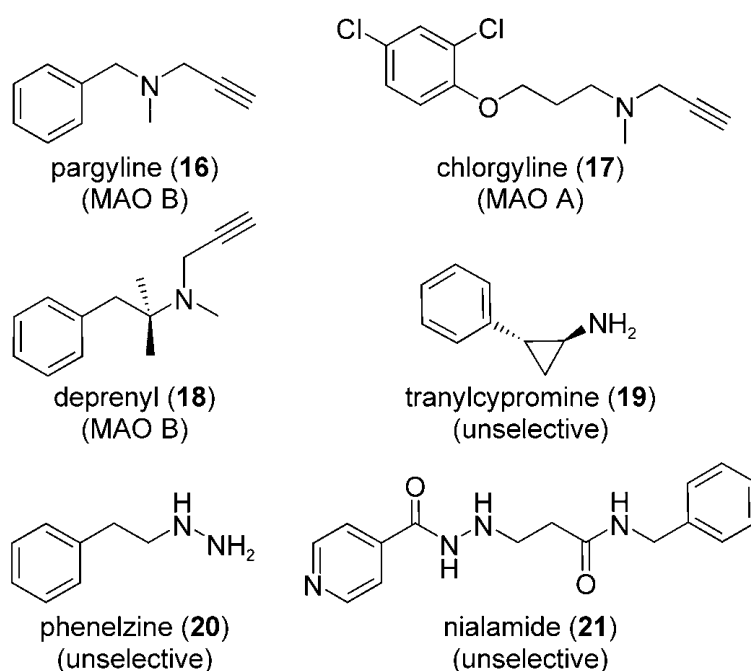


**Figure 1.9: Various monoamine oxidase inhibitors showing activity against LSD1.** Compounds 16, 17 and 18 show specificity towards MAO A whereas compounds 18, 20 and 21 are not selective towards a specific MAO (Spannhoff *et al.*, 2009). Tranylcypromine is an irreversible LSD1 inhibitor.

Tranylcypromine is an irreversible LSD1 inhibitor and its mode of action involves the formation of a covalent tranylcypromine-FAD cofactor intermediate. It has an  $IC_{50}$  value of 21  $\mu$ M against the human recombinant LSD1 enzyme and does not interact strongly with the LSD1 active site. Substitutions of the phenyl ring of tranylcypromine increased the selectivity



and potency of this molecule for LSD1 (Spannhoff *et al.*, 2009). Phenelzine (Figure 1.9) exhibited high potency as an inhibitor of LSD1. The inhibitory potential of pargyline was associated with the LSD1-AR complex, which could be the result of a conformational change in the active site of the enzyme. Pargyline compounds were modified to propylamine-derived H3 peptides, which are potent and highly selective (Woster and Casero, 2011).

Recent reports show that bisguanidine and biguanidine polyamine analogues result in the re-expression of silenced genes suppressing colon cancer development due to LSD1 inhibition (Huang *et al.*, 2007). As polyamine analogues represent a novel chemotype involved in epigenetic regulatory enzymes, they are discussed in more detail below.

### **1.7. Polyamines and polyamine analogues**

The natural polyamines shown in Figure 1.10 (putrescine, spermidine and spermine) are aliphatic, poly-cationic nitrogenous bases consisting of methylene moieties. They are present in significant amounts in all prokaryotic and eukaryotic cell types and have the ability to stabilise acidic cellular constituents such as phospholipids, DNA and RNA (Clark *et al.*, 2010). The interactions of polyamines and nucleic acids extend to DNA-protein binding and are especially important concerning gene-regulatory proteins such as histones and transcription factors (Woster and Casero, 2011). DNA is a major target of natural polyamines. Therefore, polyamine-nucleic acid interactions effect DNA conformational stabilisation, transitions and gene-regulatory protein binding (Wang *et al.*, 2003).

Polyamine analogues are based on the natural polyamine backbone, to which specific chemical groups (alkylating agents, anti-proliferative agents and DNA intercalators among others) have been conjugated. As polyamines are positively charged in physiological environments, they have a high affinity for DNA, which is hypothesized to be important in chromatin remodelling. Due to the similarities in structure, polyamine analogues might also alter chromatin structure, histone-modifying enzymes, apoptosis, cell cycle regulation and

specific gene expression. Polyamine analogues remain cationic in nature and typically possess a high affinity for the energy-dependent polyamine transport system. They are therefore accumulated by cells and target negatively charged chromatin (Holley *et al.*, 1992, Feuerstein *et al.*, 1988, Wallace and Niiranen, 2007).

Generally, polyamine analogues could act as polyamine mimics, polyamine antimetabolites, or inhibitors of the polyamine transport mechanism(s); however, their function may also be completely independent of the polyamine pathway i.e. regulating epigenetic mechanisms.

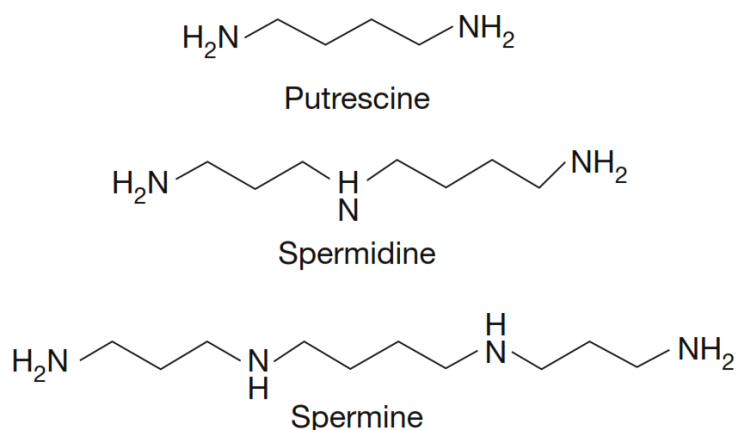


**Figure 1.10: Three natural polyamines.** Found in prokaryotic and eukaryotic cells, polyamines are aliphatic, poly-cationic nitrogenous bases consisting of methylene moieties.

The similarity in structures between polyamine oxidases and MOA inhibitors prompted the testing of polyamine analogues as epigenetic regulators and more specifically as inhibitors of LSD1. Huang and colleagues tested a small library of bisguanidine and biguanidine analogues against purified, recombinant LSD1. Nine compounds exhibited >50% inhibition against LSD1 activity at concentrations less than 1  $\mu\text{M}$ . Verlindamycin (Figure 1.11) exhibited non-competitive inhibition kinetics at concentrations less than 2.5  $\mu\text{M}$ . This analogue does not seem to be competing directly with H3K4me2 at the active site of LSD1 and it is possible that it is blocking the FAD binding site. This might induce fundamental structural changes to LSD1, affecting its substrate binding affinity (Huang *et al.*, 2007). In human colon carcinoma cells, this results in epigenetic changes on H3K4me2, evident then as

changes in gene expression due to re-expression of inappropriately silenced genes. A better understanding of the action of the polyamine analogues on LDS1 will aid in novel approaches for the treatment of cancer and cellular pathologies (Huang *et al.*, 2007).

From the bisguanidine and biguanidine analogue study stemmed a subsequent library of (bis)urea and (bis)thiourea compounds, which were studied by Sharma and colleagues. Results indicated that these compounds induced increased methylation of H3K4 in Calu-6 lung carcinoma cells (Sharma *et al.*, 2010). This same series has subsequently been screened for antimalarial activity against chloroquine-sensitive and -resistant strains of *P. falciparum* parasites, based on the verlindamycin backbone (Verlinden *et al.*, 2011) (Figure 1.11).

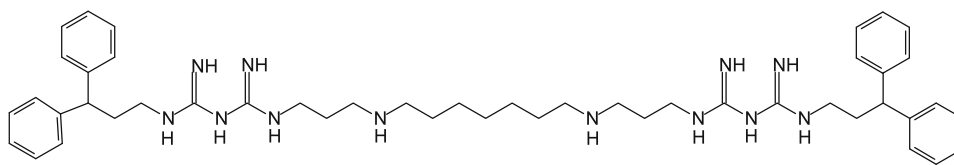


**Figure 1.11: Verlindamycin.** A polyamine analogue (1,15-bis{N5-[3,3-(diphenyl)propyl]-N1-guanido}-4,12-diazapentadecane) showing LSD1 inhibitory activity in colon and breast cancer cells (Zhu *et al.*, 2012, Huang *et al.*, 2007).

The (bis)urea and (bis)thiourea polyamine analogues showed growth inhibitory activity against *P. falciparum* parasites at less than 3  $\mu\text{M}$  concentrations with  $\text{IC}_{50}$  values in the 100-650 nM range (Verlinden *et al.*, 2011). The leading compound (compound 30; Figure 1.12) had a low nanomolar  $\text{IC}_{50}$  (88 nM), was >7000-fold more selective towards the parasites and arrested asexual parasite development within 24 hours of exposure (Verlinden *et al.*, 2011).

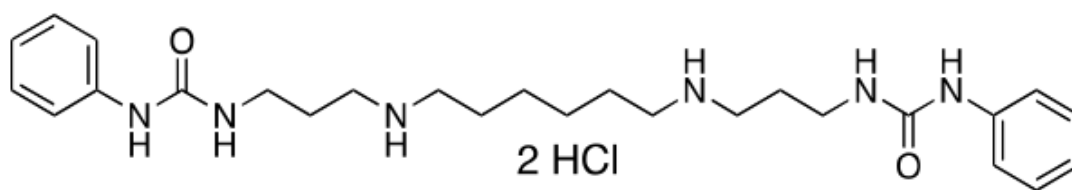


**Figure 1.12: Compound 30.** A (bis)urea polyamine analogue (RJB-92-04: 1,1'-((hexane-1,6-diylbis(azanediyl))bis(propane-3,1-diyl)) showing *P. falciparum* antimalarial activity at a low nanomolar concentration.

However, although compound 30 seemed highly promising *in vitro* as a novel antimalarial agent, subsequent *in vivo* analysis of its ability to cure *P. berghei* infected murine malaria indicated that compound 30 was not curative in this murine malaria model. Dissection of the compound's *ex vivo* pharmacokinetics and pharmacodynamics revealed that the compound was not metabolically stable as evaluated in a microsomal stability assay (Verlinden *et al.* Unpublished Results). These results imply that compound 30 would need to be modified to result in a metabolically stable derivative whilst retaining its biological activity against *P. falciparum* parasites.

Medicinal chemistry principles dictate that fluorination of a parent compound can increase its' metabolic stability and lipid solubility, thereby enhancing the rate of absorption and transport of the fluorinated compound across the blood-brain barrier (Filler R, 2009). As such, a series of compound 30 derivatives was synthesised, which incorporated fluorination on the terminal aromatic rings of the parent compound. The objective of this study was to investigate the antiparasmodial potential of a new series of compound 30-fluorinated derivatives. Additionally, the ability of the (bis)urea polyamine analogues to inhibit parasite LSD1 was investigated as a potential epigenetic target of these inhibitors.

## **1.8. Null hypothesis of research objective**

Fluorinated (bis)urea polyamine analogues will not have improved antiparasmodial activity and will not specifically target lysine specific demethylase 1 in *P. falciparum* parasites.

## **1.9. Aims**

- Determine the antiplasmodial activity and selectivity of a series of fluorinated polyamine analogues.
- Determine the activity changes in recombinant human LSD1 untreated and treated with fluorinated polyamine analogues.
- Compare methods required to determine the global epigenetic changes in histone methylation in *P. falciparum* parasites.

### **The following manuscript resulted from this study:**

Novel Symmetrical, Terminally Alkylated Oligoamine Isosteres with Potent Antimalarial Activity Against Intraerythrocytic *Plasmodium falciparum* Parasites

*Bianca K. Verlinden, Marna de Beer, Boobalan Pachaiyappan, Bernice Barnard, Warren A. Andayi, Janette Reader, Jandeli Niemand, Abraham I Louw, Colin Dubick, Ethan Marrow, Youxuan Li, Gloria Holbrook, Fangyi Zhu, Lubbe Wiesner, Timothy Egan, Kiplin Guy, Patrick M. Woster and Lyn-Marie Birkholtz*

Submitted: Journal of Medicinal Chemistry.

### **Research findings were also presented at the following international conferences:**

1. Bernice Barnard, Bianca Verlinden, Patrick Woster, Braam Louw and Lyn-Marie Birkholtz. Polyamine analogues, targeting epigenetic regulatory mechanisms, has anti-proliferative activity against *Plasmodium falciparum*. Malaria Gordon Research Conference: Molecular and Cellular Biology of Malaria. Tuscany, Italy. August 2013. Presented as a poster presentation.
2. Bernice Barnard, Bianca Verlinden, Patrick Woster, Braam Louw and Lyn-Marie Birkholtz. Polyamine analogues, targeting epigenetic regulatory mechanisms, have anti-proliferative activity against *Plasmodium falciparum*. 6<sup>th</sup> MIM PAN-African Conference. Durban, South-Africa. October 2013. Presented as a poster presentation.

## **Chapter 2**

---

### **Materials and Methods**

## 2.1. *In silico* compound pharmacokinetics

The Discovery Studio Modeling Environment (Accelrys Software Inc., release 3.0) was used to determine the ADME descriptors and Lipinski's rule of 5 for all polyamine analogues. These physiochemical descriptors incorporate *in silico* models for intestinal absorption, aqueous solubility, blood brain barrier penetration, plasma protein binding, cytochrome P450 2D6 inhibition, and hepatotoxicity. Lipinski's 5 rules state that a compound is more likely to exhibit poor absorption and permeation when two parameters are out of range. The parameters of a compound should not have a molecular weight more than 500 g/mol, not have more than 5 Hydrogen Bond Donors (HBD) or 10 Hydrogen Bond Acceptors (HBA) and a LogP value (the logarithm of the octanol/water partition coefficient) less than 5.

The Quantitative Estimate of Drug-likeness (QED) was determined *in silico* using Silicos-it QED (Chemoinformatics Services and Software; Biscu-it). QED values range from zero (all properties unfavourable) to one (all properties favourable). The QED method is better at differentiating between drug and non-drug compounds than Lipinski's rules because it is not based on cut-off values of four rules only.

## 2.2. *In vitro* cultivation of *P. falciparum*

*P. falciparum* strain 3D7 (sulfadoxine resistant, CQ sensitive), strain W2 (CQ resistant) and strain HB3 (pyrimethamine resistant, CQ sensitive) (Llinas *et al.*, 2006) were cultivated in 30 ml RPMI 1640 medium supplemented with 200  $\mu$ M hypoxanthine (Sigma-Aldrich), 25 mM HEPES (Sigma-Aldrich), 24  $\mu$ g/ml gentamycin (Invitrogen), 20 mM D-Glucose (Sigma-Aldrich), 0.5% Albumax II (Invitrogen) and O<sup>+</sup> human erythrocytes. HEPES is a zwitterionic buffering agent that is used when a cell culture requires extended periods of manipulation outside a CO<sub>2</sub> incubator and buffers the incomplete medium between pH 7.2-7.6. Gentamycin, which is an aminoglycoside antibiotic is added to the medium to inhibit growth of bacterial contaminants. Albumax II is a lipid-rich supplemented bovine albumin based human serum replacement (Trager and Jensen, 1997). Thin Giemsa stained blood smears were

developed to determine the parasitaemia and parasite life cycle stage (Trager and Jensen, 1997). Giemsa is a combination of methylene blue, eosin and azure B and it is specific towards the phosphate groups of DNA (Shapiro *et al.*, 2013). A thin blood smear is made and fixed in 100% methanol for 5 s. The slide is placed in a 5% (v/v) Giemsa solution prepared in distilled water for 5 min, rinsed and viewed under a light microscope. The parasitaemia is defined as the percentage of infected erythrocytes, calculated counting a minimum of 1000 erythrocytes (Allen and Kirk, 2010).

The synchronisation process is based on the changes in membrane permeability of parasitised erythrocytes and the selective destruction of the later stages of parasites due to the activation of new permeation pathways (Lambros and Vanderberg, 1979). To pellet the cells, cultures were centrifuged at 3500g for 5 min and the supernatant discarded. Cultures were synchronised with 10 ml of a 5% (w/v) pre-heated D-sorbitol solution made in 1×PBS (Lambros and Vanderberg, 1979) for 15 min at 37°C, to obtain ring stage parasites at >95% synchronicity. After synchronisation, the cells were centrifuged at 3500g for 5 min and the sorbitol discarded. To the pelleted cells, 10 ml incomplete culture medium was added and mixed well, in order to remove any excess sorbitol. Cells were centrifuged at 3000g for 3 min and the excess culture medium discarded. Using *in vitro* sterile techniques during cultivation, parasitaemia levels were maintained between 1-8% in 5% haematocrit by diluting the culture after synchronisation with the addition of fresh erythrocytes in 30 ml complete culture medium. The cultures were placed in 75 cm<sup>3</sup> culture flasks containing a special gas mixture (5% O<sub>2</sub>, 5% CO<sub>2</sub> and 90% N<sub>2</sub>) to optimise parasite proliferation. Culture flasks were incubated in a shaking incubator (Allen and Kirk, 2010) at 37°C.

### **2.3. *In vitro* assessment of antiplasmodial activity**

The leading compound from a previous series was an alkylated (bis)urea 3-6-3 carbon backbone polyamine analogue (Figure 1.12) with high selectivity and a nanomolar growth inhibitory concentration in *P. falciparum* strain 3D7 (Verlinden *et al.*, 2011). However, it was not metabolically stable (Verlinden *et*



*al.*, Unpublished Results) and changes to its' structure included the fluorinated series of compounds tested in this thesis. The antiplasmodial activity of the four fluorinated (bis)urea polyamine analogues were determined by using the Malaria SYBR Green I fluorescence based (MSF) assay to define dose response curves and the associated IC<sub>50</sub> concentration (concentration of compound resulting in 50% inhibition of parasite proliferation) using the three above-mentioned strains of *P. falciparum* parasites. SYBR Green I is a DNA intercalating dye, which prefers G and C base pairs. It is highly fluorescent when intercalated with DNA showing a maximum blue absorbance wavelength at 497 nm with minor peaks at 290 nm and 380 nm and a green emission wavelength at 520 nm. However, it fluoresces poorly if it has not been intercalated with DNA (Bennett *et al.*, 2004). The intercalation of DNA and SYBR Green I allows for the DNA content to be directly correlated to parasite growth, permitting the calculation of an IC<sub>50</sub> value.

The MSF assay was set up using sterile culturing techniques. Ring stage *P. falciparum* strain 3D7 parasite suspension (2% haematocrit, 1% parasitaemia) was treated with the fluorinated compounds and 0.5 µM starting concentration of CQ (positive drug control). The fluorinated polyamine analogues were 2-fold serially diluted to 187.5 pM with a starting concentration of 100 µM. The 96-well plates were incubated at 5% O<sub>2</sub>, 5% CO<sub>2</sub> and 90% N<sub>2</sub> within a stationary incubator at 37°C for 96 h. After incubation, lysis buffer (20 mM Tris, pH 7.5; 5 mM EDTA; 0.015% (w/v) saponin; 0.08% (v/v) Triton X-100) was prepared with the addition of SYBR-Green (0.2 µl/ml lysis buffer; Molecular Probes, Inc) and added to the 96-well plates. The plates were stored in the dark at RT for an hour and the fluorescence readings were recorded using a Fluoroskan Ascent FL microplate fluorometer (Thermo Scientific, excitation at 488 nm and emission at 522 nm).

#### **2.4. *In vitro* culturing of human hepatocellular liver carcinoma cells**

Human hepatocellular liver carcinoma cells (HepG2, kind gift from Duncan Cromarty, University of Pretoria) were maintained in Dulbecco's Modified

Eagle's Medium (DMEM), supplemented with 10% heat inactivated foetal bovine serum and 1% penicillin/streptomycin in a stationary incubator at 37°C (5% CO<sub>2</sub>, 90% humidity). Once flasks reached 70-80% confluence, cells were trypsinised as explained below, to obtain single cell layers once cells have been dislodged. The spent medium was aspirated and the monolayer washed three times with 1×PBS. To each flask, trypsin-EDTA was added and incubated in a stationary incubator at 37°C for 7 min. The EDTA helps to dislodge the cells by chelating calcium. Afterwards, DMEM media was added to deactivate the trypsin and cells were centrifuged at 1000 rpm for 2 min. Cells were counted using a haemocytometer and a 0.2% trypan blue solution. To new culture flasks, 200 000 cells were seeded and fresh DMEM media added, after which flasks were placed in a stationary incubator at 37°C.

## **2.5. Lactate dehydrogenase cytotoxicity determinations in mammalian cells**

The Lactate Dehydrogenase Cytotoxicity assay is a fast and simple assay based on the quantification of activity of the enzyme lactate dehydrogenase (LDH). LDH is a stable cytoplasmic enzyme released into the culture medium when the plasma membrane is damaged. During this assay, LDH oxidizes lactate to pyruvate, which reacts with tetrazolium salt to form formazan. The amount of formazan released is directly correlated to the number of lysed cells and can be detected spectrophotometrically at 500 nm (BioVision) (Fotakis and Timbrell, 2006).

HepG2 cells ( $\pm 200\ 000$ ) were seeded in a 96-well plate and allowed to proliferate for 24 h at 37°C. To the cells various concentrations ( $8000 \times IC_{50}$  and  $5000 \times IC_{50}$ ) of each of the four fluorinated polyamine analogues were added and maintained at 37°C for 48 h. After 48 h exposure, 10  $\mu$ l of lysis buffer was added to each well and incubated at RT for 15 min. The cells were pelleted at  $600 \times g$  for 10 min to precipitate the cells. The clear supernatant (10  $\mu$ l) of each well was transferred to a plate containing LDH reaction mix (100  $\mu$ l) and incubated in the dark at RT for 20 min. Colorimetric detection of NADH levels was measured at 450 nm every 10 min (BioVision). Experiments were

performed in triplicate for at least two independent biological repeats. The percentage cytotoxicity ( $GI_{50}$ ) was calculated from the raw data as presented in the results.

## 2.6. Recovery of parasite proliferation

The SYBR Green I Fluorescence dye was used to correlate the changes in treated parasite DNA levels, as explained below. The data were used to determine the changes in DNA concentration resulting from compound treatment. Highly synchronised ring cultures (2% parasitaemia; 5% haematocrit) were treated for 12 hours, with each of the two of the four polyamine analogues at their respective  $IC_{90}$  values. After the treatment, parasites were washed once with RPMI 1640 culture medium. A 1:40 dilution was made of the washed parasites and then further incubated for 2 days at 37°C to assess proliferation at specific time points.

## 2.7. Detergent Initiated $\beta$ -Haematin Crystallisation assay

The ability of the polyamine analogues to inhibit  $\beta$ -haematin formation was tested using the Detergent Initiated  $\beta$ -haematin Crystallisation Assay. During the digestion of haemoglobin, the parasite clears toxic haem from the system through sequestering haem aggregates into haemozoin. Native haemozoin is crystallographically identical to its synthetic analogue  $\beta$ -haematin. The process of haemozoin formation is thought to be a lipid-mediated process. This assay uses detergents, which effectively mimic the needed neutral lipid environment, allowing haem localisation for dimer formation (Carter *et al.*, 2010).

Compound 30, fluorinated compounds (compound 3 and compound 4) and CQ were made to 20 mM stock solutions in DMSO. In a 96-well plate, the compounds were added at a starting concentration of 1 mM and 2-fold serially diluted in an NP40/DMSO buffer (70% water; 20% NP40 and 10% DMSO (v/v)). Haemin (25 mM; Fluka) was made up in DMSO and sonicated for 1 min. To a 1 M acetate buffer (4.1 g sodium acetate and 2.4 ml acetic acid in

water, pH 4.75 – 4.9), haemin (222.2  $\mu\text{M}$ ) was added, vortexed and immediately plated into the 96-well plate. It is important for the haem to be uniformly suspended throughout the 96-well plate as it precipitates quickly. Plates were incubated for  $\pm 5$  h at  $37^\circ\text{C}$ , after which a pyridine solution (20% water, 20% acetone, 10% 2 M HEPES and 50% pyridine (v/v)) and acetate was added. The absorbance was recorded at 405 nm and sigmoidal graphs plotted using GraphPad Prism.

## **2.8. Lysine-Specific Demethylase 1 Chemiluminescence assay optimisation**

In order to determine if this series of polyamine analogues specifically target LSD1, a chemiluminescence assay was adapted from cancer cell research protocol (Huang *et al.*, 2007). Chemiluminescence is the emission of electromagnetic radiation in the energy range of visible light as a result of a chemical reaction. The assay adapted in this dissertation, is based on the oxidation of luminol by horseradish peroxidase (HRP) in the presence of hydrogen peroxide ( $\text{H}_2\text{O}_2$ ) as substrate, to form aminophthalic acid and nitrogen. The luminescence can be recorded using a luminometer at 430 nm (Deshpande, 2001). For these experiments, the demethylation reaction of H3K4me2 to H3K4me1 conducted by the parasites, resulted in the production of  $\text{H}_2\text{O}_2$ , which was used as the indicator to measure the activity of lysine-specific demethylase via the oxidation of luminol. Experiments performed in Section 2.8.1 to Section 2.8.4 are based on the above experimental design.

### **2.8.1. Kinetic study of luminol activity**

In the presence of  $\text{H}_2\text{O}_2$ , the chemiluminescent reaction occurs quickly and could easily be missed. This experiment was set up to determine the rate of decomposition of the chemiluminescent reaction once the  $\text{H}_2\text{O}_2$  has been added to the reaction well. To a single well in a white 96 well luminescent plate, ddd $\text{H}_2\text{O}$  was combined with 6  $\mu\text{g}/100 \mu\text{l}$  HRP (0.4 mg/ml stock solution; Sigma-Aldrich) and 15  $\mu\text{M}$  luminol (100 mM stock solution; Sigma-Aldrich). Prior to reading, 500 nM  $\text{H}_2\text{O}_2$  (1 mM  $\text{H}_2\text{O}_2$  stock solution; Merck) was added

to a final volume of 200  $\mu$ l per well and the luminescence was continuously recorded for 2 min using a Bio-Tek Instrument (FLx800) at 425 nm and Gen5 Software.

### **2.8.2. Reagent effects on chemiluminescence**

The use of three reagents in the cancer assay (Huang *et al.*, 2007) was confirmed by means of testing the effect of each reagent separately and all three in combination. Tris-HCl is a buffering agent and KCl and  $MgCl_2$  are cofactors, which enhance the chemiluminescent reaction (Blanchard, 1990). A final volume of 200  $\mu$ l per well in a white luminescence 96-well plate was set up per experiment. In each well dddH<sub>2</sub>O was combined with 6  $\mu$ g/100  $\mu$ l HRP (0.4 mg/ml stock solution; Sigma-Aldrich) and 15  $\mu$ M luminol (100 mM stock; Sigma-Aldrich). The HRP uses the H<sub>2</sub>O<sub>2</sub> as a substrate to oxidise luminol. To a single well, 50 mM Tris-HCl (1 M stock) was added. To a single well, 50 mM KCl (1 M stock) was added. To a single well 5 mM  $MgCl_2$  (1 M stock) was added. To a single well 50 mM Tris-HCl (1 M stock), 50 mM KCl and 5 mM  $MgCl_2$  (1 M stock) was added. Seconds before placing the 96-well plate in the luminometer, 500 nM H<sub>2</sub>O<sub>2</sub> (1 mM H<sub>2</sub>O<sub>2</sub> stock solution; Merck), was added to each well and the chemiluminescence was recorded using a Bio-Tek Instrument (FLx800) at 425 nm and Gen5 Software.

### **2.8.3. LSD1 enzymatic activity**

Due to the large size of the *Plasmodium* LSD1 gene and the unavailability of the recombinant parasite enzyme, the activity of the recombinant human LSD1 enzyme (1.2 mg/ml) was measured using the luminol dependent chemiluminescence assay. This assay served as a positive assay control, confirming the inhibition of LSD1. In a white luminescence 96-well plate, a buffer mix (6  $\mu$ g/100  $\mu$ l HRP, 50 mM Tris-HCl, 50 mM KCl, 5 mM  $MgCl_2$ , 15  $\mu$ M luminol and 5  $\mu$ M H3K4me2) and recombinant enzyme of 3  $\mu$ g was added. Tranylcypromine, compound 30 and compound 3 (leading fluorinated compound) were added at 1 mM and 10 mM concentrations. Each well was placed at 37°C for 2 min and the luminescence was recorded at 425 nm (Bio-Tek Instrument – FLx800) directly after the incubation step.

#### 2.8.4. LSD1 activity of isolated parasites

The activity of *P. falciparum* LSD1 enzyme was measured with the luminol dependent chemiluminescence assay, using parasites isolated from the erythrocytes. *P. falciparum* strain 3D7 trophozoite cultures (6-8% parasitaemia, 5% haematocrit) were treated with Tranylcypromine, Compound 30 and Compound 3 at various concentrations ( $1 \times IC_{50}$ ,  $5 \times IC_{50}$  and  $10 \times IC_{50}$ ). To each treated culture, 10 ml of a 0.15% (w/v) saponin solution made in  $1 \times$ PBS was added and incubated on ice for 15 min. The culture was centrifuged at 3500g for 5 min and the supernatant discarded. The above step was performed again, without an incubation step on ice. The isolated pellets were re-suspended in 1 ml of  $1 \times$ PBS and kept on ice till used. In a white 96-well plate, a reagent mix (6  $\mu$ g/100  $\mu$ l HRP, 50 mM Tris-HCl, 50 mM KCl, 5 mM  $MgCl_2$ , 15  $\mu$ M luminol and 5  $\mu$ M H3K4me2) was added. Tranylcypromine, Compound 30 and Compound 3 (leading fluorinated compound) treated, isolated parasites were added (85  $\mu$ l) to the 96-well plate one at a time. Each well was placed at 37°C for 2 min once isolated parasites were added and the luminescence was recorded (Bio-Tek Instrument – FLx800) directly after the incubation step.

#### 2.9. Comparison of histone isolation protocols

Histones were isolated and used for mass spectrometry to determine if the fluorinated polyamine analogues caused notable epigenetic changes. Three histone isolation protocols (Issar *et al.*, 2009; Trelle *et al.*, 2009 and Merrick *et al.*, 2008) were compared in terms of isolated histone concentrations. Many of the buffers contain useful reagents such as EDTA and EGTA, which are both metal chelators responsible for sequestering metals into solution where they have lowered activity and as such, prevent metals from reacting with proteins. EGTA has a lower affinity towards  $Mg^{2+}$  compared to EDTA and therefore, prefers chelating  $Ca^{2+}$  (Blanchard *et al.*, 1990). Salts, such as NaCl, are added to selectively release the histones from chromatin (Yager *et al.*, 1989). The Issar *et al.* (2009) protocol uses Nonidet-P40, a non-ionic surfactant, for the isolation of membrane complexes and to prevent the adsorption to surfaces. Merrick *et al.* (2008) uses the reducing reagent DTT, which could

counteract oxidative effects. Acid extraction partially neutralises the DNA phosphates, diminishing ionic interactions. The remaining lyophilisates are freely soluble in low ionic strength solutions. All three protocols use trichloroacetic acid (TCA) to precipitate proteins, after which acetone is used to remove any remaining TCA or acid (Sivaraman *et al.*, 1997). To increase storage effectiveness, glycerol and sugar are added to certain buffers (Jiang and Nail, 1998).

### **2.9.1. Issar *et al.* (2008) Protocol**

The centrifugal steps followed in the histone isolation protocol were performed at 4°C in a Thermo Scientific SL 16R centrifuge (Thermo Fisher Scientific). *P. falciparum* synchronised trophozoite cultures of 6-8% parasitaemia and 5% haematocrit were centrifuged at 3500g for 5 min. The supernatant was aspirated and the cultures were treated twice with 0.15% (w/v) saponin lysis buffer in 1×PBS, mixed gently and placed on ice for 10 min. After the incubation on ice, 1×PBS (137 mM NaCl, 2.7 mM KCl, 10 mM KH<sub>2</sub>PO<sub>4</sub>, 10 mM Na<sub>2</sub>HPO<sub>4</sub>) was added to the samples and they were centrifuged at 3500g for 5 min. Samples were washed with 1×PBS multiple times, until the supernatant appeared clear of visible haemoglobin. Up to this point, all three histone isolation protocols followed the same isolation process and wash steps.

The resulting pellet was washed 2-3 times with haemoglobin removal buffer (25 mM Tris-HCl, pH 7.8, 1 mM EDTA, 0.2% v/v Nonidet P40) and centrifuged at 12000g for 1 min until the supernatant appeared clear. The pellets were re-suspended in 4°C dddH<sub>2</sub>O and centrifuged at 7500g for 2 min. A 0.8 M NaCl solution was added to the samples and after mixing, samples were centrifuged at 7500g for 2 min. The pellets were acid extracted with the addition of 0.25 M HCl. Following grinding with an eppie grinder, samples were incubated at 4°C for 2 h.

The acid insoluble proteins were recovered by centrifugation at 4°C and 12 000g for 30 min. To the supernatant, an equal volume of 20% (w/v) TCA was

added, mixed gently and incubated on ice for 15 min. After a 30 min, 12000g centrifugation step, the supernatant was discarded. The pellet was gently washed with 500  $\mu$ l acetone and centrifuged at 12000g for 15 min. The supernatant was aspirated and the acetone was allowed to evaporate. The pellet containing histones was re-suspended in SDS-PAGE sample buffer (See section 2.11.) and stored at  $-20^{\circ}\text{C}$  (Issar *et al.*, 2009, Lopez-Rubio *et al.*, 2007). The protein concentration was calculated using the BCA quantification assay (See section 2.10) and protein pellets were dissolved in SDS-PAGE reducing buffer before analysis on SDS polyacrylamide gels as described in section 2.11.

### **2.9.2. Merrick *et al.* (2010) Protocol**

The centrifugal steps followed in the histone isolation protocol were performed at  $4^{\circ}\text{C}$  in a Thermo Scientific SL 16R centrifuge (Thermo Fisher Scientific). *P. falciparum* synchronised parasites of 6-8% parasitaemia and 5% haematocrit were centrifuged at 3500g for 5 min. Samples were saponin lysed (0.15%) and washed with 1 $\times$ PBS until the supernatant appeared clear of visible haemoglobin as described in section 2.9.1. The samples were centrifuged at 6000g for 2 min. To the resulting pellet, NP-40 lysis buffer (20 mM HEPES, pH 7.8, 10 mM KCl, 1 mM EDTA, 1 mM EGTA, 1 mM DTT, 1 $\times$ Protease inhibitor cocktail (PI, Roche), 0.65% v/v NP-40) was added, mixed well and incubated on ice for 5 min. Following centrifugation at 2500g for 5 min at  $4^{\circ}\text{C}$  the supernatant, containing cytoplasmic proteins, was aspirated. The pellet containing nuclear proteins was washed another three times with the NP-40 lysis buffer, without the incubation step, until the supernatant appeared clear and free of cytoplasmic protein contaminants (Voss *et al.*, 2002).

The remaining insoluble material, containing histones and DNA, was treated twice with 0.5 M ice-cold HCl (vortex and grind sample) and incubated at  $4^{\circ}\text{C}$  for 1 h. The sample was centrifuged at 12 000g for 30 min and the supernatant discarded. The pellet was treated with 20% TCA and placed on ice for 15 min. Following centrifugation at 12 000g for 30 min the supernatant was discarded and the pellet was washed in ice-cold acetone. Samples were



centrifuged at 12 000g for 15 min and the acetone allowed to evaporate. The pellet containing histones was re-suspended in SDS-PAGE sample buffer (See section 2.11) and stored at  $-20^{\circ}\text{C}$  (Issar *et al.*, 2009, Lopez-Rubio *et al.*, 2007). The protein concentration was calculated using the BCA quantification assay (section 2.10) and protein pellets were dissolved in SDS-PAGE reducing buffer before analysis on SDS polyacrylamide gels as described in section 2.11.

### **2.9.3. Trelle *et al.* (2009) Protocol**

The centrifugal steps followed in the histone isolation protocol were performed at  $4^{\circ}\text{C}$  in a Thermo Scientific SL 16R centrifuge (Thermo Fisher Scientific). Synchronised *P. falciparum* trophozoite parasites at 6-8% parasitaemia and 5% haematocrit were centrifuged at 3500g for 5 min. Samples were saponin lysed and washed with PBS until the supernatant appeared clear of visible haemoglobin as described in section 2.9.1. Following the addition of hypotonic lysis buffer (10 mM Tris-HCl, pH 8, 3 mM  $\text{MgCl}_2$ , 0.2% NP-40, 0.25 M sucrose, 1 $\times$ PI), the sample was homogenized with an eppie grinder and centrifuged at 500g for 10 min. The resulting pellet was washed twice in the hypotonic lysis buffer and washed once with a hypotonic buffer not containing NP-40 (10 mM Tris-HCl, pH 8, 3 mM  $\text{MgCl}_2$ , 0.25 M sucrose, 1 $\times$ PI). The sample was centrifuged at 500 $\times$ g for 10 min and the supernatant discarded.

The pellet was re-suspended, drop wise in a NaCl buffer (10 mM Tris-HCl, pH 8, 1 mM EDTA, 0.8 M NaCl, 1 $\times$ PI) and incubated on ice for 10 min. After centrifugation at 500g for 5 min, the nuclear pellet was re-suspended in 0.25 M HCl and ground using an eppie grinder for further homogenisation. Samples were rotated at  $4^{\circ}\text{C}$  for 1 h (Heto Rotamix RK 20-1; Heto Lab Equipment) and after a centrifugation step at 11 000g for 30 min an equal volume of 20% (w/v) TCA was added to the sample. The sample was incubated on ice for 15 min, centrifuged at 12 000g for 30 min and the supernatant discarded. The pellet was washed in ice-cold acetone and centrifuged at 12 000g for 15 min, after which the acetone was allowed to evaporate. The pellet containing histones was re-suspended in SDS-PAGE

sample buffer (See section 2.11) and stored at  $-20^{\circ}\text{C}$  (Issar *et al.*, 2009; Lopez-Rubio *et al.*, 2007). The protein concentration was calculated using the BCA quantification assay (section 2.10) and protein pellets were dissolved in SDS-PAGE reducing buffer before analysis on SDS polyacrylamide gels as described in section 2.10.

## 2.10. Protein quantitation analysis

To quantify the amount of protein isolated, the bicinchoninic acid Protein Quantitation Kit (BCA Kit; Pierce) was used. The assay is based on the reduction of  $\text{Cu}^{2+}$  to  $\text{Cu}^{+}$  by protein binding in an alkaline medium, resulting in a purple product with the binding of bicinchoninic acid to  $\text{Cu}^{+}$ . The resulting absorbance is recorded at 562 nm. This assay is more detergent-compatible than the Bradford assay and the Lowry method (Smith *et al.*, 1985).

A BSA 10 mg/ml stock solution was used, from which standards (2000  $\mu\text{g/ml}$ , 1000  $\mu\text{g/ml}$ , 750  $\mu\text{g/ml}$ , 500  $\mu\text{g/ml}$ , 250  $\mu\text{g/ml}$ , 125  $\mu\text{g/ml}$  and 62.5  $\mu\text{g/ml}$ , 25  $\mu\text{g/ml}$ ) were prepared. In a 96 well plate, replicates of 10  $\mu\text{l}$  of each sample, standard and sample buffer (blank reading) was added to 200  $\mu\text{l}$  of BCA working reagent (50 parts reagent A + 1 part reagent B). Reagent A consists of sodium bicinchoninate,  $\text{Na}_2\text{CO}_3$ , sodium tartrate,  $\text{NaOH}$ , and  $\text{NaHCO}_3$  (pH 11.25). Reagent B consists of  $\text{CuSO}_4 \cdot 5\text{H}_2\text{O}$  dissolved in  $\text{ddH}_2\text{O}$ . Both reagents are stable at room temperature (Noble, 2009). The plate was covered in foil, mixed in a plate shaker for 30 s and incubated at  $37^{\circ}\text{C}$  for 30 min-2 h. Longer incubations at  $37^{\circ}\text{C}$  result in improved protein-to-protein variability (Noble, 2009). After incubation, the plate was left for 30 min to cool to room temperature and the absorbance was read using a Multiskan Ascent V1.24 and software version 1.3.1 (Thermo Lab Systems) with a 595 nm filter.

## 2.11. SDS-Polyacrylamide Gel Electrophoresis

SDS-PAGE is the most widely used method for analysing protein mixtures quantitatively (Hames, 2001; Walker, 2010). The anionic detergent sodium dodecyl sulfate (SDS) gives the denatured sample a constant mass to charge

ratio and identical charge densities resulting in the proteins being separated according to size. On average, one SDS molecule binds every 2 amino acids on the rod-shaped, denatured protein structure. The protein samples were placed in SDS sample buffer (0.06 M Tris-HCl, pH 6.8, 10% glycerol, 2% (w/v) SDS) and boiled at 95°C for 4 min. The glycerol forms part of the running buffer to increase the samples' density, preventing convective migration out of the wells (Walker, 2010; Pilch, 1964). The protein concentrations were calculated using the BCA protein quantitation kit. Samples were stored at -20°C in SDS sample buffer.

Once the samples were ready to be loaded onto the gel, the protein samples were diluted 1:1 or 4:1 in SDS reducing buffer (5% v/v 2 $\beta$ -mercaptoethanol, 0.025% w/v bromophenol blue). The 2 $\beta$ -mercaptoethanol prevents the oxidation of cysteines and reduces the disulphide bridges keeping tertiary structures together. The ionisable bromophenol blue dye is used to track the electrophoretic run. Samples were loaded with the Spectra multicolour low range protein ladder (1.7–40 kDa, Thermo Scientific Pierce Protein Research Products). AnyKD (range of 10-100 kDa) precast SDS-PAGE gels were purchased from Bio-Rad and used to separate proteins using a Mini-Protean Bio-Rad system in a running buffer (25 mM Tris, 192 mM glycine and 0.1% SDS) at 300 V for 20 min. The stacking gel, with a large pore size, is used to concentrate the protein into a band before entering the separating gel. The SDS-protein complexes separate according to size as they move through the separating gel due to molecular sieving (Walker, 2010).

After protein separation, gels were stained overnight at 37°C using (0.1% (w/v) Coomassie Brilliant Blue R-250 (Sigma), 40% (v/v) methanol (Merck) and 10% (v/v) acetic acid (Merck), followed by an overnight de-stain with 25% methanol. Gels were then stored in 1% acetic acid solution for future analysis.

## **2.12. Mass spectrometry analysis**

The basis of mass spectrometry is the conversion of sample molecules into gaseous ions, which are further separated and detected in a mass

spectrometer according to their mass-to-charge ratio (Walker, 2010). Mass spectrometry was performed by Dr Salome Smit at the Central Analytical Facility, University of Stellenbosch.

All experiments were performed on a Thermo Scientific EASY-nLC II connected to a LTQ Orbitrap Velos mass spectrometer (Thermo Scientific, Bremen, Germany) equipped with a nano-electrospray source. The nano-electrospray technique was used for improved sensitivity of limited amounts of sample (Walker, 2010). For liquid chromatography, separation was performed on an EASY-Column (2 cm, ID 100 $\mu$ m, 5  $\mu$ m, C18) pre-column followed by XBridge BEH130 NanoEase column (15 cm, ID 75  $\mu$ m, 3.5  $\mu$ m, C18) with a flow rate of 300 nl/min. The gradient used was from 5-17 % B in 5 min, 17-25% B in 90 min, 25-60% B in 10 min, 60-80% B in 5min and kept at 80% B for 10 min. Solvent A was 0.1 % (v/v) formic acid in water, and solvent B was 0.1% formic acid in acetonitrile.

The mass spectrometer was operated in data-dependent mode to automatically switch between Orbitrap-MS and LTQ-MS/MS acquisition. Data were acquired using the Xcaliber software package. The precursor ion scan MS spectra ( $m/z$  400 – 2000) were acquired in the Orbitrap with resolution  $R = 60000$  with the number of accumulated ions being  $1 \times 10^6$ . The 20 most intense ions were isolated and fragmented in a linear ion trap (number of accumulated ions  $1.5 \times 10^4$ ) using collision-induced dissociation. The lock mass option (polydimethylcyclsiloxane;  $m/z$  445.120025) enabled accurate mass measurement in both the MS and MS/MS modes. In data-dependent LC-MS/MS experiments, dynamic exclusion was used with 60 s exclusion duration. Mass spectrometry conditions were 1.8 kV, capillary temperature of 250 °C, with no sheath and auxiliary gas flow. The ion selection threshold was 500 counts for MS/MS and an activation Q-value of 0.25 and activation time of 10 ms were also applied for MS/MS. Thermo Proteome Discoverer 1.3 (Thermo Scientific, Bremen, Germany) was used to identify proteins via automated database searching (Mascot, Matrix Science, London, UK, and Sequest) of all tandem mass spectra against the PlasmoDB 7.2 database.

### **2.13. Statistical Analyses**

All statistical analyses were performed using a student *t*-test and the program GraphPad InStat (Version 3). The *t*-test was used to determine if the means of two groups were statistically different from each other, with a 95% confidence interval. Using ICEstimator, the IC<sub>90</sub> values of all four polyamine analogues were calculated for the reversibility experiments. Figures were developed using GraphPad Prism (Version 5) and SigmaPlot (Version 11).

## **Chapter 3**

---

### **Results**

### 3.1. ADME profile of fluorinated polyamine analogues

Verlinden and colleagues showed that a series of symmetrical alkylated (bis)urea and (bis)thiourea polyamine analogues exhibited antiparasitic activity in the low nanomolar range (100-650 nM), additionally showing high selectivity to *P. falciparum* parasites (Verlinden *et al.*, 2011). To further evaluate the antimalarial capacity of the (bis)urea and (bis)thiourea polyamine analogue series, the three leading compounds (compound 20, 30 and 39 from (Verlinden *et al.*, 2011) were sent for *ex vivo* pharmacology evaluation and *in vivo* efficacy testing in the murine malaria model (Verlinden *et al.* Unpublished Results). The *ex vivo* pharmacology analysis was performed at St Jude's Children's Hospital, USA in the group of Kip Guy and the murine *in vivo* analysis was performed by Lubbe Wiesner at the pharmacology department, University of Cape Town.

The solubility of the leading compounds was measured at various pH values, in order to mimic certain biological environments as closely as possible. These pH environments were mimicking the pH of an empty stomach (pH 3), the pH of a full stomach (pH 5) and the pH of blood (pH 7.4). The results showed that the average solubility was moderate to good for all three leading compounds, ranging from 9.3-62.5  $\mu$ M (Table 3.1). Furthermore, the microsomal stability assay used assessed the half-life of the compounds, which is an indicator of *in vivo* clearance. Due to the majority of drug metabolism occurring in the liver, clearance times of the compounds were measured in mouse, rat, dog and human liver microsomes. Microsomal stability could not be determined for compound 30 and 39. However, the half-life of compound 20 measured above 4 hours (Table 3.1) and the clearance time in rat and human liver microsomes is comparable to known antimalarial compounds.

The predicted plasma levels of compounds, after oral administration, were measured using the Caco-2 cell permeability model, in order to assess the permeability of the leading compounds tested. The apparent permeability (Papp) measurement is indicative of absorption characteristics. Where a Papp value of  $>10 \times 10^6$  cm/sec are likely to be well absorbed, whilst those with a

low Papp ( $<10 \times 10^6$  cm/sec) are less likely to have good absorption characteristics, compound 30 falls well within range of good absorption (Table 3.1). An efflux ratio (Papp B>A/Papp A>B) of  $>2$  indicates active efflux of the compound, via transporter molecules, from the cells' apical surface. From the three leading compounds tested, compound 39 was the only one with an efflux ratio  $>2$ .

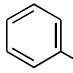
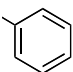
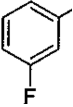
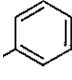
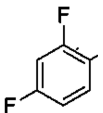
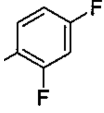
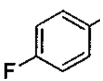
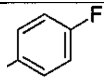
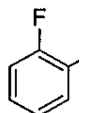
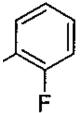
**Table 3.1:** Solubility and permeability determination of selected compounds from the first (bis)urea and (bis)thiourea-alkylated polyamine analogue library, with *in vitro* metabolic stability determined in mouse, rat, dog and human liver microsomes (Verlinden *et al.* Unpublished Results).

Compounds	Solubility		Caco permeability		Concentration (uM)	Microsomal stability							
	pH	Avg. Solub. (uM)	AVG Papp A/B (nm/s)	Efflux Ratio (B2A/A2B)		Mouse	Rat	Dog	Human				
Carbamazepi	7.4	73.4	452.88	0.96	ND								
Rifampin	ND	ND	16.38	3.44	ND								
20	3	14.5	ND	ND	High (20) Medium (4) Low (0.8)	t(1/2) /hr	CLint (ml/mi)	t(1/2) /hr	CLint (ml/mi)	t(1/2) /hr	CLint (ml/mi)	t(1/2) /hr	CLint (ml/mi)
	5	14.8				0.7	73.7	>4	<11.7	3.7	8.9	>4	<5.2
	7.4	33.7				0.7	72.1	>4	<11.7	1.3	24.7	>4	<5.2
						None detected	3.3	14.3	1.1	30.5	>4	<5.2	
30	3	9.3	188.16	0.73	ND								
	5	13.5											
	7.4	31.3											
39	3	48.5	10.88	3.24	ND								
	5	62.5											
	7.4	43.6											

Furthermore, compounds 20, 30 and 39 were evaluated in a malaria infected mouse model for *in vivo* efficacy; compound 30 was further evaluated for *in vivo* bioavailability. During the *in vivo* pharmacokinetic evaluation, most of the concentrations of compound 30 were below the limit of quantification. The cause of the low bioavailability is unclear, but may be due in part to low absorption of the compound or rapid metabolism in the gastrointestinal tract of the mice. As no effect on parasite multiplication was observed during *in vivo* studies and microsomal stability could not be indicated for this compound, the lack of efficacy could be explained by either low bioavailability or metabolic stability of compound 30. As such, it was decided to halogenate the lead compound, (compound 30) to create four altered analogues, each with a fluorination on the terminal phenyl substituents, without altering the 3-6-3 backbone or the internal urea substituents (Table 3.2).



**Table 3.2: Alkylated 3-6-3 carbon backbone fluorinated polyamine analogues.**

Compound number	Compound ID	Molecular Weights	Chemical Structure		Alkylation	Type
			R1	R2		
30	RJB-92-04	541.56			(Bis)diphenyl	Urea
1	BP-113-15	577.54			(Bis)diphenyl	Urea
2	BP-113-17	613.52			(Bis)diphenyl	Urea
3	EM-109-35	577.54			(Bis)diphenyl	Urea
4	EM-109-37	577.54			(Bis)diphenyl	Urea

1. BP-113-15:1,1'-((hexane-1,6-diylbis(azanediyl))bis(propane-3,1-diyl))bis(3-(3-fluorophenyl)urea)
2. BP-113-17:1,1'-((hexane-1,6-diylbis(azanediyl))bis(propane-3,1-diyl))bis(3-(2,4-difluorophenyl)urea)
3. EM-109-35:1,1'-((hexane-1,6-diylbis(azanediyl))bis(propane-3,1-diyl))bis(3-(4-fluorophenyl)urea)
4. EM-109-37:1,1'-((hexane-1,6-diylbis(azanediyl))bis(propane-3,1-diyl))bis(3-(2-fluorophenyl)urea)

Considering the unpublished *in vivo* efficacy and *ex vivo* pharmacology results of compound 30, the series of four fluorinated polyamine analogues were evaluated by means of *in silico* ADME profiling to evaluate their *ex vivo* pharmacokinetic profiles. These physiochemical descriptors incorporate *in silico* models for intestinal absorption, aqueous solubility, blood brain barrier penetration, plasma protein binding, cytochrome P450 2D6 inhibition and hepatotoxicity.

**Table 3.3: ADME data of the series of fluorinated polyamine analogues.** *In silico* physiochemical predictors were obtained using the Discovery Studio Modelling Environment program.

Properties	CQ	30	1	2	3	4
<b>Molecular Weight</b>	319.9	468.6	506.6	542.6	506.6	506.6
<b>Human Intestinal Absorption (HIA)<sup>a</sup></b>	0	0	0	0	0	0
<b>Aqueous Solubility</b>	-5.014	-1.372	0.39	-1.09	0.42	0.36
<b>Aqueous Solubility level<sup>b</sup></b>	2	4	5	4	5	5
<b>Blood Brain Barrier (BBB)</b>	0.755	N/A	-1.34	-1.22	-1.34	-1.34
<b>BBB Level<sup>c</sup></b>	0	4	3	3	3	3
<b>Cytochrome P450 2D6 (CYP2D6)</b>	10.68	-3.90	-6.15	-6.15	-6.15	-6.15
<b>CYP2D6 prediction</b>	True	False	False	False	False	False
<b>Hepatotoxicity</b>	0.38674	0.7099 1	3.24	3.45	3.91	2.25
<b>Hepatotoxicity prediction</b>	True	True	True	True	True	True
<b>Plasma protein binding (PPB)</b>	-1.84539	3.0968	-2.48	-2.66	-2.09	-2.16
<b>PPB prediction</b>	True	True	False	False	True	True

<sup>a</sup> Absorption: Good absorption (0), Moderate absorption (1), Low absorption (2), Very low absorption (3).

<sup>b</sup> Aqueous Solubility: Extremely low (0), Very low but possible (1), Yes, low (2), Yes, good (3), Yes optimal (4), No, too soluble (5).

<sup>c</sup> Blood brain penetration: Very high penetrant (0), High (1), Medium (2), Low (3), Undefined (4).

Table 3.3 indicates that all four fluorinated analogues and CQ are predicted to absorb well due to predicted human intestinal absorption (HIA) scores of zero. Compound 2 and compound 30 have optimal levels of aqueous solubility in terms of drug-likeness, whereas the other three fluorinated compounds are too soluble. The predicted solubility data of CQ is low. From these predicted values, the polyamine analogues seem to be more soluble than CQ. Expected values for blood brain barrier (BBB) penetration indicate: 1) the BBB value of the fluorinated analogues imply low BBB penetration, 2) compound 30 shows undefined BBB penetration values and 3)

CQ is predicted to easily penetrate the BBB. The program predicted hepatotoxicity values increasing from 0.3 (CQ) and 0.7 (compound 3) to values all above 3 for the fluorinated analogues.

All values indicate hepatotoxic natures for the tested compounds possibly indicating that the fluorination makes polyamine analogues more hepatotoxic. For the fluorinated analogues, predicted plasma protein binding (PPB) values also changed drastically to negative values, similar to CQ (-1.84539), in comparison to the positive value of compound 30 (3.0968). This could indicate that the fluorinated analogues do not bind to as many plasma proteins as compound 30, which could result in improved permeability and absorption.

Lipinski's rule of five implies that a compound is more likely to exhibit poor absorption and permeation if two or more parameters are out of range. Ideal chemotypes should have molecular weights less than 500 g/mol. They should contain no more than 5 hydrogen bond donors (HBD) or 10 hydrogen bond acceptors (HBA) and should have a LogP (octanol/water partition coefficient) value less than 5.

The Quantitative Estimate of Drug-likeness (QED) value was calculated because it is not based on cut-off values of four rules only, ranking compounds across a wide value range. The QED values range from zero (all properties unfavourable) to one (all properties favourable), ranking compounds according to their predicted drug-likeness (Bickerton *et al.*, 2012).

Data from Table 3.4 indicates that all four fluorinated analogues have less than 5 HBD, less than 10 HBA and AlogP values less than 5. Compared to the AlogP value of CQ (4.4), all polyamine analogues have lowered ALogP values (2.3-2.6) in the same range as compound 30.

**Table 3.4: The Quantitative Estimate of Drug-likeness calculated for the series of fluorinated polyamine analogues.** Physiochemical and QED predictors of the fluorinated polyamine analogues, compound 30 and CQ, predicted using the Biscu-it QED on Silicos-it program.

Properties	CQ	30	1	2	3	4
Molecular Weight	319.9	468.6	506.64	542.62	506.64	506.64
AlogP	4.4	2.6	2.375	2.654	2.375	2.375
Hydrogen bond donors	1	6	2	2	2	2
Hydrogen bond acceptors	3	8	6	6	6	6
Number of rotatable bonds	8	17	21	21	21	21
Number of aromatic rings	2	2	2	2	2	2
QED*	-	0.158	0.146	0.107	0.146	0.146

\*Quantitative Estimate of Drug Likeness

Although the molecular weights of the analogues exceed 500 g/mol, the compounds comply with three of Lipinski's rules, according to the Biscu-it QED on Silicos-it program. The predicted QED values for all five polyamine analogues are very low, ranging from 0.107-0.158. The range of values is very close to 0, which is associated with unfavourable properties for drug-likeness or low drug-likeness (Bickerton *et al.*, 2012).

### 3.2. Antiplasmodial activity of polyamine analogues in *P. falciparum* parasites

To determine if the fluorination of compound 30 (Table 3.1; Verlinden *et al.*, 2011) has an effect on the *in vitro* potency of the compound against *P. falciparum* parasite proliferation, the Malaria SYBR Green I Fluorescence assay was performed to determine the dose-response effects and the IC<sub>50</sub> values.

The fluorinated analogues were tested against *P. falciparum* strain 3D7 (CQ sensitive), strain HB3 (pyrimethamine resistant) and strain W2 (CQ resistant). The recorded fluorescence values were used to create dose-response curves

for each compound in each strain. Using the data obtained from the dose-response curves (Figure 3.1), the corresponding  $IC_{50}$  values for each strain were calculated as summarised in Table 3.5.

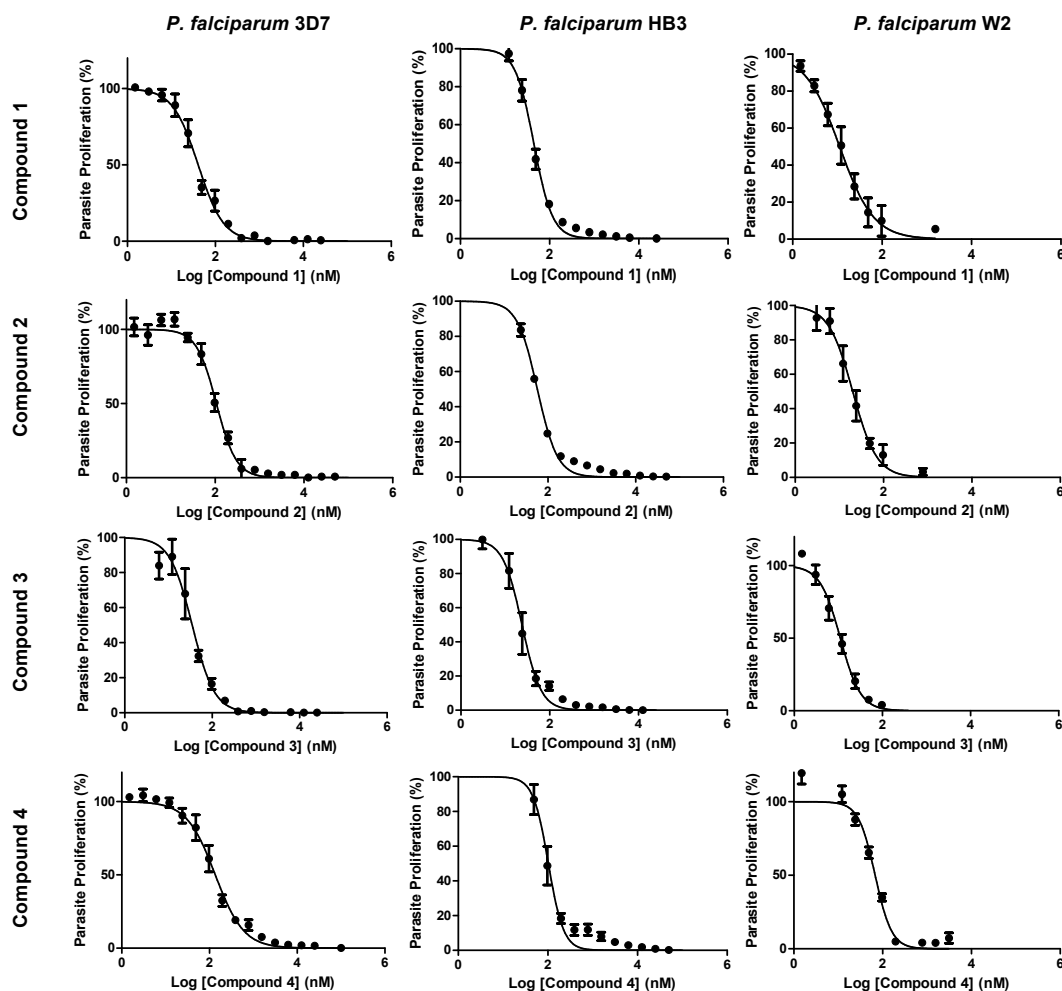


**Figure 3.1: Dose-response curves of four fluorinated polyamine analogues against three strains of *P. falciparum* parasites.** The MSF assays were set up using synchronised ring stage *P. falciparum* parasite suspensions (1% parasitaemia, 2% haematocrit), which were treated with the fluorinated analogues, 2-fold serially diluted to 187.5 pM and a starting concentration of 100  $\mu$ M. The 96-well plates were incubated at 5%  $O_2$ , 5%  $CO_2$  and 90%  $N_2$  within a stationary incubator at 37°C for 96 h. *P. falciparum* strain 3D7, strain HB3 and strain W2 were used to obtain the dose-response curves above, from which the corresponding  $IC_{50}$  values were calculated. Data are the means of at least three independent experiments performed in triplicate  $\pm$ S.E.

Results of the antiplasmodial activity of the fluorinated polyamine analogue series against *P. falciparum* proliferation showed that compound 3 had the lowest  $IC_{50}$  value in all three tested *P. falciparum* strains (11 nM – 35 nM), followed by compound 1 (11 nM – 45 nM). Compound 2 (107 nM) and

compound 4 (136 nM) necessitated the highest concentrations for 50% inhibition of *P. falciparum* strain 3D7 parasite proliferation. From the data obtained in the panel of strains, the resistance index for the compounds could also be calculated (Table 3.5).

**Table 3.5: *In vitro* antiplasmodial activity of fluorinated 3-6-3 carbon backbone polyamine analogues.** Analogues were screened against a panel of intraerythrocytic *P. falciparum* parasite strains using the MSF assay. Data from the various strains were used to calculate the resistance index and are representative of 3 individual experiments, each performed in triplicate,  $\pm$  S.E.

Compound	<i>P. falciparum</i> IC <sub>50</sub> (nM)			RI <sup>a</sup>
	3D7	W2	HB3	
30	88 $\pm$ 7	26 $\pm$ 1	-	0.29
1	41 $\pm$ 5	11 $\pm$ 6	45 $\pm$ 7	0.27
2	107 $\pm$ 1	20 $\pm$ 7	57 $\pm$ 6	0.19
3	35 $\pm$ 2	11 $\pm$ 2	24 $\pm$ 6	0.31
4	136 $\pm$ 2	68 $\pm$ 1	103 $\pm$ 3	0.50
CQ	15 $\pm$ 7	62 $\pm$ 2	19 $\pm$ 2	4.13

<sup>a</sup> Resistance index (RI) is defined as the ratio of the IC<sub>50</sub> values of the resistant strain (W2) divided by the IC<sub>50</sub> values of the sensitive strain (3D7).

Table 3.5 compares the IC<sub>50</sub> values of compound 30 and the fluorinated polyamine analogues in three *P. falciparum* strains. The IC<sub>50</sub> values calculated for the compounds in strain 3D7 were higher than the corresponding compound values calculated in strain HB3. Strain W2 resulted in the overall lowest IC<sub>50</sub> values for each corresponding compound. Compound 3 had an IC<sub>50</sub> value of 35 nM in *P. falciparum* strain 3D7, 24 nM in *P. falciparum* strain HB3 and 11 nM in *P. falciparum* strain W2 (Table 3.5). The same trend is followed by all four fluorinated analogues. These results indicate that the compounds show antiplasmodial activity against a wide range of *P. falciparum* phenotypes, and no cross-resistance is evident.

Both leading compounds (compound 1 and compound 3) are (bis)diphenyl, urea 3-6-3 carbon backbone polyamine analogues. However, compound 1 has *meta* monofluorinated terminal rings and compound 3 has *para* monofluorinated terminal rings. Compound 2 has *ortho/para* difluorinated terminal rings and compound 4 has *ortho* monofluorinated terminal rings. The difference in placement of the fluorine molecules affects the reactivity of the compounds towards the parasites (Table 3.5). Possibly, the positioning could affect the binding of the compounds in the target active site, making the inhibition less effective or more effective. The resistance indices of this library of polyamine analogues are well below the RI value calculated for CQ (4.1). The low resistance indices could be indicative of a distinct resistance mechanism as compared to that of CQ, suggesting a distinct mode of action.

### **3.3. Selectivity indices of the fluorinated polyamine analogues**

Selectivity of a compound is important for drug development, as the compound has to be specific to the parasite-infected red blood cells and not attack the host cells. The parent compound (Compound 30) has been shown to be >7000-fold selective towards the parasite as compared to mammalian cells (Verlinden *et al.*, 2011). Therefore, the concentration responsible for 50% inhibition of cell growth ( $GI_{50}$ ) was determined against human hepatocellular liver carcinoma cells (HepG2), after 96 h compound treatment with the fluorinated polyamine analogues (Table 3.6).

**Table 3.6: Cytotoxicity and selectivity determination of 3-6-3 carbon backbone fluorinated polyamine analogues determined using HepG2 mammalian cells.** Data represents the mean of 3 independent biological repeats, performed in triplicate  $\pm$  S.E.

Compound	HepG2 GI <sub>50</sub> ( $\mu$ M)	Selectivity Index (SI) <sup>a</sup>
CQ	43.09 $\pm$ 2.4	4787
30	619.3 $\pm$ 25.8	7038
1	126.2 $\pm$ 28	3078
2	649.2 $\pm$ 2.1	6067
3	9579 $\pm$ 3.9	>8000
4	519.3 $\pm$ 2.7	3818

<sup>a</sup> Selectivity index (SI) was determined as the compound GI<sub>50</sub> mammalian cell/ IC<sub>50</sub> *P. falciparum*.

The GI<sub>50</sub> values calculated (Table 3.6) were all in the  $\mu$ M range, one order of magnitude higher than that calculated for *P. falciparum* parasite IC<sub>50</sub> values (Table 3.5). The selectivity index, which is defined as the ratio of HepG2 GI<sub>50</sub> over *P. falciparum* IC<sub>50</sub>, ranged from >3000-fold to >8000-fold more selective for *P. falciparum* parasites compared to mammalian cells. Of the four analogues, compound 3 was the most selective towards parasite cells, followed by compound 2. The lowest selectivity index for this series was compound 1, showing 3078-fold more selectivity towards *P. falciparum* parasites (Table 3.6).

### 3.4. Recovery of parasites after short-term exposure with compounds 1 and 3

The inhibition of polyamine biosynthesis results in an *in vitro* parasite cytostatic phenotype, which is not ideal for antimalarial drug development as re-infection can occur (Niemand *et al.*, 2012). Parasite recovery experiments, based on work done by Malmquist *et al.* (2012), were performed to determine if the fluorinated polyamine analogues resulted in cytostatic or cytotoxic parasite phenotypes. Synchronised ring stage parasites (2% parasitaemia, 5% haematocrit) were treated at  $3 \times IC_{90}$  and  $10 \times IC_{90}$  of compound 1 ( $IC_{90}$ -187.3 nM) and compound 3 ( $IC_{90}$ -136.6 nM) following a short-term exposure



of 12 h. After incubation the cultures were washed with culture medium and parasite proliferation recorded at 4 time points using SYBR Green I fluorescence (Malmquist *et al.*, 2012).

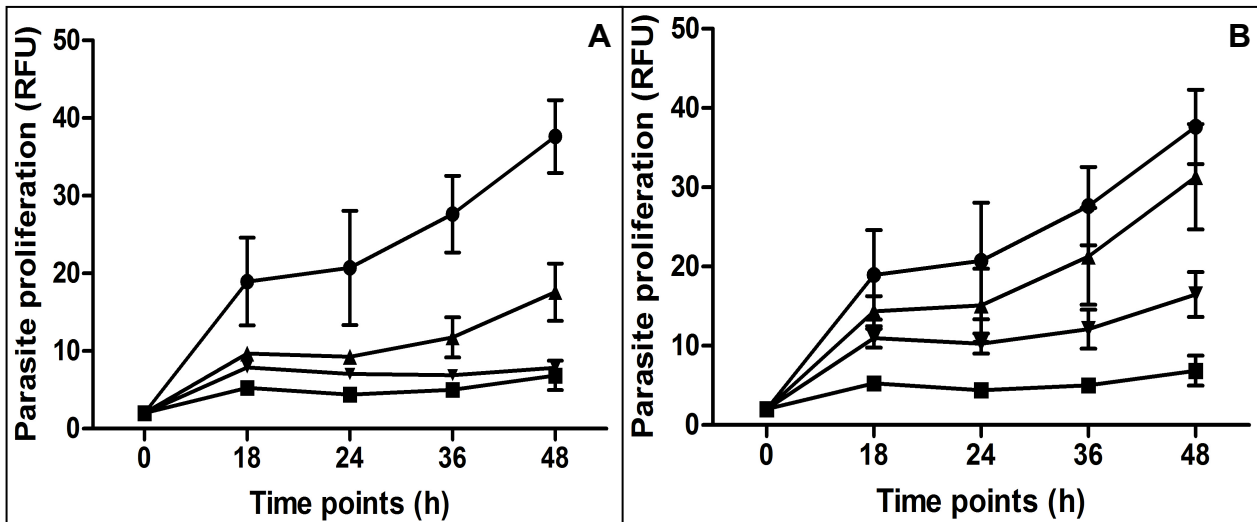


**Figure 3.2: Parasite proliferation measured using SYBR Green I Dye, after removal of drug pressure.** *P. falciparum* ring stage parasites (strain 3D7) were treated with compound 1 (A) and compound 3 (B) for 12 h at  $3\times IC_{90}$  (upright triangle) and  $10\times IC_{90}$  (downward triangle). Parasites were washed with warm culture medium and subsequent parasite proliferation was measured at 4 time points using the Malaria SYBR Green I Fluorescence assay. A circle represents untreated parasites as positive growth controls. A square represents CQ treated parasites ( $0.5\ \mu M$ ) as negative growth controls. Data are the means of 3 independent repeats performed in duplicate  $\pm$  S.E.

Compound 1-treated cultures showed continued parasites proliferated after drug removal at  $3\times IC_{90}$  but no parasite proliferation was evident at  $10\times IC_{90}$ . By contrast, compound 3-treated parasites were able to fully recover and continued to proliferate after drug removal when treated at both  $3\times IC_{90}$  and  $10\times IC_{90}$  (Figure 3.2). Due to the proliferation assay being unable to distinguish between dead and living parasites, the parasite proliferation when treated with compound 3 at  $10\times IC_{90}$  could be as a result of the assay reading DNA of dead parasites. However, further time studies would have to confirm this. The data could lend itself to the assumptions that compound 1-treated parasites result in a cytotoxic phenotype. Only at 36 h after a low dose of compound-1 were the parasites able to start proliferating again. However, the data recorded from compound 3-treated parasites, after a 12 h pulse, indicated that the parasites were able to recover after drug removal.

Results recorded from all mentioned proliferation assays established that the different placements of the fluorine molecules did affect the inhibitory capacity of the compounds towards the parasites (Table 3.2) and provided information on the antiplasmodial structure-activity relationships (SAR) of compounds 1-4. Possible modes of action were investigated in the next sections.

### 3.5. $\beta$ -Haematin Crystallisation Studies

The basic scaffold of the fluorinated polyamine analogues and CQ both consists of a benzene ring and the latter has been implicated as the mode of action of CQ in preventing haemozoin formation. In order to avoid haem toxicity, parasites sequester haem into aggregates of dimeric ferriprotoporphyrin IX called haemozoin ( $\beta$ -haematin crystals) (Carter *et al.*, 2010).

Keeping this similarity in mind,  $\beta$ -haematin crystallisation studies were performed to investigate a possible similar mode of action for the polyamine analogues. The detergent initiated  $\beta$ -haematin crystallisation assay is based on the ability of compounds to inhibit the formation of  $\beta$ -haematin crystals, which can be detected by means of determining the amount of pyridine reacting with haemin and not  $\beta$ -haematin. The non-ionic and non-denaturing detergent NP-40 has been used in this assay to nucleate the formation of  $\beta$ -haematin crystallisation, while pyridine coordinates with ferriprotoporphyrin IX, displacing water. Therefore the absorbance has been proven to be directly proportional to haematin concentration (Ncokazi and Egan, 2005). Investigations concerning current novel antimalarial compounds use this assay to determine if a mechanism of action similar to that of CQ is probable.

Therefore, this assay was performed using the fluorinated series of polyamine analogues. Compound 30, compound 3 (leading analogue) and compound 4 (weakest analogue) were therefore tested for the ability to inhibit  $\beta$ -haematin formation (Figure 3.3).

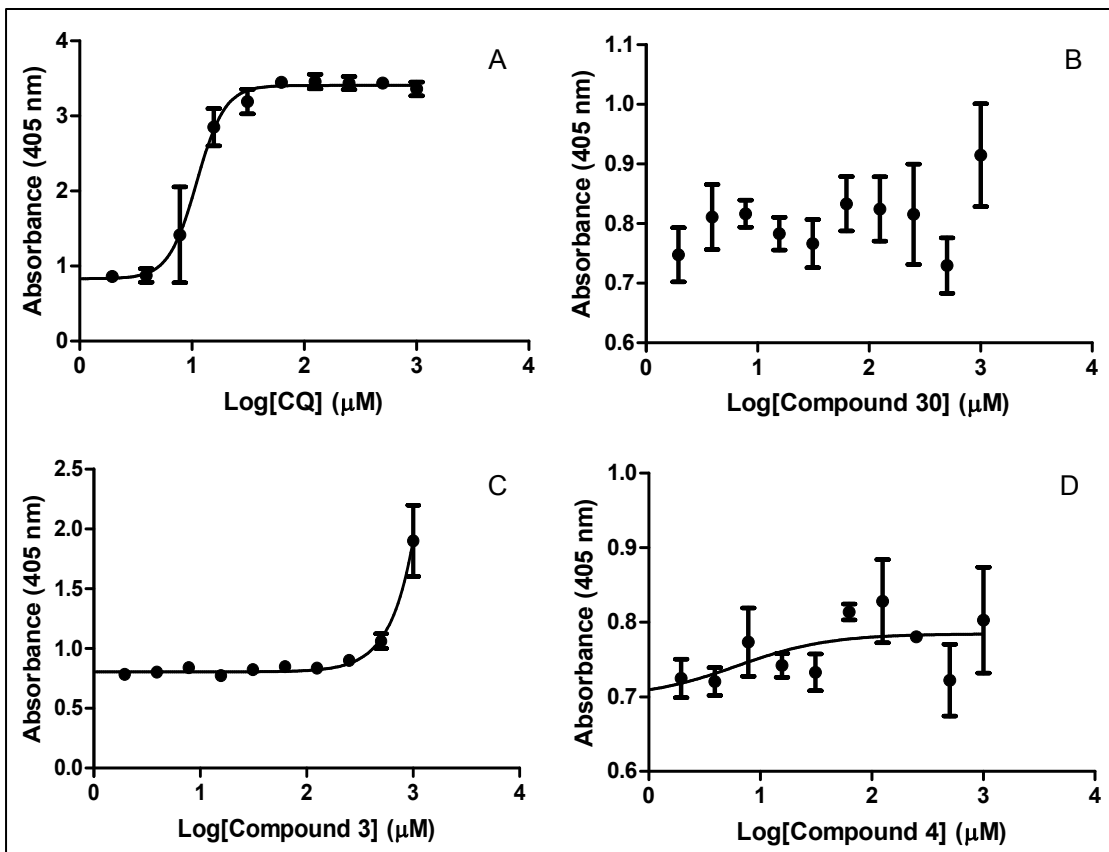


**Figure 3.3: Sigmoidal  $\text{IC}_{50}$  graphs of  $\beta$ -haematin inhibition studies with 3-6-3 carbon backbone polyamine analogues and CQ.** Compound 30 (B), compound 3 (C), compound 4 (D) and CQ (A) were used at a starting concentration of 1 mM from which they were 2-fold serially diluted in an NP40/DMSO buffer. To the compounds a haemin/acetate buffer was added and the 96-well plates were incubated at  $37^\circ\text{C}$  for 5 h. After incubation, a pyridine/acetate buffer was added and the absorbance was measured at 405 nm. Data are representative of three independent repeats performed in duplicate  $\pm$  S.E.

CQ was determined to have an  $\text{IC}_{50}$  value of  $11 \mu\text{M}$  for the formation of  $\beta$ -haematin crystals. From Figure 3.3, it is evident that compound 3 had the ability to inhibit  $\beta$ -haematin formation but only at a concentration above 1 mM. This suggests that haematin inhibition may not be the primary mechanism of inhibition of compound 3. Comparatively, both compounds 30 and compound 4 were unable to inhibit  $\beta$ -haematin formation at all of the concentrations tested (98 nM to 1 mM) indicating that these compounds do not have the ability to prevent haematin formation.

### 3.6. LSD1 Chemiluminescence Assay Optimisation

Previously, the (bis)urea and (bis)thiourea polyamine analogues were shown to inhibit LSD1 activity in mammalian breast cancer cells (Sharma *et al.*, 2010, Huang *et al.*, 2007). Therefore, in this study, the fluorinated analogues of compound 30 (Verlinden *et al.*, 2011) were tested for their ability to inhibit LSD1. An LSD1 chemiluminescent assay has been developed based on the oxidation of luminol by HRP in the presence of H<sub>2</sub>O<sub>2</sub> (Parejo *et al.*, 2000, Chen *et al.*, 2007) and was optimised in this study for use against malaria parasites as described below.

#### 3.6.1. Kinetic study of chemiluminescence

The reaction of this assay is based on the oxidation of luminol by HRP in the presence of H<sub>2</sub>O<sub>2</sub> (Chen *et al.*, 2007). This experiment was set up to determine the rate of decomposition of the chemiluminescent reaction once the H<sub>2</sub>O<sub>2</sub> has been added to the reaction well (Figure 3.4). Luminol is oxidised in the presence of H<sub>2</sub>O<sub>2</sub> to 3-aminophthalate anions, of which the luminescence was recorded using a luminometer at 425 nm.

Figure 3.4 indicates that the activity of luminol decreased from ±275 000 RLU/Sec to 225 000 RLU/Sec within the first 2 minutes of chemiluminescent recordings. From the rapid decrease in the rate of reaction shown in Figure 3.4, it was optimal to record further experimental readings directly after the addition of recombinant enzyme or parasites. This is due to the recombinant enzyme and the parasites being able to activate the oxidation of luminol in the presence of HRP and H<sub>2</sub>O<sub>2</sub>. Once the rate of luminol decomposition was established, the negative or positive effects of various components of the reaction mixture on chemiluminescent readings were tested.

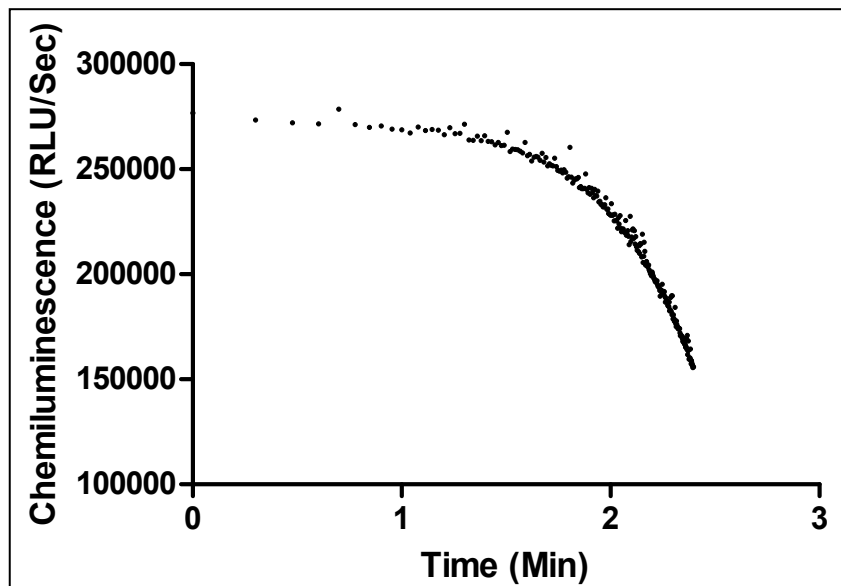


**Figure 3.4: Kinetic study of the decomposition of luminol.** The rate of decomposition of luminol, in the presence of horseradish peroxidase (HRP) and hydrogen peroxide ( $H_2O_2$ ), recorded over a period of 2 min at 425 nm. Data represents two independent repeats performed in duplicate.

### 3.6.2. Reagent effect on chemiluminescence

The original LSD1 assay protocol (Huang *et al.*, 2007) used for study in human colon carcinoma cells included the buffering agent Tris-HCl (pH 8.5) and two electrolytes KCl and  $MgCl_2$  in the reaction mixture containing luminol, HRP and the LSD1 substrate (H3K4me2). These reagents were tested individually and in combination in order to establish if their presence resulted in improved chemiluminescent readings (Figure 3.5).

The data shows that Tris-HCl, as a buffering agent at pH 8.5, makes a considerable difference to the chemiluminescent reading as compared to the readings observed of the single electrolytes (KCl or  $MgCl_2$ ) without buffering (Figure 3.5). The combined effect of all three reagents resulted in an improved chemiluminescent reading just below  $1.5 \times 10^6$  RLU/Sec compared to  $0.9 \times 10^6$  RLU/Sec for Tris-HCl alone.

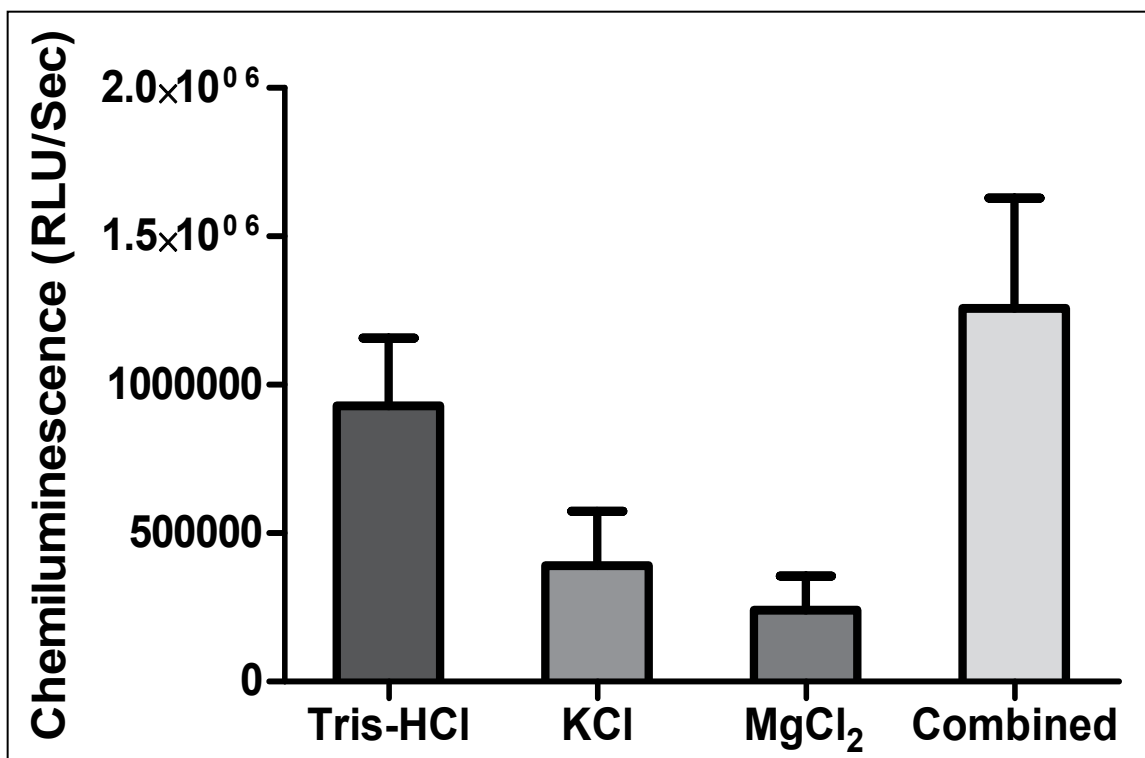


**Figure 3.5: The effect of reagent composition on chemiluminescent readings.** Reagents were pipetted into a white 96-well plate at the following concentrations: 15  $\mu$ M luminol, 6  $\mu$ g/100  $\mu$ l HRP, 50 mM Tris-HCl (pH 8.5) or, 50 mM KCl, or 5 mM MgCl<sub>2</sub>. The plate was incubated at 37°C for 2 min, after which 500 nM H<sub>2</sub>O<sub>2</sub> was added and chemiluminescence recorded at 10 s and 425 nm. Data are representative of three independent repeats performed in duplicate  $\pm$  S.E.

### 3.6.3. Inhibition of human recombinant LSD1 enzyme activity

Recombinantly expressed *P. falciparum* LSD1 (350 kDa) enzymes are not currently available. To confirm the specificity of the assay towards LSD1 activity, inhibition of human recombinant LSD1 activity was tested in the presence of an LSD1 specific inhibitor and the polyamine analogues (Table 3.6). The recombinant human LSD1 enzyme, which is 103 kDa in size, was purchased (Sigma-Aldrich) and used to confirm the specificity and functioning of the LSD1 specific assay and the effect of the analogues on human recombinant LSD1 activity (Figure 3.6).

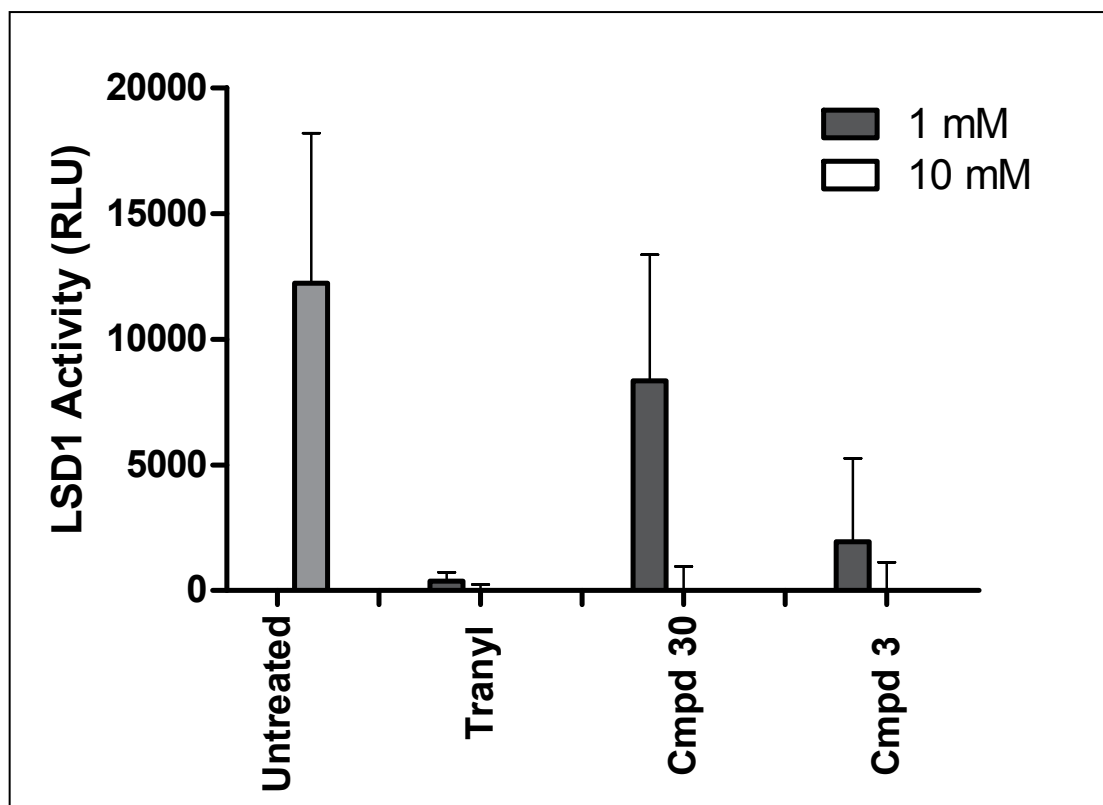


**Figure 3.6: Effect of compounds on recombinant human LSD1 activity.** Each reaction mixture consisted of 15  $\mu$ M luminol, 6  $\mu$ g/100  $\mu$ l HRP, 5  $\mu$ M H3K4me2, 50 mM Tris-HCl (pH 8.5), 50 mM KCl, 5 mM MgCl<sub>2</sub>. The reactions were incubated at 37°C for 2 min, 500 nM H<sub>2</sub>O<sub>2</sub> was added and luminol chemiluminescence recorded at 10 s and 425 nm. Data are representative of a single experiment performed in duplicate  $\pm$  S.D.

Tranlycypromine (trans-2-phenylcyclopropylamine hydrochloride), a known human LSD1 inhibitor (Maojun Yang, 2007) completely inhibited recombinant human LSD1 activity at both 1 mM and 10 mM. Compound 30 was able to inhibit LSD1 activity by 30% at 1 mM, with complete inhibition seen at 10 mM. However, compound 3 potently inhibited 84% of LSD1 activity at 1 mM, followed also by complete inhibition of the protein at 10 mM (Figure 3.6). The effect of these inhibitors on *P. falciparum* LSD1 activity was subsequently determined on parasite lysates.

#### 3.5.4. Antiplasmodial activity of tranlycypromine

As a positive control for LSD1 inhibition, tranlycypromine was used in the luminol based chemiluminescence assay. This molecule is a non-specific monoamine oxidase inhibitor, which also targets LSD1. However, no

information is available on the effect of this drug on whole cell parasites and this necessitated determining this effect prior to using tranlycypromine as control to inhibit LSD1 activity in *P. falciparum* parasite lysates. A dose-response curve was obtained and used to determine the 50% inhibitory concentration of tranlycypromine against intraerythrocytic *P. falciparum* parasites (strain 3D7)(Figure 3.7). The compound was 2-fold serially diluted from a starting concentration of 800  $\mu\text{M}$  to a final concentration of 31.25  $\mu\text{M}$ .

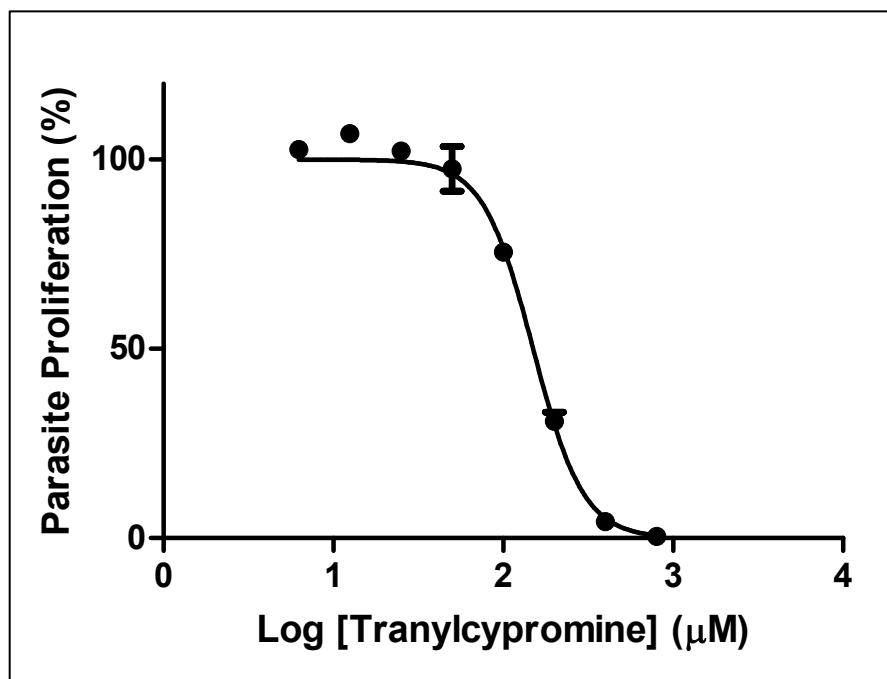


**Figure 3.7: A dose-response curve of tranlycypromine activity against 3D7 *P. falciparum* parasites.** Using synchronised *P. falciparum* ring stage parasites, a Malaria SYBR Green I Fluorescence based assay was set up (2% haematocrit, 1% parasitaemia) with tranlycypromine at a starting concentration of 800  $\mu\text{M}$ , which was 2-fold serially diluted to 31.25  $\mu\text{M}$ . The 96-well plate was incubated at 37°C for 96 h and absorbance was measured at 560 nm. The  $\text{IC}_{50}$  concentration was subsequently calculated from the sigmoidal graph. Data are representative of three independent repeats performed in triplicate  $\pm$  S.E. Where not shown, error bars fall within the symbols.

From the sigmoidal curve in Figure 3.7, it was calculated that tranlycypromine had an  $\text{IC}_{50}$  value of 150  $\mu\text{M}$  against intraerythrocytic *P. falciparum* parasites (strain 3D7) as compared to the  $\text{IC}_{50}$  value of 20  $\mu\text{M}$  in human colon carcinoma cells (Maojun Yang, 2007). Although there is a substantial difference in the  $\text{IC}_{50}$  values of tranlycypromine inhibitory activity in human cells compared to parasites, the  $\text{IC}_{50}$  values are both in the  $\mu\text{M}$  range.



Therefore, tranylcypromine could be used as a positive control for LSD1 inhibition in further parasite specific LSD1 experiments.

### 3.6.5. Inhibition of *P. falciparum* LSD1 activity in parasites

This LSD1-specific chemiluminescent assay has never before been attempted in *in vitro* *P. falciparum* parasites. To determine the effect of compound 3 on *P. falciparum* strain 3D7 parasites, the LSD1-specific optimised assay was therefore performed using parasite lysates. The assays were performed using trophozoite stage parasites due to multiple rounds of nuclear division and increased activity of epigenetic enzymes such as LSD1 (Cui *et al.*, 2008a).

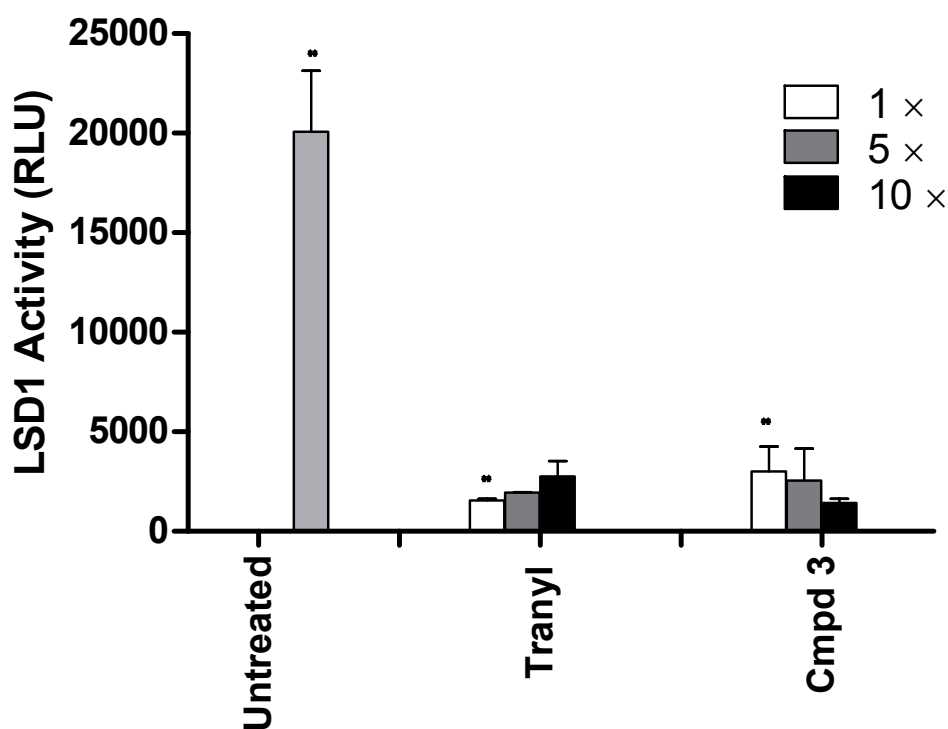


**Figure 3.8: The effect of compound 3 on LSD1 enzyme activity of isolated *P. falciparum* trophozoites.** Synchronised, trophozoite parasites (6% parasitaemia, 5% haematocrit) were treated with tranylcypromine (Tranyl) and compound 3 (Cmpd 3) at three concentrations ( $1 \times IC_{50}$ ,  $5 \times IC_{50}$ ,  $10 \times IC_{50}$ ) as indicated, for 24 h. Parasites were isolated using 0.15% (w/v) saponin and were used in the LSD1 assay. The reactions were incubated at  $37^{\circ}C$  for 2 min,  $\pm 1 \times 10^7$  parasites added and the luminol chemiluminescence was recorded at 10 s at 425 nm. Data are representative of a single experiment performed in duplicate  $\pm$  S.D. Significance between the untreated results and compound 3 ( $1 \times IC_{50}$ ) and tranylcypromine ( $1 \times IC_{50}$ ) is indicated by *P*-value  $\leq 0.01$  (\*\*), as determined with a Student *t*-test.

After a 24 h treatment of trophozoite-stage parasites in culture, the parasites were isolated from their erythrocytes and used in the LSD1 assay in the presence of various concentrations of the inhibitors (Figure 3.8). There was a significant difference ( $P \leq 0.01$ ) between the untreated and treated samples. At  $1 \times IC_{50}$  compound 3 is less active against LSD1 inhibition than tranylcypromine but at  $10 \times IC_{50}$ , compound 3 appears to be more active against LSD1 than tranylcypromine. Future repeats of this experiment could, according to the above results, confirm a possible concentration dependent reaction of compound 3. Results shown in Figure 3.8 indicate an inhibition of LSD1 enzyme activity in isolated *P. falciparum* trophozoite resulting from parasite treatment with the fluorinated polyamine analogue, compound 3.

### **3.7. Isolation of *P. falciparum* histones**

To determine if possible epigenetic changes were affected due to LSD1 inhibition observed in section 3.6, parasite histones were isolated and used for MS analysis to identify the presence of histones and possible PTM pattern changes. The inhibition of an epigenetic enzyme, such as LSD1, will cause a change in the histone code. Parasite histones were acid extracted and MS analysis used to compare three extraction protocols to identify and confirm which histones were present and the coverage rates of each histone.

#### **3.7.1. Protein concentration standard curve**

Dye based protein quantification methods include the Bradford assay, the BCA assay, the Lowry method, detergent-based fluorescent detection and amine derivatisation, to name a couple. The BCA assay was chosen for experiments as it is more detergent-compatible than the Bradford and Lowry methods (Smith *et al.*, 1985). Bovine serum albumin (BSA) is often used as a protein standard as it is commercially available (Noble, 2009). Using the BSA standards, a line graph was plotted, from which the sample protein concentrations were calculated.

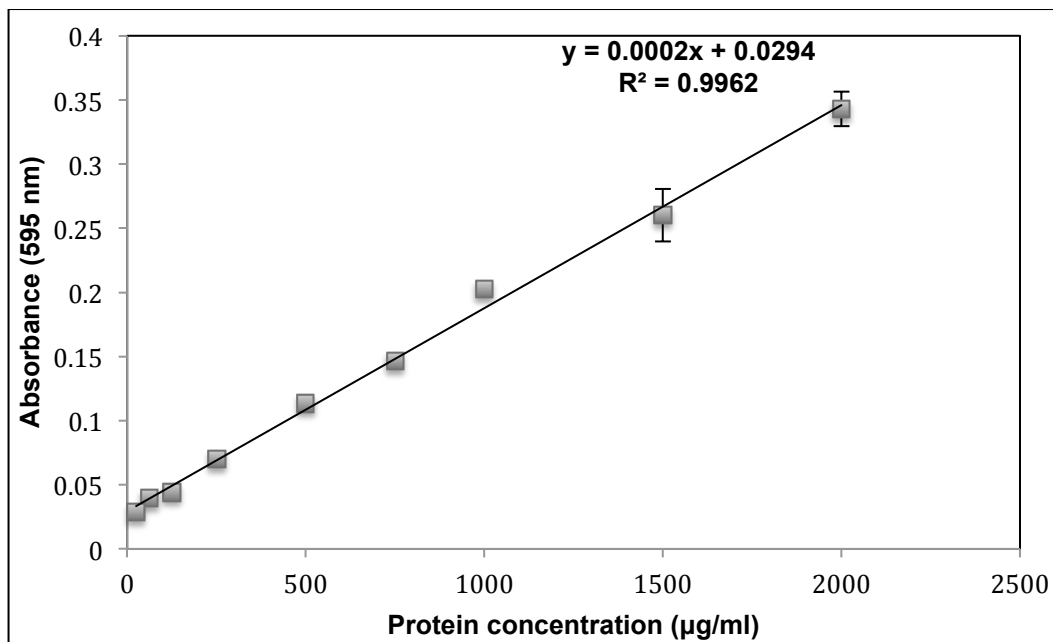


**Figure 3.9: A regression line graph of BSA standards.** Using the BCA kit and supplier instructions, BSA protein standards (2000 µg/ml; 1500 µg/ml; 1000 µg/ml; 750 µg/ml; 500 µg/ml; 125 µg/ml; 62.5 µg/ml; 25 µg/ml; 0 µg/ml) were used to construct a line graph. Standards were incubated with 50 parts reagent A and 1 part reagent B and incubated at 37°C for 30 min-2 h. The 96-well plate was allowed to cool to RT and absorbance was measured at 595 nm. Data are representative of three independent experiments performed in duplicate ± S.E. Where not shown, error bars fall within the symbols.

The BSA standards' absorbance values were recorded at 595 nm and a coefficient of correlation ( $R^2$ ) was calculated equal to 0.99.  $R^2$  is a measure of the strength of the linear relationship of two variables and is calculated by the division of the covariance of the variables by their standard deviations. The  $R^2$  of Figure 3.9 is acceptable (>0.95) and was used to determine the protein concentrations of the isolated histone samples listed in Table 3.7 and Table 3.8.

### 3.7.2. Concentrations of *P. falciparum* acid extracted histone proteins

Data compiled in Table 3.7 compares the differences in protein concentrations when histones were isolated from freshly saponin lysed parasites as opposed to histones isolated from parasites stored at -20°C before saponin lysis occurred.

**Table 3.7: Concentrations of acid extracted histone proteins from fresh and frozen *P. falciparum* parasites.** Synchronised, trophozoite strain 3D7 parasites (6-8% parasitaemia, 5% haematocrit) were lysed using 0.15% (w/v) saponin. Three histone acid extraction procedures (Issar and Scherf *et al.*, Merrick *et al.*, Trelle *et al.*) were used on both fresh saponin lysed parasites and saponin lysed parasites stored at -20°C before histone isolations (frozen parasites were allowed to thaw at RT). Protein concentrations were determined using the BCA protein quantitation kit and absorbance was recorded at 595 nm. Data are representative of two independent repeats.

Samples	[Protein] isolated from fresh samples (µg/ml)	[Protein] isolated from frozen samples (µg/ml)
Issar and Scherf <i>et al.</i>	246	1064
Merrick <i>et al.</i>	276	671
Trelle <i>et al.</i>	384	722

Protein concentration values (Table 3.7) show that higher histone concentrations were obtained from parasite isolates after freeze-thawing than from fresh isolates. These results concurred with those of Merrick *et al.* who isolated only 276 µg protein/ml histones from fresh parasites but 671 µg/ml histones from frozen parasite samples. A possible reason could be because the ice crystals, which form during freezing of the samples, disrupt and burst parasites much better upon thawing than only extractions directly from intact, isolated parasites (Deutcher, 2009). Therefore, further experiments performed in this study used thawed parasite samples for histone extractions and comparisons. Furthermore, following protein quantification, samples were separated according to size on an SDS-PAGE gel and isolated histone protein bands were identified by MS analysis.

### 3.7.3. SDS-PAGE separation of *P. falciparum* acid extracted histone preparations.

Before analysis of histone preparations by SDS-PAGE their concentrations were determined using the BCA quantitation kit (Table 3.8).

**Table 3.8: Concentration of acid extracted *P. falciparum* histone proteins.** Histone samples were isolated using three acid extraction methods (Issar and Scherf *et al.*, Merrick *et al.*, Trelle *et al.*) and the concentrations determined using a BCA protein quantitation kit. From each sample, 10  $\mu$ l was incubated with 50 parts reagent A and 1 part reagent B and incubated at 37°C for 30 min-2 h. After incubation, samples were allowed to cool to RT and absorbance was measured at 595 nm. Data are representative of two independent repeats.

<b>Samples</b>	<b>[Protein] (<math>\mu</math>g/ml)</b>
<b>Issar and Scherf <i>et al.</i> (Lane 1)</b>	4334
<b>Issar and Scherf <i>et al.</i> (Lane 2)</b>	4145
<b>Trelle <i>et al.</i> (Lane 3)</b>	4320
<b>Trelle <i>et al.</i> (Lane 4)</b>	4009
<b>Merrick <i>et al.</i> (Lane 5)</b>	4378
<b>Merrick <i>et al.</i> (Lane 6)</b>	4290

The concentrations calculated (Table 3.8) were all in the same range, indicating that all three histone acid extraction procedures were effective in isolating high concentrations of protein. Therefore, to determine which protocol resulted in the isolation of high concentrations of histone 3, MS analysis was used to determine the coverage ranges of isolated histones from all three extraction protocols, after SDS-PAGE separation. About 16  $\mu$ g of each sample was loaded and separated on an AnyKD pre-cast SDS-PAGE gel (Bio-Rad) and stained with Coomassie Brilliant Blue dye (Figure 3.10). The pre-cast gel has an optimum separation range of 10-100 kDa and is run at a constant voltage (300 V) for 20 min.

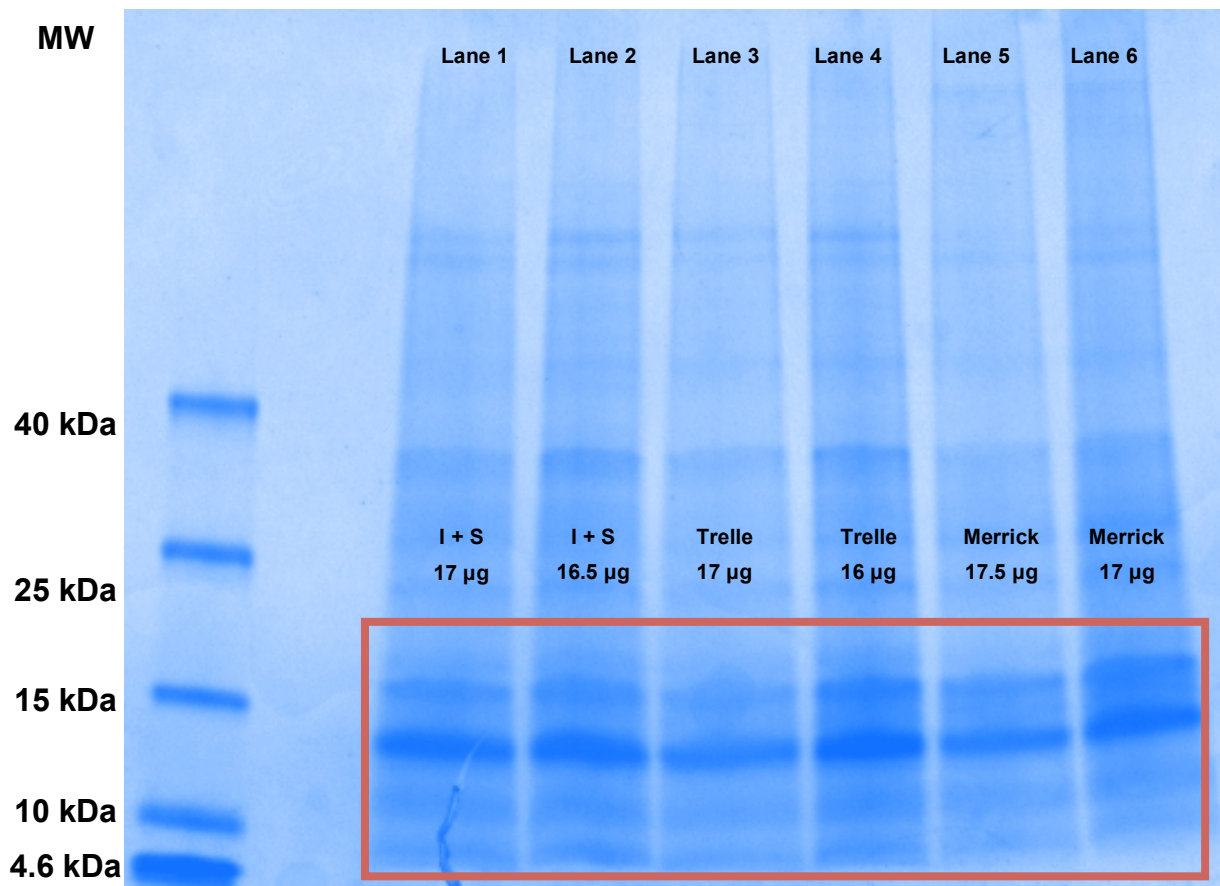


**Figure 3.10: Separation of acid extracted *P. falciparum* histones on an AnyKD SDS-PAGE gel.** Separated histone proteins, indicated by the red block (10-17 kDa), were isolated using three acid extraction protocols: Issar and Scherf *et al.* (I+S); Trelle *et al.* (Trelle); Merrick *et al.* (Merrick). For each sample, about 16 µg of protein was loaded in each well of the AnyKD pre-cast SDS-PAGE gel. The gel was run at a constant voltage (300 V) for 20 min in a running buffer (25 mM Tris, 192 mM glycine, 0.1% SDS). After protein separation, the gel was stained overnight in 0.1 % Coomassie Brilliant Blue R-250, 40% methanol and 10% acetic acid at 37°C and de-stained overnight at 37°C in 25% methanol. Data are representative of two independent repeats, performed in duplicate.

The separated histones on the SDS-PAGE gel were originally identified using mass spectrometry in the Salcedo-Amaya thesis (2012). There should preferentially be five clear bands representing all eight known *P. falciparum* histones (Trelle *et al.*, 2009). From Figure 3.10, the two most prevalent histone bands separated from all three acid extraction protocols were speculated to be H3, H3.3 and H2A, H2Bv. The two bands representing H2B and H4 are very faintly visible just above the 10 kDa and 4.6 kDa markers, respectively. The band indicative of H2A.Z and centromeric H3 was not clearly visible using any of the three acid extraction procedures (Figure 3.10).

The ability to clearly draw distinct conclusions regarding band presence is affected negatively by the specific visibility on this gel, but the method has been validated previously (Trelle *et al.*, 2009). Subsequently, MS analysis was performed on the potential histone bands to identify the proteins.

### 3.8. Mass spectrometry analysis of isolated histone samples

The bands containing the suspected histone proteins (red block, Figure 3.9) were analysed with MS at the CAF, University of Stellenbosch. The histones identified by the different isolation protocols are listed in Table 3.9.

**Table 3.9: The histones isolated using three acid extraction protocols and identified by mass spectrometry.** Histone samples were isolated using three acid extraction procedures (Issar and Scherf *et al.*, Merrick *et al.*, Trelle *et al.*). The protein concentration was calculated using a BCA kit and about 16 µg proteins were separated on an anyKD SDS-PAGE gel. Histones were analysed with MS at the CAF, University of Stellenbosch. The coverage of all eight known histone proteins were compared and averaged for each sample. Data are representative of two repeats, performed in duplicate.

Histones	Issar and Scherf <i>et al.</i>		Trelle <i>et al.</i>			Merrick <i>et al.</i>			
	Coverage	Average (%)	Coverage	Average (%)	Coverage	Average (%)	Coverage	Average (%)	
H2A	33	80	57	83	82	82	58	81	70
H2A.Z	85	71	78	90	86	88	72	91	81
H2B	74	100	87	97	76	87	92	69	80
H2B.Z	83	85	84	93	80	86	72	86	79
H3.1	73	79	76	98	78	88	77	84	81
H3.3	47	88	67	74	88	81	-	74	37
H3 cen	-	-	-	-	-	-	-	-	-
H4	68	85	77	93	75	84	78	84	81

In Table 3.9, the MS analyses identified seven of the eight known histone proteins expected in *P. falciparum* parasites, which were isolated using both the Issar and Scherf *et al.* and Trelle *et al.* protocols. These two acid extraction protocols allowed for the isolation of all four canonical histone classes (H2A, H2B, H3 and H4) as well as an H2A variant (H2A.Z), an H2B variant (H2B.Z), and an H3 variant (H3.3). The protocol from Merrick *et al.* did isolate all four canonical histones but did not isolate H3.3 in both samples, and as such could not be accepted as significant. None of the protocols isolated centromeric H3 (H3 cen).

## **Chapter 4**

---

### **Discussion**



Affecting mostly developing countries of the world, malaria is caused by the protozoan genus *Plasmodia*, which is transferred to the human host via female *Anopheles* mosquitoes during a blood meal. The most severe disease symptoms and highest rate of mortality is associated with *P. falciparum* parasites. According to the WHO report, malaria affects about 250 million people annually, of which sub-Saharan Africa carries the largest burden (WHO, 2013). Although progress in disease treatment and control has been achieved, continuous advances are required to eradicate and eliminate the disease. Due to increasing problems posed by parasite and mosquito resistance towards currently available control treatments, a continued search is justified for novel antimalarial chemotypes.

Certain aspects of current cancer and antimalarial research have been focusing on polyamine analogues as inhibitory agents. Polyamine analogues are structurally similar to natural polyamines and in some instances can functionally replace polyamines therefore offering therapeutic value. Polyamines can be found at increasing concentrations in rapidly proliferating cells, such as cancerous cells and parasitic protozoa. They are essential to cell growth and development (Birkholtz *et al.*, 2011) and interference in polyamine biosynthesis has been successfully applied to the treatment of African sleeping sickness, a disease caused by a closely related protozoan parasite. (Bellevue *et al.*, 1996). The death pathway resulting from polyamine analogues is exclusively apoptosis, defined as programmed cellular death.

Polyamines are aliphatic amines functioning by means of reversible ionic interactions with negatively charged macromolecules such as nucleic acids and membrane proteins (Muller *et al.*, 2008). In *P. falciparum* parasites, 14% of the metabolome consists of polyamines and due to distinct polyamine biosynthesis features in these parasites, novel drug targets in this pathway are being concentrated on (Birkholtz *et al.*, 2011). The usefulness of single polyamine pathway enzyme inhibitors, such as DFMO is limited for a variety of reasons. The rationale behind polyamine analogue design and synthesis is that the analogues deplete polyamine content by single/multiple mechanisms. Traditionally, polyamine analogues can either inhibit polyamine biosynthesis

(polyamine antimetabolite), compete for uptake or displace the natural polyamines within the cell (polyamine mimetics), block polyamine uptake mechanisms, or induce both catabolic enzymes and polyamine export (Wallace and Niiranen, 2007). However, polyamine analogues can also act via mechanisms that are independent of the polyamine pathway, such as targeting epigenetic regulation.

From previous studies concerning polyamine analogues, results indicated that the analogues were epigenetic modulators by means of their LSD1 inhibitory activity in cancer cells (Huang *et al.*, 2007). From experimental results in cancer cells, the leading compounds of the two guanidine and biguanidine polyamine analogue libraries consisted of a (thio)urea and a bulky aromatic N-terminal substituent (allowing for increased activity) as opposed to an alkyl or benzyl substituent (Sharma *et al.*, 2010).

Following the promising results from the above mentioned cancer studies, a third series of alkylated (bis)urea and (bis)thiourea compounds were synthesised and tested for antiplasmodial activity (Verlinden *et al.*, 2011). These analogues showed growth inhibitory activity at low nanomolar IC<sub>50</sub> values (100-650 nM), were highly selective and cytotoxic and arrested parasite proliferation within 24 hours of exposure by means of arresting nuclear division. The leading compound (Compound 30) consisted of a 3-6-3 carbon backbone and a (bis)urea constituent, exhibiting an *in vitro* IC<sub>50</sub> of 88 nM against *P. falciparum* parasites. (Verlinden *et al.*, 2011).

The predicted plasma levels, used to assess permeability, showed that compound 30 would probably be absorbed well. To assess the half-life of compound 30, a microsomal stability assay was used with human, rat, dog and mouse liver microsomes. However, the microsomal stability and rate of *in vivo* clearance for compound 30 could not be established. Furthermore, the *in vivo* efficacy studies in the *P. berghei* murine model revealed that most of the concentrations of compound 30 were below the limit of quantification. The reason for the low bioavailability is unclear, but could be a result of low

absorption or rapid metabolism of the compound in the murine gastrointestinal tract (Verlinden *et al.*, Unpublished Results).

There is increasing evidence that minor modifications to a drug candidate can result in major changes in pharmacological properties. The fluorination of a compound should allow for it to maintain or improve its inherent biological activity and metabolic stability (Skagerberg *et al.*, 1989). Fluorine molecules are sufficiently similar in steric size and lipophilicity compared to hydrogen and should therefore be able to fit into the enzyme active site without added hindrance (Filler, 2009). The fluorine molecule acts as a hydrogen bond acceptor, which increases its binding strength to the drug target via hydrogen bond formation (Skagerberg *et al.*, 1989). The carbon-fluorine bond is extremely strong, making compounds more resistant to metabolic degradation and allowing for increased lipophilicity. The best drug candidates are usually balanced – not too hydrophilic, nor too lipophilic. Therefore, four fluorinated structural polyamine derivatives, based on the 3-6-3 (bis)urea backbone of compound 30 were synthesised. Fluorine molecules were added to each compound at strategic positions on the aromatic rings, as indicated in Table 3.1 and the analogues were tested for their drug-likeness and pharmacokinetic features, using ADME profiles.

ADME profiles are used to predict the disposition of compounds within an organism and as such, its' drug-likeness, which is expressed as rules such as Lipinski's Rule of Five (Bickerton *et al.*, 2012). Lipinski's rules state that a compound is more likely to exhibit poor absorption and permeation when two parameters are out of range. The parameters a compound should not have a molecular weight more than 500 g/mol, not have more than five HBD or ten HBA and a LogP value (the logarithm of the octanol/water partition coefficient) less than five. It is often referred to as the "rule of five" because the cut off values for all four parameters are most often close to the number five or multiples of five (Lipinski *et al.*, 2001). To investigate the ADME properties of a compound it is important to review how the compounds are administered and the processes in the body that affect a good pharmacokinetic profile (Vugmeyster, 2012; Voet&Voet., 2011).

An orally administered drug needs adequate absorption from the gut wall into the blood circulatory system. It is transported to the liver where it is acted on by hepatic enzymes, after which the compound is excreted via the bile or metabolised. It is transported via arterial blood to the rest of the body and to its' target organ. Once the effect of the drug has been triggered, it should be adequately eliminated to avoid bioaccumulation (Schneider *et al.*, 2013). Increased lipophilicity refers to the improved ability of compounds to dissolve in fats, oils, lipids, plasma proteins and non-polar solvents. The increase in lipophilicity of the polyamine analogues due to the addition of fluorine molecules could improve compound quality and likelihood of therapeutic success (Arnott, 2012).

The ALogP value refers to the lipophilicity of a compound and is important for compound absorption, drug-membrane interactions, metabolism, promiscuity and toxicity (Leeson, 2012). In terms of absorption from the gut wall into blood circulation, the predicted data ranges comparing the four fluorinated polyamine analogues to compound 30 are, however, very similar and it cannot be deduced from the model that the fluorination specifically impacted or improved lipophilicity of the polyamine analogues. However, the ALogP values differ a lot from that of CQ, possibly predicting that the compounds are more lipophilic than CQ. All five polyamine analogues and CQ exhibited HIA values of 0, which is indicative of good intestinal absorption with at least 90% predicted to be absorbed into the blood circulation.

The aqueous solubility, which is critical to drug delivery, depends on a variety of factors such as the HBD and HBA properties of the molecule as well as that of water and the energy costs related to the disruption of the molecule's crystal lattice to allow for solubilisation (Lipinski *et al.*, 2001). An excessive number of HBD and HBA has a negative effect on the permeability of compounds across a lipid bilayer due to them being too polar (Lipinski *et al.*, 2001; Voet&Voet., 2011). All five polyamine analogues showed HBA and HBD numbers, which were much higher than that of CQ (HBA-3 & HBD-1). This could be a factor further affecting solubility. Furthermore, the fluorinated polyamine analogues all have lowered HBA and HBD numbers, compared to

compound 30. Possibly, these results could be perceived as a positive prediction towards an improved metabolic profile for the fluorinated chemotypes.

Data from Table 3.3 shows that compound 1, compound 3 and compound 4 tested too soluble in water at 25°C, indicating that the compounds would be directly excreted without proper absorption. Compound 30 and compound 2 showed data correlating to optimal solubility for drug-likeness. The solubility of compound 30 was confirmed with the *in vivo* efficacy data (Verlinden *et al.*, Unpublished Results). The difference between compound 2 and the other fluorinated analogues being that: 1) it has difluorinated terminal rings and 2) the highest molecular weight of the series (613.52 g/mol). However, the high throughput screening of compounds often predicts compounds to be more soluble than the true thermodynamically solubility achieved *in vivo* (Lipinski *et al.*, 2001).

Results show a drastic difference in values of PPB between compound 30, the fluorinated analogues and CQ. Compound 30 has a high, positive PPB value (3.0968), whereas the values for the fluorinated analogues and CQ are negative, ranging from -1.84 to -2.66. Plasma proteins include proteins such as lipoproteins, glycoproteins and serum albumin. The lowered likelihood of binding to plasma proteins could result in the improved ability of compounds to diffuse through membranes and have greater therapeutic effects (KOMMMU, 2013). Due to plasma protein binding being important for improved *in vivo* efficacy, this result is an additional positive prediction towards an improved metabolic profile.

The QED value can range between zero and one, a range from all properties unfavourable for drug-likeness to all properties favourable for drug-likeness, respectively (Bickerton *et al.*, 2012). The QED method is better at differentiating between drug and non-drug compounds than Lipinski's rules because it is not based on cut-off values of four rules only. It was used to show that compounds, which do not comply with the five Lipinski rules, have a range of drug-likeness that can be correlated with those which do comply with

the Lipinski rules (Leeson, 2012). The polyamine analogues had low QED values, ranging from 0.107 to 0.14, which suggests that according to this classification these compounds have a low favourability for drug-likeness.

It has been suggested that few classes (except most antibiotics, antifungals, vitamins and cardiac glycosides) do comply with the "rule of five" because these orally available classes can act as substrates for naturally occurring transporter molecules (Lipinski *et al.*, 2001). According to the Biscu-it QED on Silico-it program, the fluorinated analogues comply with three of Lipinski's rules, 1) an ALogP value less than five, 2) two HBD each and 3) six HBA each. These rules deal, however, only with permeability and solubility as barriers to absorption. Intestinal metabolism and intestinal wall transporter molecules, which influences the measurements of drug bioavailability, are mostly beyond the scope of these specific rules (Lipinski *et al.*, 2001) and *in vivo* efficacy experiments on this series are underway.

Ideally, an antimalarial should be selective and non-toxic to the human host. It should be orally bioavailable and cure the disease within a few days, so as to decrease the spread and materialisation of resistance (Birkholtz *et al.*, 2011). Compared to compound 30, the fluorinated molecules share similar pharmacokinetic *in silico* results for several aspects. *In vivo* data (Verlinden *et al.*, Unpublished Results) showed that compound 30 was unable to appreciatively diminish *P. berghei* parasitaemia. With the dosing scheme used, most concentrations were below the limit of quantification during pharmacokinetic *in vivo* experiments and results pointed towards a lack of oral bioavailability or to metabolic instability. Therefore, due to similarity in the *in silico* predictions, one can assume that there is a chance that the fluorinated derivatives might not show improved *in vivo* model results. However, there is a drastic difference in the plasma protein binding capacity of compound 30 and the fluorinated polyamine analogues. The fluorinated analogues have negative binding energies and as such, fluorination might have a significant effect on efficacy *in vivo*. However, the focus of this study was not to confirm improved bioavailability of the fluorinated series, but rather to investigate the antiparasitic capacity and selectivity of this series.

The *in vitro* IC<sub>50</sub> values of the fluorinated series of (bis)urea polyamine analogues were calculated using a panel of *P. falciparum* strains. These positive *in vitro* IC<sub>50</sub> values in the low nanomolar range shows that there are no signs of cross-resistance and that the compounds are effective acting against a range of parasite phenotypes. The results show that the *meta* fluorinated compound 1 and the *para* fluorinated compound 3 are the leading analogues of this series. Both showed a decrease of approximately 50% in antimalarial activity (Table 3.5) compared to the IC<sub>50</sub> value of the original unfluorinated compound 30 in strain 3D7 (drug sensitive) and W2 (drug resistant). The *ortho/para* fluorinated compound 2 and the *ortho* fluorinated compound 4 were the least active analogues. The *para* fluorination is prone to hydroxylation in the phase I metabolism and as such is important for improved metabolic stability. The hydroxylation converts lipophilic compounds into more water soluble compounds, resulting in the compounds being more readily excreted (Filler, 2009). Therefore, the presence of this fluorine molecule could aid the oral bioavailability of the compound *in vivo*, especially regarding the *in silico* bioavailability results obtained.

The fluorine group may also affect the pK<sub>a</sub> and hydrogen bonding properties of the adjacent urea nitrogen (N). The proximity of the fluorine to the terminal urea N determines the strength of hydrogen bonding between the urea N-H and the F. Consequently the N-H easily forms a hydrogen bond with the *ortho* fluorine whereas the chances of it forming with the *para* and *meta* fluorine are remote (Filler, 2009). This hydrogen bonding and not the *ortho* fluorine steric bulk may distort the polyamine chain conformation and the aromatic ring spatial orientation. The uptake by the polyamine transporter could possibly be affected by this distortion. The hydrogen bonding on its own will also affect the cationic charge magnitude on the N and this could also potentially be affecting the binding to a polyamine transporter.

The therapeutic activity of most current antimalarials is severely compromised due to either toxicity or resistance (Schrader *et al.*, 2012). Due to the extremely high percentage of children under the age of five and pregnant

women who are prone and more susceptible to malaria, antimalarials need to act quickly and efficiently (Biamonte *et al.*, 2013). Following the antiplasmodial activity results, the resistance index (Table 3.5) was calculated by dividing the  $IC_{50}$  value of the chloroquine resistant strain (W2) by the  $IC_{50}$  value of the non-resistant strain (3D7). The resistance index represents the drugs' efficacy against resistant cell lines versus the corresponding non-resistant cell line.

The RI values of all fluorinated compounds (except compound 4) are in close range to that of compound 30, which indicates a similar level of efficacy towards resistant cell lines. The *ortho* fluorination of compound 4 seems to increase the RI value and decrease the selectivity index of this compound with regards to that of compound 30, making it less effective against resistant cells lines and less selective towards parasite cells. *In vitro* data shows that compound 4 also had the highest  $IC_{50}$  value in this series. The *para* fluorination (compound 3) results in the lowest  $IC_{50}$  value, lowest RI and highest SI. All favourable *in vitro* results compared to that of compound 30 with the added benefit of an  $IC_{50}$  value, which is 2.5-fold more active in terms of antiplasmodial activity. RI results indicated that fluorinated derivatives (0.25-0.5) are lower than that of CQ (4.1), indicating a probable different mechanism of resistance than for CQ. Therefore, the fluorinated series is less prone to be affected by resistance mechanisms associated with, e.g., mechanistically distinct modes of action such as mutations of the *P. falciparum* CQ Resistance Transporter (Janni Papakrivos *et al.*, 2012; Zishiri *et al.*, 2011).

For further *in vitro* cytotoxicity and selectivity data (Table 3.6), compounds were screened using HepG2 cancer cells. Selectivity is an important drug property to evaluate as cytotoxicity of drugs may result in the death of mammalian cells once the compound has been ingested. These two parameters were investigated because ideally a new drug should be efficacious against drug-resistant strains and be safe and suitable for use by small children and pregnant women (Fidock *et al.*, 2013). The calculated selectivity indices are an indication that all four compounds are indeed exceedingly more selective towards the parasites than mammalian cells.



From the cytotoxicity and selectivity data towards mammalian cells, compound 1 had the lowest selectivity index being 3078-fold more selective towards parasite cells than mammalian cells. Not only is the leading fluorinated compound (compound 3) more selective but also more effective against resistant strains and shows the lowest  $IC_{50}$  value, it has a mode of action, which is most probably not similar to that of CQ.

Recent reports have shown that artemisinin-treated parasites, once in the ring stage of the life cycle, has the ability to enter into a state of hibernation (Hoshen *et al.*, 2000; Teuscher *et al.*, 2010). During this dormant phase, specifically ring-stage parasites are protected from lethal effects of drugs. Once the drug pressure has been removed, viable parasites return within a few days and parasitaemia increases accordingly (Codd *et al.*, 2011). Owing to the important link between dormancy and antimalarial treatment failure, the two leading compounds of the fluorinated polyamine analogues series were screened for the ability to suppress parasite proliferation after removal of drug treatment.

A recovery assay was performed as previously explained (Malmquist *et al.*, 2012) with slight modification. Parasite proliferation reversibility refers to excess available substrate competing and displacing inhibitor compounds or a secondary pathway delivering the missing elements, which allows for normal cellular processes to continue. Alternatively, parasite proliferation rescue refers to the required elements (of which production is inhibited) being absorbed from the environment. The results (Figure 3.2) showed that only compound 1 had a cytotoxic component, whereas compound 3 did not have a cytotoxic or cytostatic component. Future experiments should include both reversibility and rescue assays as the results might point to a possible mode of action or classify the analogues as polyamine antimetabolites or polyamine mimetics. The recovery assay results show that, similarly to dormancy, parasite proliferation continues after inhibitor removal.

Looking at the differences in results obtained for the fluorinated series, it can be assumed that the positioning of the fluorine molecule affects the efficacy of the compounds. More data, such as drug-active site binding strength needs to be collected or alternatively, computational models should be created to determine the best positioning of the fluorine molecules (*meta* versus *para*), resulting in optimum parasite inhibition. Parallel to this study, experiments were being performed using the fluorinated polyamine analogue series, to determine polyamine-dependent modes of action. Therefore, in order to shed light on the cellular pathways and proteins affected by these polyamine analogues, assays to establish or eliminate certain polyamine-independent modes of actions were done. These included  $\beta$ -haematin formation inhibition and LSD1 inhibition.

Strategies for target identification and mode of action determination rely on genetic, computational and biochemical principles (Ong *et al.*, 2009), and an antimalarial drug discovery goal is to achieve rapid parasite death (Malmquist *et al.*, 2012). A possible mechanism of action considered, due to the heterocyclic nature of the analogues, was the inhibition of  $\beta$ -haematin formation (Carter *et al.*, 2010). The haematin inhibition assays (Figure 3.3), revealed that compound 30 and compound 3 do not have a strong haematin inhibitory capacity, with higher  $IC_{50}$  values than that of CQ (11  $\mu$ M). The results could indicate that the primary mode of action of these compounds is different compared to that of CQ, due to the difference in  $IC_{50}$  values calculated. The inhibition of  $\beta$ -haematin formation could be a secondary or tertiary mode of action of these analogues as compounds were not able to inhibit  $\beta$ -haematin formation at low inhibitory concentrations. This hypothesis is supported by the RI values of these analogues, which suggests that analogues have a mechanism of action that is distinct to that of CQ. These results are promising as novel mechanisms of action are beneficial for future antimalarial compound development.

In 2010, a series of (bis)urea and (bis)thiourea polyamine analogues were shown to affect certain aspects of epigenetic regulation in cancer cells, such as the inhibition of LSD1 (Sharma *et al.*, 2010). A demethylase enzyme

specific assay was used to confirm changes in epigenetic enzyme activity in the presence of these analogues. Compared to screens done with the previous (bis)urea and (bis)thiourea library of compounds (Sharma *et al.*, 2010), the chemiluminescent assay (Huang *et al.*, 2007) was optimised for use on malaria parasites and used to determine the inhibitory effect on PfLSD1 activity. Chemiluminescent assays are widely used due to the high sensitivity with low detection limits, rapid signal detection and a wide dynamic range (Chaichi *et al.*, 2013). In order to optimise the reagents of the assay for later testing on the parasite, the recombinant human LSD1 enzyme was initially used as an indicator for changes in epigenetic regulation.

Specific enzymatic activity of LSD1 was determined optimising a luminol-dependent chemiluminescence assay, with H3K4me2 as substrate, to measure the production of H<sub>2</sub>O<sub>2</sub> (Huang *et al.*, 2007). The substrate purchased (H3K4me2) contained 21 amino acids because LSD1 requires at least 15 residues for efficient demethylation (Culhane *et al.*, 2010). In the presence of H<sub>2</sub>O<sub>2</sub> and luminol, HRP oxidised luminol, resulting in the production of chemiluminescence, which was recorded at 425 nm (Walker, 2010, Vdovenko *et al.*, 2012). Hydrogen peroxide is analytically the most useful oxidant of luminol but it requires the simultaneous use of an electrode, metal ion or enzyme such as horseradish peroxidase. Due to the assay being designed for use in cancer cells, the effect of each reagent on chemiluminescence was assessed. Luminol was oxidised at a very fast rate; about 50% of the activity was lost within 2 min after addition of substrate (Figure 3.4). Considering the buffer constituents, the presence of Tris-HCl showed a significant increase in activity due to its buffering capabilities at pH 8.5 (Mohan *et al.*, 2003). As supporting electrolytes, MgCl<sub>2</sub> and KCl had no effect on activity when added separately. However, all three reagents together resulted in a noteworthy increase in the luminescent readings. These results validate that the chemiluminescent activity of luminol has been found to be optimal in an alkaline solution, in the presence of supporting electrolytes such as KCl (Vdovenko *et al.*, 2012).

The recombinant parasite LSD1 enzyme is not commercially available and the possibility of recombinantly expressing the parasite enzyme was considered. As indicated on the PlasmoDB website ([www.plasmodb.org](http://www.plasmodb.org)), the enzyme is 350 kDa in size. Many malaria proteins are much larger than their homologues in other organisms. This increased length is due to the presence of inserts, which are disordered, and of low complexity and due the nature of these inserts, recombinant expression is not amenable. Another problem involving parasite protein expression is the A+T richness of the genome, which results in different codon usage compared to *E. coli*. Furthermore, the introductions of sporadic mutations of low complexity sequences, which are introduced by *E. coli*, are also problematic to protein expression (Birkholtz *et al.*, 2006). Therefore, the human recombinant LSD1 enzyme was purchased (Sigma-Aldrich), which was expressed in *E. coli* and had a molecular weight of 103 kDa.

The active site of LSD1 has considerable sequence homology to monoamine oxidase A and B, N-acetylpolyamine oxidase and spermine oxidase (Sharma *et al.*, 2010). Therefore, tranylcypromine, a monoamine oxidase A and B inhibitor was used as a positive control for LSD1 inhibition as no *Pf*LSD1 specific inhibitor has been identified to date (Hauser *et al.*, 2012). Tranylcypromine, acting as a time-dependent inhibitor of LSD1, inactivates nucleosomal demethylation at the LSD1/CoRest complex (Culhane *et al.*, 2010). As a known human LSD1 inhibitor, tranylcypromine had a very high IC<sub>50</sub> value in *P. falciparum* parasites, which was in the micromolar range (Figure 3.7). The high IC<sub>50</sub> value of tranylcypromine could be due to parasite specific attributes, such as factors affecting the movement of the compounds into the cells. The polyamine analogues could be entering the cells via a polyamine-specific transporter molecule and as such, this could be a reason for their improved IC<sub>50</sub> values when compared to tranylcypromine.

Using the luminol-dependent chemiluminescent LSD1 assay, tranylcypromine, the parent compound and the leading fluorinated analogue was screened for human LSD1 inhibition. In this study, we showed that tranylcypromine inhibited 97% of recombinant human LSD1 activity at 1 mM compared to the

untreated control. At a concentration of 1 mM, Compound 30 showed 30% enzyme activity inhibition compared to the untreated human LSD1 activity and Compound 3 was 5-fold less effective than tranylcypromine, but showed 84% enzyme activity inhibition compared to the untreated control. At a concentration of 10 mM all the compounds exhibited 100% enzyme inhibition (Figure 3.6).

Furthermore, *P. falciparum* parasites were isolated and tested for *Pf*LSD1 inhibitory activity. Compound 3 showed significant *Pf*LSD1 inhibition compared to both the untreated control (Figure 3.8). Due to the high activity of the untreated sample compared to the treated samples, these results indicate that the isolated trophozoite parasites were able to take up the polyamine analogue and tranylcypromine as substrates, showing significant LSD1 inhibition. The significant results obtained in Figure 3.8 are very promising because LSD1 is a validated drug target, involved in important epigenetic regulatory processes required for parasite survival, and there are currently no *Pf*LSD1 specific inhibitors available. These highly selective polyamine analogues are a structurally distinct, novel class of antimalarials (Verlinden *et al.*, 2011) that do not show general cytotoxicity in mammalian cells and do show appreciable antiplasmodial activity. To further validate the above-mentioned results, three histone extraction procedures were compared. The best extraction procedure could be used in future experiments to determine the global epigenetic changes in histone methylation in compound 3 treated *P. falciparum* parasites.

As highly conserved and abundant proteins (Shechter *et al.*, 2007), histones are small, basic proteins that form nucleosomes of about 150bp DNA (Croken *et al.*, 2012). They are bound to DNA by non-covalent forces, among which the ionic interactions between positively charged histone tails and DNA phosphate are the most important. Initial histone isolation studies showed that increased concentrations of histone proteins ( $\geq 50\%$ ) could be isolated from frozen and thawed parasites, instead of using freshly isolated parasites, due to disruption of red blood cell membranes by ice crystal formation (Deutcher, 2009).

Looking at the three protocols comparatively, the salts added to the various buffers of all three protocols, selectively release the histones from the chromatin (NaCl) and maintain the ionic strength of the buffer (KCl and MgCl<sub>2</sub>). The addition of acid to the sample decreases the pH of the solution, allowing for the extraction of histones from the nuclear material. The proteins are precipitated with TCA and washed with acetone to remove acid from the solution without dissolving the protein pellet (Shechter *et al.*, 2007). Acid extraction partially neutralizes the DNA phosphates, diminishing the ionic interactions. The histones are denatured but the lyophilisates are freely soluble in solutions with low ionic strength. The salts then allow the condensation of parts of the charged molecules into compact, globular structures that interact with one another or possibly other histone molecules.

Furthermore, all three protocols used TCA for precipitation, although the mechanism of action by this monovalent anion is still not clearly understood. It has been shown that the three chloro- groups of the acetic acid molecule are very important for the precipitation reaction and that the pH of the solution is not the only determining factor of protein precipitation (Sivaraman *et al.*, 1997). The suggested mechanism of action is hydrophobic aggregation, due to an increase in intermolecular interactions and increased exposure of hydrophobic regions (Xu *et al.*, 2003).

Looking at factors affecting the differences in results obtained from the three protocols, the Trelle *et al.* protocol and the Merrick *et al.* protocol both added a protease inhibitor cocktail (PI) to their buffers, which was not present in the Issar and Scherf *et al.* buffers. The PI used, inhibits a broad-spectrum of serine, cysteine and metalloproteases as well as calpains and is used to prevent proteolytic degradation and preserves cellular protein compositions (cOmplete ULTRA tablets, Roche). As indicated in Table 3.9, the Trelle *et al.* protocol, using the PI cocktail had equal or higher coverage percentage for all eight histones present, when compared to coverage of Issar and Scherf *et al.* The Merrick *et al.* protocol had higher coverage for histones H2A, H2A.Z, H3.1 and H4, in comparison to Issar and Scherf *et al.* The only other notable

difference between the three procedures is the acid extraction times. Trelle *et al.* extracts histone proteins for an hour and a half, whereas Merrick *et al.* and Issar and Scherf *et al.* acid extracts for two and a half hours. Acid extraction does, however, denature cellular modifying enzymes and proteases faster than high-salt extraction procedures and this could be a factor affecting isolated protein yields (Shechter *et al.*, 2007).

Separation on an SDS-PAGE gel showed that the most prevalent histone bands separated by all three acid extraction protocols was firstly H3 and H3.3 in line with the 15 kDa marker, and secondly H2A and H2B.Z ( $\pm 14$  kDa). Two slightly less visible but existent bands, indicative of H2B and H4, lay between the 10 kDa and 4.6 kDa markers respectively. The band indicative of H2A.Z and H3cen, which should be above the 15 kDa marker, was not even slightly visible to the naked eye in any of the three protocols used. The contaminating bands are a collection of human and *P. falciparum* proteins (Trelle *et al.*, 2009). MS analysis was used to determine the coverage percentage of each histone band present per extraction procedure, as seen on the SDS-PAGE gel (Figure 3.10).

MS analysis is an extremely valuable analytical technique. It is based on the conversion of sample molecules into gaseous ions, which are further separated and detected in a mass spectrometer according to their mass-to-charge ratio (Walker, 2010). According to the MS data of this study, all three protocols allow for the isolation of the 4 canonical *P. falciparum* histones (H2A, H2B, H3 and H4). Issar and Scherf *et al.* and Trelle *et al.* both allow for the isolation of three of the variant histones, namely H2A.Z, H2B.Z and H3.3. Merrick *et al.* allows for the isolation of all four canonical *P. falciparum* histones but isolates only 2 variant histones (H2A.Z and H2B.Z). The average coverage of the H3.3 variant is extremely low (37%) as isolated by the Merrick *et al.* protocol, due to it being present in a single sample only. This could be due to experimental error.

None of the protocols compared isolated H3cen (Table 3.9). H3cen is primarily associated with chromosome centromeres and are involved in

chromatin condensation. Therefore, it is expected to be present at lower concentrations compared to the canonical histones (Trelle *et al.*, 2009). Mostly, PTMs studied at genome level are associated with gene expression. However, *P. falciparum* H3cen is defined only as a structural domain within the genome (Duffy *et al.*, 2014). From this data, no coverage of H3cen was recorded with any of the three extraction procedures used. In terms of further studies concerning LSD1 inhibition, the histone extraction technique used should result in optimal isolation of H3 because LSD1 demethylates H3K4me1 and H3K4me2 residues. Therefore, from the data collected, it is recommended that due to the high concentration of histone proteins extracted ( $\pm 4000 \mu\text{g/ml}$ ), the ease of assay use, the coverage of H3 ( $\pm 85\%$ ), the Trelle *et al.* histone extraction protocol is the best extraction protocol for further studies.

Due to the promising results discussed thus far, the effect of LSD1 inhibition on parasite PTMs by means of compound 3 treatment should be a definite future perspective. These changes could be selected for using polyclonal antibodies specific for core histone H3, H3K4me1, H3K4me2, H3K4me3, H3K9me3 and H3K9ac. The canonical histone H3 detection can be used as a control to show its definite presence as all modifications that should be focussed on are on H3. Once the LSD1 enzyme is inhibited, there should be an increase in the concentration of H3K4me1 and H3K4me2 (Huang *et al.*, 2007). This is due to the enzyme being able to demethylate only mono- and dimethylated residues. The level of H3K4me3 residues should not be affected, as it is not a substrate for LSD1 (Huang *et al.*, 2007, Sharma *et al.*, 2010).

Results obtained from this dissertation shows that the fluorination of compound 30 led to improved antiplasmodial activity (at a low nanomolar  $\text{IC}_{50}$  range) and improved selectivity. The leading fluorinated polyamine analogue (compound 3) inhibits the epigenetic *P. falciparum* enzyme LSD1. The best histone extraction protocol for future PTM studies was determined to be Trelle *et al.*, as confirmed by MS data of histone coverage. Future experiments should consist of both MS data and Western Blot data comparing the levels of



methylated H3 residues of fluorine polyamine analogue treated and untreated *P. falciparum* parasite samples.

## **Chapter 5**

---

### **Concluding Discussion**

After *in vivo* studies on the parent compound of a (bis)urea polyamine analogue series showed signs of metabolic instability, the terminal rings of the 3-6-3 polyamine analogue backbone underwent minor changes to determine if improved antiplasmodial activity and selectivity could be achieved. Furthermore, this series of compounds were tested for their ability to inhibit the activity of the epigenetic enzyme LSD1 within malaria parasites.

The results obtained from this research project showed that by changing the terminal ring constituents of the 3-6-3 polyamine backbone, with the addition of fluorine molecules, various positive changes occurred. Firstly, the *in vitro* antiplasmodial activity improved as tested against a panel of *P. falciparum* parasites, showing no signs of cross-resistance. The *para* and *meta* monofluorination of the terminal rings resulted in the lowest nanomolar IC<sub>50</sub> concentrations of 35 nM and 41 nM in *P. falciparum* strain 3D7 parasites. Secondly, the compounds had enhanced selectivity towards parasites, ranging from ~3000-fold to >8000-fold as compared to mammalian HepG2 cells. Thirdly, studies concerning possible mode of action options showed that  $\beta$ -haematin formation inhibition is not likely the primary target of the parent analogue or of the fluorinated polyamine analogues. Low RI values were calculated for the fluorinated analogues, suggesting that they do most likely not have a mode-of-action similar to that of CQ.

Moreover, this dissertation shows results concerning the optimisation and first time use of a luminol-dependent chemiluminescence assay in malaria parasites, specific towards epigenetic LSD1 enzyme activity inhibition. With using the human recombinant enzyme, results provided clear evidence that the leading fluorinated compound inhibited human LSD1 enzyme activity. There was a difference in inhibitory activity between the parent compound and the leading fluorinated analogue, of which the significance should be confirmed in future experiments. Furthermore, significant inhibition of *P. falciparum* LSD1 enzyme activity was achieved with the leading fluorinated compound. This assay, as has been adapted for use in malaria parasites, can be used to further establish the effect of novel and existing compounds on the validated, epigenetic drug target LSD1.

After comparison of three parasite histone protein acid extraction protocols, the Trelle *et al.* protocol resulted in the most accurate histone isolation results for further epigenetic-based studies. These future studies should include MS analysis (possibly also Western Blot Analysis) to show the differences in H3K4me2 and H3K4me1 methylation marks of untreated, compound 30 treated and compound 3 treated parasites. This would confirm that *Pf*LSD1 is the epigenetic target of the leading fluorinated polyamine analogue. Furthermore, this procedure can then be easily adapted for the analysis of novel LSD1 epigenetic inhibitory compounds.

Additionally, these analogues are being tested for improved metabolic stability and bioavailability, and as such the results of this dissertation has made an impact on the study of fluorinated polyamine analogues on epigenetic factors in the field of antiplasmodial research.

## References

- ALLEN, R. J. & KIRK, K. 2010. Plasmodium falciparum culture: the benefits of shaking. *Molecular and biochemical parasitology*, 169, 63-5.
- ANDREWS, K. T., HAQUE, A. & JONES, M. K. 2012. HDAC inhibitors in parasitic diseases. *Immunol Cell Biol*, 90, 66-77.
- ARNOTT JA, P. S. 2012. The influence of lipophilicity in drug discovery and design. *Expert Opinion Drug Discovery*.
- BANNISTER, L. H., HOPKINS, J. M., FOWLER, R. E., *et al.* 2000. A brief illustrated guide to the ultrastructure of Plasmodium falciparum asexual blood stages. *Parasitol Today*, 16, 427-33.
- BARTFAI, R., HOEIJMAKERS, W. A., SALCEDO-AMAYA, A. M., *et al.* 2010. H2A.Z demarcates intergenic regions of the plasmodium falciparum epigenome that are dynamically marked by H3K9ac and H3K4me3. *PLoS Pathog*, 6, e1001223.
- BELL, A. 2005. Antimalarial drug synergism and antagonism: mechanistic and clinical significance. *FEMS Microbiol Lett*, 253, 171-84.
- BIAMONTE, M. A., WANNER, J. & LE ROCH, K. G. 2013. Recent advances in malaria drug discovery. *Bioorg Med Chem Lett*, 23, 2829-43.
- BICKERTON, G. R., PAOLINI, G. V., BESNARD, J., *et al.* 2012. Quantifying the chemical beauty of drugs. *Nat Chem*, 4, 90-8.
- BIRKHOLTZ, L. M., BASTIEN, O., WELLS, G., *et al.* 2006. Integration and mining of malaria molecular, functional and pharmacological data: how far are we from a chemogenomic knowledge space? *Malaria journal*, 5, 110.
- BIRKHOLTZ, L. M., BORNMAN, R., FOCKE, W., *et al.* 2012. Sustainable malaria control: transdisciplinary approaches for translational applications. *Malar J*, 11, 431.
- BIRKHOLTZ, L. M., WILLIAMS, M., NIEMAND, J., *et al.* 2011. Polyamine homeostasis as a drug target in pathogenic protozoa: peculiarities and possibilities. *Biochem J*, 438, 229-44.
- BLANCHARD, J. S. 1990. Buffers: Principles and Practice. *Methods in Enzymology*, 104, 404.
- BRADFORD, M. M. 1976. A rapid and sensitive method for the quantitation of microgram quantities of protein utilizing the principle of protein-dye binding. *Analytical biochemistry*, 72, 248-54.
- BURROWS, J. N. 2012. Antimalarial drug discovery: where next? *Future medicinal chemistry*, 4, 2233-5.
- BURROWS, J. N., BURLLOT, E., CAMPO, B., *et al.* 2014. Antimalarial drug discovery - the path towards eradication. *Parasitology*, 141, 128-39.
- CALDERÓN, F. D. M. W., FRANCISCO-JAVIER GAMO 2013. Antimalarial Drug Discovery: Recent Progress and Future Directions. *Progress in Medical Chemistry*, 52.
- CARTER, M. D., PHELAN, V. V., SANDLIN, R. D., *et al.* 2010. Lipophilic mediated assays for beta-hematin inhibitors. *Comb Chem High Throughput Screen*, 13, 285-92.
- CHAICHI, M. J., KHAJVAND, T., MEHRZAD, J., *et al.* 2013. Indirect chemiluminescence-based determination of catecholamines in pharmaceutical formulations by furandicarboxylate derivative as a novel blue fluorescer in peroxyoxalate-H<sub>2</sub>O<sub>2</sub> system. *Analytical*

- sciences : the international journal of the Japan Society for Analytical Chemistry*, 29, 815-21.
- CHEN, H., GAO, F., HE, R., *et al.* 2007. Chemiluminescence of luminol catalyzed by silver nanoparticles. *Journal of colloid and interface science*, 315, 158-63.
- CHOOKAJORN, T., DZIKOWSKI, R., FRANK, M., *et al.* 2007. Epigenetic memory at malaria virulence genes. *Proceedings of the National Academy of Sciences of the United States of America*, 104, 899-902.
- CLARK, K., NIEMAND, J., REEKSTING, S., *et al.* 2010. Functional consequences of perturbing polyamine metabolism in the malaria parasite, *Plasmodium falciparum*. *Amino Acids*, 38, 633-44.
- CODD, A. F. T., KYLE, D.E., CHENG, Q., GATTON, M.L., 2011. Artemisinin-induced parasite dormancy: a plausible mechanism for treatment failure. *Malaria Journal*, 10.
- CORTES, A., CROWLEY, V. M., VAQUERO, A., *et al.* 2012. A view on the role of epigenetics in the biology of malaria parasites. *PLoS Pathog*, 8, e1002943.
- CROKEN, M. M., NARDELLI, S. C. & KIM, K. 2012. Chromatin modifications, epigenetics, and how protozoan parasites regulate their lives. *Trends in parasitology*, 28, 202-13.
- CUI, L., FAN, Q. & MIAO, J. 2008a. Histone lysine methyltransferases and demethylases in *Plasmodium falciparum*. *Int J Parasitol*, 38, 1083-97.
- CUI, L. & MIAO, J. 2007. Cytotoxic effect of curcumin on malaria parasite *Plasmodium falciparum*: inhibition of histone acetylation and generation of reactive oxygen species. *Antimicrobial agents and chemotherapy*, 51, 488-94.
- CUI, L. & MIAO, J. 2010. Chromatin-mediated epigenetic regulation in the malaria parasite *Plasmodium falciparum*. *Eukaryot Cell*, 9, 1138-49.
- CUI, L., MIAO, J., FURUYA, T., *et al.* 2008b. Histone acetyltransferase inhibitor anacardic acid causes changes in global gene expression during in vitro *Plasmodium falciparum* development. *Eukaryot Cell*, 7, 1200-10.
- CULHANE, J. C., WANG, D., YEN, P. M., *et al.* 2010. Comparative analysis of small molecules and histone substrate analogues as LSD1 lysine demethylase inhibitors. *Journal of the American Chemical Society*, 132, 3164-76.
- DALY, M. M., MIRSKY, A. E. & RIS, H. 1951. The amino acid composition and some properties of histones. *J Gen Physiol*, 34, 439-50.
- DESHPANDE, S. S. 2001. Principles and applications of luminescence spectroscopy. *Critical reviews in food science nutrition.*, 41, 155-224.
- DEUTCHER, M. P. 2009. Maintaining protein stability. *Methods in Enzymology*, 463.
- DUFFY M. F., S. S., JOSLING GA, PETTER M. 2014. Epigenetic regulation of the *Plasmodium falciparum* genome. *Briefings in Functional Genomics*, 13, 203 - 216.
- DUFFY, M. F., SELVARAJAH, S., JOSLING, G. A., *et al.* 2012. The role of chromatin in *Plasmodium* gene expression. *Cellular microbiology*.
- FAHRNER, J. A., EGUCHI, S., HERMAN, J. G., *et al.* 2002. Dependence of histone modifications and gene expression on DNA hypermethylation in cancer. *Cancer research*, 62, 7213-8.

- FEUERSTEIN, B. G., BASU, H. S. & MARTON, L. J. 1988. Theoretical and experimental characterization of polyamine/DNA interactions. *Advances in experimental medicine and biology*, 250, 517-23.
- FILLER R, S. R. 2009. Fluorine in medicinal chemistry: a century of progress and a 60-year retrospective of selected highlights. *Future medicinal chemistry*, 1, 777-791.
- FORNERIS, F., BINDA, C., BATTAGLIOLI, E., *et al.* 2008. LSD1: oxidative chemistry for multifaceted functions in chromatin regulation. *Trends in biochemical sciences*, 33, 181-9.
- FOTAKIS, G. & TIMBRELL, J. A. 2006. In vitro cytotoxicity assays: comparison of LDH, neutral red, MTT and protein assay in hepatoma cell lines following exposure to cadmium chloride. *Toxicol Lett*, 160, 171-7.
- FRENCH, J. B., CEN, Y. & SAUVE, A. A. 2008. Plasmodium falciparum Sir2 is an NAD<sup>+</sup>-dependent deacetylase and an acetyllysine-dependent and acetyllysine-independent NAD<sup>+</sup> glycohydrolase. *Biochemistry*, 47, 10227-39.
- GILL, J., KUMAR, A., YOGAVEL, M., *et al.* 2010. Structure, localization and histone binding properties of nuclear-associated nucleosome assembly protein from Plasmodium falciparum. *Malaria journal*, 9, 90.
- GOMEZ, C., ESTHER RAMIREZ, M., CALIXTO-GALVEZ, M., *et al.* 2010. Regulation of gene expression in protozoa parasites. *Journal of biomedicine & biotechnology*, 2010, 726045.
- GRIFFITH, K.S., LEWIS, L.S., MALI, S. & PARISE, M.E.  
Treatment of malaria in the united states-a systematic review.  
*Journal of the American Medical Association* (2007) **297**, 2264-2277.
- HAUSER, A. T., BISSINGER, E. M., METZGER, E., *et al.* 2012. Screening assays for epigenetic targets using native histones as substrates. *Journal of biomolecular screening*, 17, 18-26.
- HERNANDEZ-RIVAS, R., PEREZ-TOLEDO, K., HERRERA SOLORIO, A. M., *et al.* 2010. Telomeric heterochromatin in Plasmodium falciparum. *Journal of biomedicine & biotechnology*, 2010, 290501.
- HOBBS, C. A., PAUL, B. A. & GILMOUR, S. K. 2002. Deregulation of polyamine biosynthesis alters intrinsic histone acetyltransferase and deacetylase activities in murine skin and tumors. *Cancer Res*, 62, 67-74.
- HOEIJMAKERS, W. A., STUNNENBERG, H. G. & BARTFAI, R. 2012. Placing the Plasmodium falciparum epigenome on the map. *Trends in parasitology*, 28, 486-95.
- HOLLEY, J., MATHER, A., CULLIS, P., *et al.* 1992. Uptake and cytotoxicity of novel nitroimidazole-polyamine conjugates in Ehrlich ascites tumour cells. *Biochemical pharmacology*, 43, 763-9.
- HOU, H. & YU, H. 2010. Structural insights into histone lysine demethylation. *Current opinion in structural biology*, 20, 739-48.
- HUANG, Y., GREENE, E., MURRAY STEWART, T., *et al.* 2007. Inhibition of lysine-specific demethylase 1 by polyamine analogues results in reexpression of aberrantly silenced genes. *Proc Natl Acad Sci U S A*, 104, 8023-8.

- HUANG, Z.Q., MARTON, L. J., *et al.* 2012. Polyamine analogs modulate gene expression by inhibiting lysine-specific demethylase 1 (LSD1) and altering chromatin structure in human breast cancer cells. *Amino Acids*, 42, 887-98.
- ISSAR, N., RALPH, S. A., MANCIO-SILVA, L., *et al.* 2009. Differential sub-nuclear localisation of repressive and activating histone methyl modifications in *P. falciparum*. *Microbes Infect*, 11, 403-7.
- ISSAR, N., ROUX, E., MATTEI, D., *et al.* 2008. Identification of a novel post-translational modification in *Plasmodium falciparum*: protein sumoylation in different cellular compartments. *Cellular microbiology*, 10, 1999-2011.
- IWATA, R., ITO, H., HAYASHI, T., *et al.* 1995. Stable and general-purpose chemiluminescent detection system for horseradish peroxidase employing a thiazole compound enhancer and some additives. *Analytical biochemistry*, 231, 170-4.
- JANNI PAPAKRIVOS, JULIANA M. SÁ & WELLEMS, T. E. 2012. Functional Characterization of the *Plasmodium falciparum* Chloroquine-Resistance Transporter (PfCRT) in Transformed *Dictyostelium discoideum* Vesicles. *Plos One*, 7.
- JIANG, S. & NAIL, S. L. 1998. Effect of process conditions on recovery of protein activity after freezing and freeze-drying. *Eur J Pharm Biopharm*, 45, 249-57.
- KING, O. N., LI, X. S., SAKURAI, M., *et al.* 2010. Quantitative high-throughput screening identifies 8-hydroxyquinolines as cell-active histone demethylase inhibitors. *PLoS One*, 5, e15535.
- KOMMMU, R., BHIMAVARAPU, R 2013. Detection of proteins in body fluids and plasma protein binding of various drugs. *International journal of inventions in pharmaceutical sciences*, 53-58.
- LACHNER, M., O'SULLIVAN, R. J. & JENUWEIN, T. 2003. An epigenetic road map for histone lysine methylation. *Journal of cell science*, 116, 2117-24.
- LACOUNT, D. J., VIGNALI, M., CHETTIER, R., *et al.* 2005. A protein interaction network of the malaria parasite *Plasmodium falciparum*. *NATURE*, 438, 103-7.
- LAMBROS, C. & VANDERBERG, J. P. 1979. Synchronisation of *Plasmodium falciparum* erythrocytic stages in culture. *J Parasitol*, 65, 418-20.
- LEESON, P. 2012. Drug discovery: Chemical beauty contest. *NATURE*, 481, 455-6.
- LIPINSKI, C. A., LOMBARDO, F., DOMINY, B. W., *et al.* 2001. Experimental and computational approaches to estimate solubility and permeability in drug discovery and development settings. *Adv Drug Deliv Rev*, 46, 3-26.
- LLINAS, M., BOZDECH, Z., WONG, E. D., *et al.* 2006. Comparative whole genome transcriptome analysis of three *Plasmodium falciparum* strains. *Nucleic Acids Res*, 34, 1166-73.
- LOPEZ-RUBIO, J. J., GONTIJO, A. M., NUNES, M. C., *et al.* 2007. 5' flanking region of var genes nucleate histone modification patterns linked to phenotypic inheritance of virulence traits in malaria parasites. *Molecular microbiology*, 66, 1296-305.



- LOPEZ-RUBIO, J. J., MANCIO-SILVA, L. & SCHERF, A. 2009. Genome-wide analysis of heterochromatin associates clonally variant gene regulation with perinuclear repressive centers in malaria parasites. *Cell host & microbe*, 5, 179-90.
- MALMQUIST, N. A., MOSS, T. A., MECHERI, S., *et al.* 2012. Small-molecule histone methyltransferase inhibitors display rapid antimalarial activity against all blood stage forms in *Plasmodium falciparum*. *Proceedings of the National Academy of Sciences of the United States of America*, 109, 16708-13.
- MASER, P. S. W., ROTTMANN, M., WENZLER, T., KAISER, M., AND BRUN, R., 2012. Antiparasitic agents: new drugs on the horizon. *Current Opinion in Pharmacology*, 12, 562-566.
- MERRICK, C. J. & DURAISINGH, M. T. 2010. Epigenetics in *Plasmodium*: what do we really know? *Eukaryotic cell*, 9, 1150-8.
- MIAO, J., FAN, Q., CUI, L., *et al.* 2006. The malaria parasite *Plasmodium falciparum* histones: organization, expression, and acetylation. *Gene*, 369, 53-65.
- MULLER, I. B., DAS GUPTA, R., LUERSEN, K., *et al.* 2008. Assessing the polyamine metabolism of *Plasmodium falciparum* as chemotherapeutic target. *Molecular and biochemical parasitology*, 160, 1-7.
- MUNSHI, A., SHAFI, G., ALIYA, N., *et al.* 2009. Histone modifications dictate specific biological readouts. *Journal of genetics and genomics = Yi chuan xue bao*, 36, 75-88.
- NCOKAZI, K. K. & EGAN, T. J. 2005. A colorimetric high-throughput beta-hematin inhibition screening assay for use in the search for antimalarial compounds. *Analytical biochemistry*, 338, 306-19.
- NIEMAND, J., LOUW, A. I., BIRKHOLTZ, L., *et al.* 2012. Polyamine uptake by the intraerythrocytic malaria parasite, *Plasmodium falciparum*. *Int J Parasitol*, 42, 921-9.
- NOBLE, J. E. 2009. Quantitation of Protein. *Methods in Enzymology*, 463, 73-95.
- ONG, S. E., SCHENONE, M., MARGOLIN, A. A., *et al.* 2009. Identifying the proteins to which small-molecule probes and drugs bind in cells. *Proceedings of the National Academy of Sciences of the United States of America*, 106, 4617-22.
- PAREJO, I., PETRAKIS, C. & KEFALAS, P. 2000. A transition metal enhanced luminol chemiluminescence in the presence of a chelator. *Journal of pharmacological and toxicological methods*, 43, 183-90.
- PATEL, V., MAZITSCHKEK, R., COLEMAN, B., *et al.* 2009. Identification and characterization of small molecule inhibitors of a class I histone deacetylase from *Plasmodium falciparum*. *Journal of medicinal chemistry*, 52, 2185-7.
- PETTER, M., SELVARAJAH, S. A., LEE, C. C., *et al.* 2013. H2A.Z and H2B.Z double-variant nucleosomes define intergenic regions and dynamically occupy var gene promoters in the malaria parasite *Plasmodium falciparum*. *Mol Microbiol*, 87, 1167-82.
- PIHLASALO, S., AURANEN, L., HANNINEN, P., *et al.* 2012. Method for estimation of protein isoelectric point. *Analytical chemistry*, 84, 8253-8.
- PILCH, D. R. 1964. Two-Dimensional Gel Analysis of Histones and Other H2AX-Related Methods. *Methods in Enzymology*, 121, 321-404.

- PONDER, E. L. & BOGYO, M. 2007. Ubiquitin-like modifiers and their deconjugating enzymes in medically important parasitic protozoa. *Eukaryotic cell*, 6, 1943-52.
- SALCEDO-AMAYA, A. M., VAN DRIEL, M. A., ALAKO, B. T., *et al.* 2009. Dynamic histone H3 epigenome marking during the intraerythrocytic cycle of *Plasmodium falciparum*. *Proceedings of the National Academy of Sciences of the United States of America*, 106, 9655-60.
- SHAPIRO, H. M., APTE, S. H., CHOJNOWSKI, G. M., *et al.* 2013. Cytometry in malaria--a practical replacement for microscopy? *Curr Protoc Cytom*, Chapter 11, Unit 11 20.
- SHARMA, S. K., WU, Y., STEINBERGS, N., *et al.* 2010. (Bis)urea and (bis)thiourea inhibitors of lysine-specific demethylase 1 as epigenetic modulators. *Journal of medicinal chemistry*, 53, 5197-212.
- SHECHTER, D., DORMANN, H. L., ALLIS, C. D., *et al.* 2007. Extraction, purification and analysis of histones. *Nature protocols*, 2, 1445-57.
- SIMS, J. S., MILITELLO, K. T., SIMS, P. A., *et al.* 2009. Patterns of gene-specific and total transcriptional activity during the *Plasmodium falciparum* intraerythrocytic developmental cycle. *Eukaryot Cell*, 8, 327-38.
- SIVARAMAN, T., KUMAR, T. K., JAYARAMAN, G., *et al.* 1997. The mechanism of 2,2,2-trichloroacetic acid-induced protein precipitation. *J Protein Chem*, 16, 291-7.
- SKAGERBERG, B., CLEMENTI, S., SJOSTROM, M., *et al.* 1989. Principal properties of aromatic substituents. *Prog Clin Biol Res*, 291, 127-30.
- SMITH, P. K., KROHN, R. I., HERMANSON, G. T., *et al.* 1985. Measurement of protein using bicinchoninic acid. *Analytical biochemistry*, 150, 76-85.
- SPANNHOFF, A., HAUSER, A. T., HEINKE, R., *et al.* 2009. The emerging therapeutic potential of histone methyltransferase and demethylase inhibitors. *ChemMedChem*, 4, 1568-82.
- SULLIVAN, W. J., JR., NAGULESWARAN, A. & ANGEL, S. O. 2006. Histones and histone modifications in protozoan parasites. *Cellular microbiology*, 8, 1850-61.
- TEUSCHER, F. M. L. G., CHEN, N., PETERS, J., KYLE, D.E., AND CHENG, Q., 2010. Artemisinin-Induced Dormancy in *Plasmodium falciparum*: Duration, Recovery Rates, and Implications in Treatment Failure. *The Journal of Infectious Diseases*, 292, 1362 - 1368.
- TIAN, X. & FANG, J. 2007. Current perspectives on histone demethylases. *Acta biochimica et biophysica Sinica*, 39, 81-8.
- TILLEY, L., DIXON, M. W. & KIRK, K. 2011. The *Plasmodium falciparum*-infected red blood cell. *The international journal of biochemistry & cell biology*.
- TONKIN, C. J., CARRET, C. K., DURAISINGH, M. T., *et al.* 2009. Sir2 paralogues cooperate to regulate virulence genes and antigenic variation in *Plasmodium falciparum*. *PLoS biology*, 7, e84.
- TRAGER, W. & JENSEN, J. B. 1997. Continuous culture of *Plasmodium falciparum*: its impact on malaria research. *Int J Parasitol*, 27, 989-1006.
- TRELLE, M. B., SALCEDO-AMAYA, A. M., COHEN, A. M., *et al.* 2009. Global histone analysis by mass spectrometry reveals a high content of

- acetylated lysine residues in the malaria parasite *Plasmodium falciparum*. *Journal of proteome research*, 8, 3439-50.
- VDOVENKO, M. M., DEMIYANOVA, A. S., CHEMLEVA, T. A., *et al.* 2012. Optimisation of horseradish peroxidase-catalyzed enhanced chemiluminescence reaction by full factorial design. *Talanta*, 94, 223-6.
- VERLINDEN, B. K., NIEMAND, J., SNYMAN, J., *et al.* 2011. Discovery of novel alkylated (bis)urea and (bis)thiourea polyamine analogues with potent antimalarial activities. *J Med Chem*, 54, 6624-33.
- VOET, V. 2011. *Biochemistry*, J. Wiley & Sons.
- VOSS, T. S., MINI, T., JENOE, P., *et al.* 2002. *Plasmodium falciparum* possesses a cell cycle-regulated short type replication protein A large subunit encoded by an unusual transcript. *J Biol Chem*, 277, 17493-501.
- WALKER, K. W. A. J. 2010. *Principles and Techniques of Biochemistry and Molecular Biology*, Cambridge University Press.
- WANG, J. D. L. U. 2004. The impact of early ADME profiling on drug discovery and development strategy. *Drug Discovery World Fall*, 73 - 86.
- WALLACE, H. M. & NIIRANEN, K. 2007. Polyamine analogues - an update. *Amino Acids*, 33, 261-5.
- WANG, C., DELCROS, J. G., CANNON, L., *et al.* 2003. Defining the molecular requirements for the selective delivery of polyamine conjugates into cells containing active polyamine transporters. *Journal of medicinal chemistry*, 46, 5129-38.
- WEINER, A., DAHAN-PASTERNAK, N., SHIMONI, E., *et al.* 2011. 3D nuclear architecture reveals coupled cell cycle dynamics of chromatin and nuclear pores in the malaria parasite *Plasmodium falciparum*. *Cellular microbiology*, 13, 967-77.
- WELLS, T. N., ALONSO, P. L. & GUTTERIDGE, W. E. 2009. New medicines to improve control and contribute to the eradication of malaria. *Nature reviews. Drug discovery*, 8, 879-91.
- WESTENBERGER, S. J., CUI, L., DHARIA, N., *et al.* 2009. Genome-wide nucleosome mapping of *Plasmodium falciparum* reveals histone-rich coding and histone-poor intergenic regions and chromatin remodeling of core and subtelomeric genes. *BMC Genomics*, 10, 610.
- WHO. 2010. *World Malaria Report 2010* [Online]. World Health Organization.
- WHO 2013. *World Malaria Report 2013*. 284.
- WOSTER, P. M. & CASERO, R. A., JR. 2011. *Polyamine Drug Design*, Royal Society of Chemistry.
- XU, Z., XIE, Q. & ZHOU, H. M. 2003. Trichloroacetic acid-induced molten globule state of aminoacylase from pig kidney. *J Protein Chem*, 22, 669-75.
- YANG, M. J. C. C., LAWRENCE M. SZEWCZUK, PEGAH JALILI, HAYDN L. BALL, MISCHA MACHIUS, PHILIP A. COLE, AND HONGTAO YU 2007. Structural Basis for the Inhibition of the LSD1 Histone Demethylase by the Antidepressant trans-2-Phenylcyclopropylamine. *Biochemistry*.
- YAGER, T. D., MCMURRAY, C. T. & VAN HOLDE, K. E. 1989. Salt-induced release of DNA from nucleosome core particles. *Biochemistry*, 28, 2271-81.

YEUNG, S. D., MOORTHY, V. S., MILLS, A. J., 2009. Artemisinin resistance on the Thai-Cambodian border. *The Lancet*, 374, 1418 - 1419.

## **Appendix 1**

*Ex vivo* pharmacology and *in vivo* efficacy testing (work performed at St Jude's Childrens Hospital, USA by Kip Guy)

### **Solubility**

Solubility assay was carried out on Biomek FX lab automation workstation (Beckman Coulter, Inc., Fullerton, CA) using mSOL Evolution software (pION Inc., Woburn, MA). The detailed method is described as following. 10 ml of 10 mM compound stock (in DMSO) was added to 190 ml 1-propanol to make a reference stock plate. 5 ml from this reference stock plate was mixed with 70 ml 1-propanol and 75 ml citrate phosphate buffered saline (isotonic) to make the reference plate, and the UV spectrum (250 nm–500 nm) of the reference plate was read. 6 ml of 10 mM test compound stock was added to 594 ml buffer in a 96-well storage plate and mixed. The storage plate was sealed and incubated at room temperature for 18 hours. The suspension was then filtered through a 96-well filter plate (pION Inc., Woburn, MA). 75 ml filtrate was mixed with 75 ml 1-propanol to make the sample plate, and the UV spectrum of the sample plate was read. Calculations were carried out by mSOL Evolution software based on the AUC (area under curve) of UV spectrum of the sample plate and the reference plate. All compounds were tested in triplicates.

### **Permeability**

Parallel Artificial Membrane Permeability Assay (PAMPA) was conducted by Biomek FX lab automation workstation (Beckman Coulter, Inc., Fullerton, CA) and PAMPA evolution 96 command software (pION Inc., Woburn, MA). The detailed method is described as following. 3 ml 10 mM test compound stock in DMSO was mixed with 597 ml of citrate phosphate buffered saline (isotonic) to make diluted test compound. 150 ml of diluted test compound was transferred to a UV plate (pION Inc., Woburn, MA) and the UV spectrum was read as the reference plate. The membrane on pre-loaded PAMPA sandwich

(pION Inc., Woburn, MA) was painted with 4 ml GIT lipid (pION Inc., Woburn, MA). The acceptor chamber was then filled with 200 ml ASB (acceptor solution buffer, pION Inc., Woburn, MA), and the donor chamber was filled with 180 ml diluted test compound. The PAMPA sandwich was assembled, placed on the Gut-box and stirred for 30 minutes. Aqueous Boundary Layer was set to 40 mm for stirring. The UV spectrum (250-500 nm) of the donor and the acceptor were read. The permeability coefficient was calculated using PAMPA evolution 96 command software (pION Inc., Woburn, MA) based on the AUC of the reference plate, the donor plate and the acceptor plate. All compounds were tested in triplicates.

### **Metabolic stability studies**

Compounds were incubated at 37°C with either pooled mouse, rat, dog or human liver microsomes (BD-Gentest, BD-Biosciences, Woburn, MA) at three concentrations (0.8 µM, 4 µM and 20 µM). The incubation mix consisted of compounds (0.8 µM, 4 µM and 20 µM), 0.2 mg/ml human microsomal protein, 2.5 mM NADPH, and 3.3 mM MgCl<sub>2</sub> in 100 mM phosphate buffer, pH 7.4. All incubations were performed in triplicate. Reactions were stopped at the end of incubation by the addition of cold acetonitrile (1×volume of reaction). The rate of loss of parent compound was determined at 0, 15, 30, and 60 min by LC-MS/MS analysis. The amount of compound in the samples was expressed as a percentage of remaining compound compared to time point zero (100%). The slope (-k) of the linear regression from ln[test compound] versus time plot was determined, and t<sub>1/2</sub> was calculated from the equation  $k = \ln(2)/t_{1/2}$ .

### **In vivo efficacy evaluation (work done at University of Cape Town, Pharmacology Dept by Lubbe Wiesner)**

The compounds were administered at two different doses (10 and 50 mg/kg) each using the Peters 4-day suppressive test model. Animals were infected with  $2 \times 10^6$  parasitised erythrocytes and treated at pre-determined time points over 4 days. Physical examinations were conducted twice daily. The parasite used was the CQ-sensitive isolate *Plasmodium berghei*, a highly virulent and

lethal strain of malaria and a suitable model system for the tests described herein. Parasites were maintained in host animals until such time as the amount was sufficient to infect all the test animals on the same day. Two host mice were infected with parasites and left untreated to allow the parasites to multiply. Parasitemia was monitored occasionally until it was sufficiently high; at that time, parasites were harvested from the host mice via cardiac puncture. The two parasite stocks were pooled and average parasitemia of the pooled stock was determined microscopically. Additionally, the total number of erythrocytes per millilitre of the pooled stock was determined; this is necessary in order to ensure test animals obtain both uniform and correct amounts of parasite to establish the infection. Test mice were divided into eight groups of five animals per group and weighed. Parasitised erythrocytes (pRBC) were transferred to microfuge tubes and maintained in phosphate-buffered saline at a level of  $5 \times 10^7$  pRBC/ml as a secondary stock, of which 200  $\mu$ L was injected intraperitoneally to each test animal in order to introduce  $2 \times 10^6$  pRBC to each mouse. Immediately thereafter, the mice in each group were treated with the pre-determined regimen for that group (Table 1). Treatments were repeated 24, 48, and 72 hours post-infection. Parasitemia levels were monitored frequently and weights were also determined at each of these times.

### ***In vivo* pharmacokinetic evaluation**

Compound 7 was evaluated for its pharmacokinetic properties in a mouse model (C57/BL6). Oral pharmacokinetic studies were conducted in two groups of mice and the exact procedures are described below:

Group 1 (N = 5): Compound 7 was administered via oral gavage at 10 mg/kg in DMSO:water (1:9, v/v). The total volume per administration was 200  $\mu$ L. Blood samples (50  $\mu$ L) were collected via tail bleeding at 0.5, 2.5, 5 and 7 hours post-dose in 0.5 ml lithium heparin microvials to prevent blood coagulation. The samples were stored at  $-80^\circ\text{C}$ .

Group 2 (N = 5): Compound 7 was also administered via oral gavage at 50 mg/kg in DMSO:water (1:9, v/v). The same protocol was used as described for group 1. The concentration of compound 7 was determined using a

quantitative LC-MS/MS method. Sample preparation was achieved with a protein precipitation extraction method, using 20  $\mu$ L whole blood and 100  $\mu$ L acetonitrile. Gradient chromatography was performed on a Phenomenex Luna PFP(2) (5 $\mu$ , C18, 100A, 50x2 mm) analytical column (Phenomenex, USA) using acetonitrile and 0.1% formic acid mixed with HPLC water as mobile phase at a flow rate of 0.75 ml/min. An AB Sciex API 3200 Q-Trap mass spectrometer was operated at unit resolution in the multiple reaction monitoring (MRM) mode, monitoring the transition of the protonated molecular ions at  $m/z$  469.2 to the product ions at  $m/z$  230.0 for compound **7**. The assay was validated over a range of 7.8 ng/ml to 125 ng/ml for compound **7**.